VILNIUS UNIVERSITY
STATE RESEARCH INSTITUTE
CENTER FOR PHYSICAL SCIENCES AND TECHNOLOGY

Giedrius
ABROMAVIČIUS

Microstructural and optical properties of metal oxide optical coatings deposited by ion beam sputtering and their application in UV spectral range

DOCTORAL DISSERTATION

Technological sciences,
Material engineering T008

VILNIUS 2020

This dissertation was prepared at Optical coatings laboratory of the Center for physical sciences and technology in 2013–2019 and is defended on an external basis.

Academic consultant:
dr. Ramutis Drazdys (Center for physical sciences and technology, Technological Sciences, Material Engineering, T008)

Chairman – prof. habil. dr. Valdas Sirutkaitis (Vilnius University, technological sciences, material engineering, T008).
Members:
prof. dr. Artūras Jukna (Vilnius Gediminas Technical University, technological sciences, material engineering, T008);
dr. Andrejus Michailovas (Center for Physical Sciences and Technology, technological sciences, material engineering, T008).
prof. dr. Tomas Tamulevičius (Kaunas University of Technology, technological sciences, material engineering, T008).
dr. Arūnas Varanavičius (Vilnius University, technological sciences, material engineering, T008);

The dissertation shall be defended at a public meeting of the Dissertation Defence Panel at 14:00 on 25th of February 2020 in meeting room of the Institute of Physics (Center for Physical Sciences and Technology).
Address: Savanorių ave. 231, Vilnius, Lithuania

The text of this dissertation can be accessed at the libraries of Vilnius University, Center for Physical Sciences and Technology, as well as on the website of Vilnius University: www.vu.lt/lt/naujienos/ivykiu-kalendorius

VILNIAUS UNIVERSITETAS
VALSTYBINIS MOKSLINIŲ TYRIMŲ INSTITUTAS FIZINIŲ IR TECHNOLOGIJOS MOKSLŲ CENTRAS

Giedrius
ABROMAVIČIUS

Jonapluoščio dulkinimo būdu suformuotos metalų oksidų optinės dangos: mikrostruktūrinės ir optinės charakteristikos bei jų panaudojimas UV diapazone

DAKTARO DISERTACIJA

Technologijos mokslai,
Medžiagų inžinerija T008

VILNIUS 2020

Disertacija rengta 2013 – 2019 metais Optinių dangų laboratorijoje, Valstybiniame mokslinių tyrimų institute Fizinių ir technologijos mokslų centre ir yra ginama eksternu.

Mokslinis konsultantas:
dr. Ramutis Drazdys (Valstybinis mokslinių tyrimų institutas Fizinių ir technologijos mokslų centras, technologijos mokslai, medžiagų inžinerija, T008)

Gynimo taryba:
Pirmininkas – prof. habil. dr. Valdas Sirutkaitis (Vilniaus universitetas, technologijos mokslai, medžiagų inžinerija, T008).
Nariai:
prof. dr. Artūras Jukna (Vilniaus Gedimino technikos universitetas, technologijos mokslai, medžiagų inžinerija – T008);
dr. Andrejus Michailovas (Fizinių ir technologijos mokslų centras, technologijos mokslai, medžiagų inžinerija – T008).
prof. dr. Tomas Tamulevičius (Kauno technologijos universitetas, technologijos mokslai, medžiagų inžinerija, T008).
dr. Arūnas Varanavičius (Vilniaus universitetas, technologijos mokslai, medžiagų inžinerija – T008);

Disertacija ginama viešame posėdyje 2020 m. vasario mėn. 25 d. 14 val. Fizinių ir technologijos mokslų centro Fizikos instituto posėdžių salėje. Adresas: Savanorių pr. 231, Vilnius, Lietuva, LT-02300.

Disertaciją galima peržiūrėti Vilniaus universiteto, Fizinių ir technologijos mokslų centro bibliotekose bei VU interneto svetainėje adresu: https://www.vu.lt/naujienos/ivykiu-kalendorius

CONTENTS

LIST OF ABBREVIATIONS

AFM	Atomic Force Microscopy
AR	Anti-Reflective
AOI	Angle Of Incidence
CRD	Cavity Ring Down
EBE	Electron Beam Evaporation
FS	Fused Silica
HR	High-Reflective
HT	High Transmittance
H	High refractive index
IBS	Ion Beam Sputtering
L	Low refractive index
LID	Laser Induced Damage
LIDT	Laser Induced Damage Threshold
MR	Magnetorheological
MRF	Magnetorheological Finishing
RMS	Root Mean Square
SSD	Sub-Surface Damage
T	Transmittance
UV	Ultraviolet
XRD	X-Ray Diffraction

INTRODUCTION

Optical thin films and coatings have been present in our world since ancient times, because they are simply just part of the nature. There are many examples, where thin layers determine surface optical properties.

Optical thin film and coating deposition is the one of many human created technologies. However, the nature is full of biological examples, which uses interference of layered structures to enhance their visual properties like reflection, color, absorption, scatter in order to modify visibility, communication, mimicry, etc. [1]. Most of them are based on alternating layers having different refractive indices, like guanine and cytoplasm in fishes, cuticles and air in butterflies.

Optical coatings are inevitable part of almost any optical system, starting from regular eyeglasses and finishing with the complicated laser systems. Since the invention of laser in 1960 by R. Maiman [2], research of dielectric optical coatings turned into a rapidly growing field. Coating resistance to laser radiation in its turn became one of the most important investigated property [3, 4]. Annual symposium called "Laser-Induced Damage in Optical Materials" was founded in Boulder, USA in 1969. It is dedicated to modelling, measuring and improving optical resistance of bulk materials and thin films. Further developments and new applications of lasers raised interests in other important coating properties and their interplay, such as microstructure, film stress, stoichiometry, optical losses, resistance to ultrashort pulse damage, etc.

Optical coating deposition technology started to develop many years before invention of the laser itself. The first substrates were coated by thin metal films using evaporation and subsequent condensation in the middle of the XIXth century [1], later followed by reactive evaporation of metal oxides under vacuum in the middle of the XXth century [5, 6]. Roots of other currently sophisticated deposition processes like magnetron sputtering or ion beam sputtering trace back to 1852, when Welsh physicist W. R. Grove described iron oxide thin film deposition on silver plate [7]. By 1932, more than hundred papers were published in this field, and several patents were issued, also a commercial sputter deposition system was already available [8, 9]. It was noticed, that sputter deposited films were more adherent, less sensitive to local delamination, had substantially higher lifetime than solution-grown or electroplated layers. Prototype of modern ion beam sputtering system emerged already in 1975, when broad-beam ion sources were engineered for thin film deposition [10]. These ion sources initially were developed for space propulsion in 1960 [11]. Application of ion beam sputtering to optical coating production was driven for the need of low loss dielectric mirrors, necessary for laser gyros. While new deposition process was slow, it provided non-contaminated process without damage by discharge and without additional substrate heating. The main advantages comparing with other existing coating technologies were low optical losses, amorphous film structure, low porosity, very good environmental stability, absence of spectral shift or degradation in time [12]. In addition, stability of the process and tight control of process variables enabled reliable realization of complex coating designs like bandpass, rugate, notch filters, chirped mirrors, etc. Due to all these advantages, IBS technology currently is well established as the main platform to realize state-of-the-art optical coatings for laboratory and extreme environments, like space applications, having precise complex optical properties, high stability, durability and resistance to laser radiation. However, constantly evolving laser systems push the requirements for optical components still further. Furthermore, IBS technology has several drawbacks; one of these is high intrinsic stress of deposited coatings. If not treated, this might deteriorate flatness of optical component and introduce unwanted beam distortion within laser system.

Laser radiation at ultraviolet (UV) spectral range was first demonstrated by Franken et al [13] using optical harmonic generation (λ = 347 nm) by ruby laser. Possibilities to generate fundamental laser harmonic at UV spectral range employing noble gas excitation were discussed in 1966. Experimentally it was realized in the 1970's after introducing excimer laser [14]. Currently, different areas routinely use UV laser technology, such as lithography, electronics, micromachining, biomedicine, spectroscopy, chemistry. Due to much higher photon energies at shorter wavelengths, such laser radiation provides unique opportunities, like more efficient interaction with matter, also better focusing. However, at the same time this spectral range adds additional challenges for performance and longevity of necessary optical components.

Presented thesis is focused on several aspects of improving properties of ion beam sputtering deposited coatings for UV spectral range. Firstly, plasma etching of fused silica substrates before coating process is investigated in order to evaluate possibilities to improve LIDT properties of transmitting optical components. Secondly, metal oxide mixture approach, combined with high temperature post-deposition annealing, enabling transition of layer microstructure, is examined for improving optical and laser resistance properties of dielectric mirrors for 266 nm radiation. Thirdly, high temperature annealing of HfO_2, Sc_2O_3 and Al_2O_3 binary mixtures, deposited by ion beam sputtering is investigated in order to identify possible candidates to design stress compensated multilayer UV coatings without degradation of optical properties.

The objective of the thesis

To extend the applicability of ion beam sputtered optical coatings for UV spectral range laser applications by optimizing plasma treatment of optical substrates, sputtering of material mixtures and post-deposition treatment of deposited coatings.

The scientific tasks of the work

1. To increase optical resistance of substrates to UV laser radiation by applying argon plasma etching without deterioration of their surface properties.
2. To develop substrate treatment method employing low energy oxygen plasma, which modifies and prepares substrate surface prior to deposition of high optical resistance coatings.
3. To investigate post deposition thermal treatment before and after crystallization onset of different hafnia-silica mixture based dielectric mirrors, focusing on their optical, microstructural, surface and laser damage resistance properties.
4. To increase optical resistance of HfO_2 and HfO_2-SiO_2 mixture based dielectric mirrors by optimizing post deposition thermal treatment process.
5. To investigate optical, surface and stress properties of binary HfO_2, Sc_2O_3 and Al_2O_3 mixtures thermally annealed at broad range of temperatures and evaluate possible applicability of this approach to develop stress-compensated multilayer coatings for UV spectral range.

Scientific novelty and practical value

Scientific novelty and practical value could be summarized in the following statements.

Scientific novelty

1. Low-energy oxygen plasma treatment of the fused silica substrates was investigated for the first time, using different etching depths and plasma ion energies. Increase of etched FS substrate surface LIDT, comparable to the laser resistance of bulk FS at 355 nm was demonstrated.

2. Combined approach using HfO_2-SiO_2 mixtures and high temperature thermal annealing was demonstrated, enabling considerable increase of LIDT and optical properties improvement of dielectric mirrors for 266 nm wavelength.
3. Binary mixtures of common metal oxides - HfO_2, Sc_2O_3 and Al_2O_3 were shown to be perspective candidates for development of stress compensated multilayer coatings for UV spectral range without degradation of optical, microstructural properties, if applying appropriate annealing temperature.

Practical benefits

1. Argon and oxygen plasma etching of fused silica substrates was developed enabling realization of transparent optical components for high power UV lasers. Part of the research was performed under collaboration with Altechna Coatings, the results are used in manufacturing of optical components.
2. High temperature annealing, triggering crystallization of HfO_2-SiO_2 mixture layers within multilayer structure was proven to be an effective technique to increase their LIDT more than 2 times, also maintaining high reflectance values. Suitable HfO_2-Al_2O_3, Sc_2O_3-Al_2O_3 and HfO_2-Sc_2O_3 mixtures and ranges of annealing temperatures were identified for development of stress-compensated multilayer coatings with improved optical loss properties. These results are important for Lithuanian optical coating companies in designing and producing optical components for UV spectral range.

Statements to defend

1. Laser induced damage threshold of fused silica surface for UV (355 nm) laser pulses is substantially increased without deterioration of surface properties by applying optimized argon plasma etching.
2. Modification and preparation of FS substrate surface by low energy oxygen plasma prior to coating deposition increases optical resistance of final optical component by 2-3 times for nanosecond UV (355 nm) laser pulses.
3. Optimized post deposition thermal treatment of HfO_2 and HfO_2-SiO_2 mixture based dielectric mirrors increases their LIDT for UV (266 nm) nanosecond laser pulses by 2.5-3 times.
4. Thin films having necessary stress values for design of stress compensated multilayer coatings for UV spectral range are deposited

by changing compositions of HfO_2, Sc_2O_3 and Al_2O_3 binary mixtures and applying suitable post-annealing temperatures.

Approbation

Scientific papers directly related to the thesis (peer-reviewed and indexed in Clarivative Analytics WoS)

1. K. Juškevičius, R. Buzelis, **G. Abromavičius**, S. Abbas, A. Belosludtsev, R. Drazdys, S. Kičas, "Argon plasma etching of fused silica substrates for manufacturing high laser damage resistance optical interference coatings," Optical Materials Express, **7** (10), 2017.
2. **G. Abromavičius**, T. Juodagalvis, R. Buzelis, K. Juškevičius, R. Drazdys, S. Kičas, "Oxygen plasma etching of fused silica substrates for high power laser optics", Applied Surface Science, **453**, 2018.
3. **G. Abromavičius**, S. Kičas, R. Buzelis, "High temperature annealing effects on spectral, microstructural and laser damage resistance properties of sputtered HfO_2 and HfO_2-SiO_2 mixture-based UV mirrors", Optical Materials **95**, 2019.
4. **G. Abromavičius**, T. Juodagalvis, "Mechanical stress, optical and surface properties of high temperature annealed HfO_2, Sc_2O_3 and Al_2O_3 binary mixture thin films deposited by ion beam sputtering", submitted to Optical Materials.

Other scientific papers

1. **G. Abromavičius**, N. Kyžas, A. Belosludtsev "Oxygen plasma etching of YAG crystals", Proc. SPIE, Advances in Optical Thin Films VI, **10691**, 2018.
2. **G. Abromavičius**, L. Grinevičiūtė, R. Buzelis, S. Kičas, A. Melninkaitis, E. Pupka, T. Tolenis, "High LIDT mirrors for 355nm wavelength based on combined ion beam sputtering and glancing angle deposition technique", Proc. SPIE, Laser-Induced Damage in Optical Materials, **10447**, 2017.
3. A. Melninkaitis, L Grinevičiūtė, **G. Abromavičius**, L. Mažulė, L. Smalakys, E. Pupka, M. Ščiuka, R. Buzelis, S. Kičas, T. Tolenis, "Next-generation all-silica coatings for UV applications", Proc. SPIE, Laser-Induced Damage in Optical Materials, **10447**, 2017.
4. **G. Abromavičius**, R. Buzelis, R. Drazdys, K. Juškevičius, S. Kičas, T. Tolenis, J. Mirauskas, M. Ščiuka, V. Sirutkaitis, A. Melninkaitis,

"Optical resistance and spectral properties of anti-reflective coatings deposited on LBO crystals by ion beam sputtering", Lithuanian Journal of Physics, **51** (4), 2011.

5. K. Starke, L. O. Jensen, M. Jupé, D. Ristau, **G. Abromavičius**, K. Juškevičius, R. Buzelis, R. Drazdys, "Investigation in oxide mixture coatings with adapted gradient index profiles", Proc. SPIE, Laser-Induced Damage in Optical Materials, **7504**, 2009.
6. **G. Abromavičius**, R. Buzelis, R. Drazdys, A. Melninkaitis, V. Sirutkaitis. "Influence of electric field distribution on laser induced damage threshold and morphology of high reflectance optical coatings", Proc. SPIE, Laser-Induced Damage in Optical Materials, **6720**, 2007.
7. **G. Abromavičius**, R. Buzelis, R. Drazdys, A. Melninkaitis, D. Mikšys, V. Sirutkaitis, A. Skrebutėnas, "Improvement of optical properties and radiation resistance of optical coatings based on Nb_2O_5 and Ta_2O_5", Proc. SPIE, Advanced Optical Materials, Technologies, and Devices, **6596**, 2007.
8. A. Melninkaitis, D. Mikšys, V. Sirutkaitis, **G. Abromavičius,** R. Buzelis, R. Drazdys, "Laser-induced damage threshold measurements of high reflecting dielectric layers", Proc. SPIE, Advanced Optical Materials, Technologies, and Devices, **6596**, 2007.
9. **G. Abromavičius**, R. Buzelis, R. Drazdys, A. Melninkaitis, D. Mikšys, V. Sirutkaitis, A. Skrebutėnas, R. Juškėnas, A. Selskis, "The microstructure and LIDT of Nb_2O_5 and Ta_2O_5 optical coatings", Proc. SPIE, Laser-Induced Damage in Optical Materials, **6403**, 2006.
10. **G. Abromavičius**, R Buzelis, R. Drazdys, R. Grigonis, A. Melninkaitis, D. Mikšys, T. Rakickas, V. Sirutkaitis, A. Skrebutėnas, R. Juškėnas, A. Selskis, "Influence of ion-assisted deposition on laser-induced damage threshold and microstructure of optical coatings", Proc. SPIE, Laser-Induced Damage in Optical Materials, **5991**, 2006.
11. A. Melninkaitis, D. Mikšys, T. Balčiūnas, V. Sirutkaitis, A. Skrebutėnas, R. Buzelis, R. Drazdys, **G. Abromavičius**, "Effect of substrate temperature and ion assistance on nanosecond laser-induced damage threshold in high reflection dielectric coatings", Proc. SPIE, Laser-Induced Damage in Optical Materials, **5991**, 2006.
12. A. Melninkaitis, M. Maciulevičius, T. Rakickas, D. Mikšys, R. Grigonis, V. Sirutkaitis, A. Skrebutėnas, R. Buzelis, R. Drazdys, **G. Abromavičius**, "Comparison of optical resistance of ion assisted

deposition and standard electron beam deposition methods for high reflectance dielectric coatings", Proc. SPIE, Advances in Optical Thin Films II, **5963**, 2005.

Conferences directly related to the thesis

1. **G. Abromavičius**, T. Juodagalvis, R. Buzelis, S. Kičas and R. Drazdys, "Plasma treatment of fused silica substrates for enhancement of resistance to UV laser radiation", Optical Systems Design, Frankfurt, Germany, 2018.
2. **G. Abromavičius**, S. Kičas, "Post-deposition annealing of ion beam sputtered dielectric mirrors based on hafnia-silica mixtures", Advanced Materials and Technologies, Palanga, Lithuania**,** 2018.
3. **G. Abromavičius**, S. Kičas, "Optical and surface properties of HfO_2-SiO_2 mixture based UV mirrors", Open Readings, Vilnius, 2018.
4. **G. Abromavičius**, T. Juodagalvis, R. Buzelis, S. Kičas and R. Drazdys, "Lydyto kvarco optinių pagrindukų ėsdinimo deguonies plazma taikymas formuojant didelės galios lazeriams skirtus optinius komponentus", Fizinių ir technologijos mokslų tarpdalykiniai tyrimai, Vilnius, Lithuania, 2018.
5. K. Juškevičius, R. Buzelis, R. Samuilovas, S. Abbas, **G. Abromavičius**, A. Puzas, R. Drazdys, "Plasma etching of fused silica substrates for manufacturing high laser damage resistance optical interference coatings", Optical Interference Coatings, Tucson, USA, 2016.

Conferences, which are not directly related to the thesis

1. **G. Abromavičius**, T. Tolenis, L. Grinevičiūtė, R. Buzelis, S. Kičas, A. Melninkaitis, E. Pupka, "High LIDT mirrors for 355nm wavelength based on combined ion beam sputtering and glancing angle deposition technique", SPIE Laser Damage, Boulder, 2017.
2. **G. Abromavičius**, T. Juodagalvis and R. Drazdys, "Optical and mechanical properties of Al_2O_3 thin films prepared by ion beam sputtering", Open Readings, Vilnius, 2017.
3. **G. Abromavičius**, R. Samuilovas, K. Juškevičius and R. Drazdys, "Al_2O_3 films prepared by reactive magnetron sputtering and their application for making dielectric mirrors", Advanced Materials and Technologies, Palanga, Lithuania**,** 2017.

4. **G. Abromavičius**, R. Drazdys, “Jonapluoščio dulkinimo būdu suformuotų metalo oksidų optinės savybės bei jų taikymas UV spektrinio ruožo aukšto atspindžio optinių dangų formavimui”, LNFK, Vilnius, Lithuania, 2015.

The contribution of the thesis author

The author designed himself, or actively participated in designing of all experiments. He also performed all necessary experiments for dielectric UV mirrors, executed their photometric, surface measurements and performed full data analysis. He actively took part in analysis of low oxygen plasma etching and HfO_2, Sc_2O_3 and Al_2O_3 binary mixture analysis. His contribution also includes all thesis related publications preparation (except the 1st) and presentation of the results in scientific conferences.

The contribution of the others

Tomas Juodagalvis performed low oxygen plasma etching experiments, as well, as HfO_2, Sc_2O_3 and Al_2O_3 binary mixture depositions and necessary measurements.

Dr. Rytis Buzelis performed LIDT and CRD measurements.

Dr. Vidas Pakštas performed and helped in interpreting of necessary XRD measurements.

Dr. Simonas Kičas gave valuable insights in experiment designs of dielectric UV mirrors and HfO_2, Sc_2O_3, Al_2O_3 binary mixtures.

Romanas Samuilovas and Dr. Kęstutis Juškevičius took important part in designing and executing argon plasma etching experiments, also analyzing obtained experimental data.

1 LITERATURE OVERVIEW

1.1 Processing of optical substrates

During manufacture of a substrate, a piece of optical material runs through the different processing steps and obtains necessary shape, flatness and surface quality. Processed substrate usually has defect layer, which could seriously degrade performance of resulting optical component after deposition of the necessary coating. In the following subsections, origin, properties of defect layer and its possible removal methods will be discussed.

1.1.1 Polishing residuals of optical substrates

Processing of optical glass or crystal typically starts from cutting and continues through grinding, lapping, polishing and post-polishing steps. All these operations bring their own contribution to the final surface quality of the optical component, which usually is even more crucial for the applications related to UV spectral range. Scratches, digs on the surface, voids in the subsurface can increase stray light, reduce optical performance and laser induced damage threshold. Lapping is the last step before the final polishing operation. Mix of water and loose abrasive, which is called slurry, is used between lapping plate and glass substrate. Generally, a transition layer called subsurface damage layer (SSD) forms between the substrate surface and its bulk at this processing stage.

Fig. 1 schematically shows defect layers beneath the surface of polished brittle material [15].

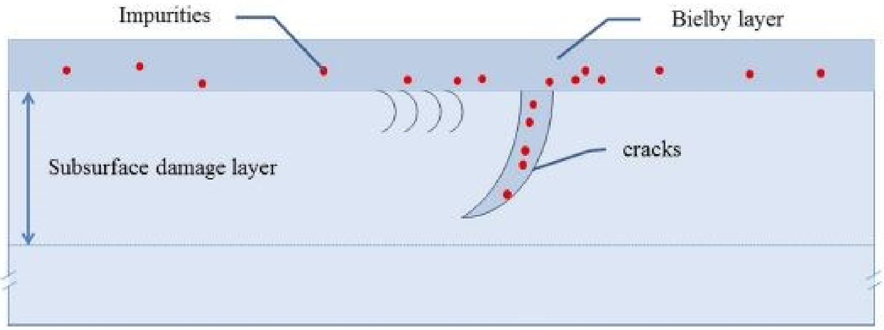

Fig. 1. Schematic of Beilby and SSD layer within the polished glass substrate [15].

If the optical component is designed for high power laser applications, careful attention should be paid to SSD layer. It has microcracks filled with light absorbing impurities [16], polishing compounds. Cracks within SSD could also amplify electric field of an incident laser pulse [17, 18]. Planar cracks can increase light intensity up to 10 times, while curved cracks or intersecting cracks can cause very high intensification [19]. The depth of SSD increases if polishing parameters such as cutting rate, grinding, polishing time are increased or larger abrasives are used [20-23]. It is also closely related with the mechanical properties of the substrate. For optical glasses, the depth of SSD can be estimated by such relation [23]:

$$H = \frac{1}{\pi}\left(\frac{K_c}{\Omega\beta\sigma_y}\right) \tag{1}$$

Where H is depth of SSD, K_c ductility index and σ_y is glass uniaxial yield stress. $\Omega \approx 1.1$ and $\beta \approx 0.08$ are geometrics factor accounting for the proximity of the free surface. Typical crack depth for BK7 glass is from 2 to 4 μm [23].

So-called Beilby layer is another very important characteristics concerning glass polishing [24], which is thin layer beneath the surface due to chemical reactions with polishing slurry. Cerium oxide is usually used in polishing and cerium penetrates under silica surface due to condensation reaction between the Si-OH silica surface and Ce-OH ceria particle surface [16]. In addition, other impurities like potassium K could penetrate into the surface by diffusion. Fig. 2 presents relative intensity of various contaminants at different depth of CeO_2 type slurry polished substrate [25]. It is clearly seen, that subsurface layer down to 60 nm is abundant with Ca, Ce and K.

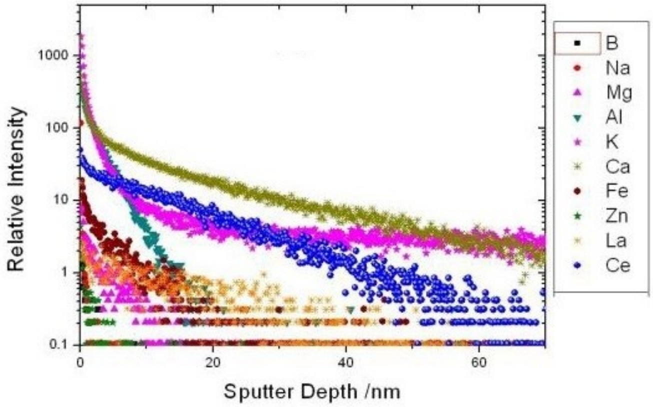

Fig. 2. Amount of residual impurities after different ion sputtering depth of polished FS substrate (polishing slurry type was CeO_2) [25].

Contaminated Beilby layer is absorbing incident ultraviolet laser energy and suppress resistance to laser damage of the optical component. Many studies have been dedicated to investigate the influence of this contamination layer. Exponential decay of metallic pollution (Ce, Zr, Al, Fe, Cu, Cr) concentration down to depth of 100-200 nm was measured in Kozlowski et al. study [26]. However, pollution depth and concentration values among different studies are scattered. For example, 0.3 μg/g concentration of Ce just below substrate surface and its significant decrease at ~25 nm depth was measured in study by Jiang et al [27], but 200 μg/g Ce concentration and its significant decrease 6-8 μm below the substrate surface was reported in study of Neauport et al [28]. Different polishing process parameters, such as surface removal rate are partly responsible for such differences. Characterization methods of impurities could also result in different values.

1.1.2 Post-polishing treatment of substrates

Many techniques has been developed to reduce SSD of polished substrates, such as chemical etching in various solutions [15, 27, 29-34], UV laser conditioning [35, 36], ion/plasma or reactive ion/plasma etching [37-41], magnetorheological finishing (MRF) [42] or combinations of these. Such additional treatment allows removing the majority of subsurface defects. LIDT of substrates and transparent optical components are also improved in this way [29].

Relatively simple technology of wet chemical etching was investigated for many years. Here, SSD layer is removed by immersing polished substrates for selected period of time into acid or alkali based concentrated solution. For example, leaching in heated (60 °C) aqueous solution with 40% HNO_3 and 10% H_2O_2 for 48 hours resulted in removal of 1 μm thickness surface layer. Also, concentration of Ce at FS surface was reduced about ten times, LIDT increased (R-on-1, $\lambda = 355$ nm, $\tau = 3$ ns) from 7 ± 4 J/cm^2 to 30 ± 2 J/cm^2 [32]. Another study used HF and NH_4F:HF (at various ratios) etching of more than 20 μm thickness to improve significantly small and large beam LIDT (R-on-1, $\lambda = 355$ nm, $\tau = 3$ ns, $d = 80$ μm and $\lambda = 351$ nm, $\tau = 5$ ns, $d = 3$ cm) [34]. Advantage of this procedure is simplicity and cost effectiveness. However, this technology brings several drawbacks, including increased surface roughness and additional contamination by re-deposition layer after substrate processing. Initial roughness increase up to $R_a = 1$ μm after 6 min HF etching [33] or to $R_a = 0.9$-1 nm after 6-15 min HF/HNO_3 etching [43].

UV laser conditioning is a procedure when polished substrate is raster scanned with overlapping UV ($\lambda = 248$, $\lambda = 355$ nm, etc.) laser pulse shots of nanosecond duration, with increased sub-damage threshold energies. Study of Brusasco et al showed that density of damaged places for FS samples made by different vendors decreased 1.25 - 3 times, depending on λ = 355 nm laser fluency and initial polishing quality. However, adding HF etching step before UV laser conditioning process allowed to decrease density of damaged places even 100 times [36].

Magnetorheological finishing (MRF) technology is used as a final polishing step for a broad range of applications, such as spherical, aspherical, freeform and plane surface polishing. Magnetic carbonyl iron and nonmagnetic abrasive particles (diamond, cerium) mixed in water with some additives constitute polishing fluid in MRF technology. The rheology of the fluid can be modified using magnetic field. MR polishing slurry is put in contact with the substrate by the polishing wheel and is stiffened using applied magnetic field. Drag and normal force of abrasive particles removes the material. Catrin et al has demonstrated successful application of MRF technology for removal SSD, when approximately 10 μm were removed from the FS substrate surface [42]. However, this investigation also demonstrated that up to 5 - 7 μm were polluted by MRF slurry elements such as iron and cerium, which degraded LIDT performance for 351 nm 2.5 ns laser pulses. Wet etching is necessary as a final step for removing polluted layer in order to increase LIDT. This approach was successfully demonstrated by several authors [35, 44].

1.1.3 Plasma and ion technologies for post-processing of substrates

Surface treatment using ion/plasma based technologies seems to be a promising tool for removing Beilby and SSD layers, since it is non-contact and non-contaminating process. Moreover, this technological step can also be successfully implemented just before coating deposition process. However, appropriate process design and parameters should be used. In addition, ion/plasma etching of substrates could also change their other important properties, like surface roughness. Increase of substrate surface roughness was reported after ion treatment, including ripple-like structure [45] and granular nanopatterns formation [46].

During the sputtering process, ions transfer their energy and momentum to the target atoms during elastic collisions. In this way, atoms obtain additional energy to overcome existing lattice and surface binding energy and substrate material is removed from the surface. Fig. 3 shows simulation of sputtering damage depth depending on incidence angle and ion energy [39].

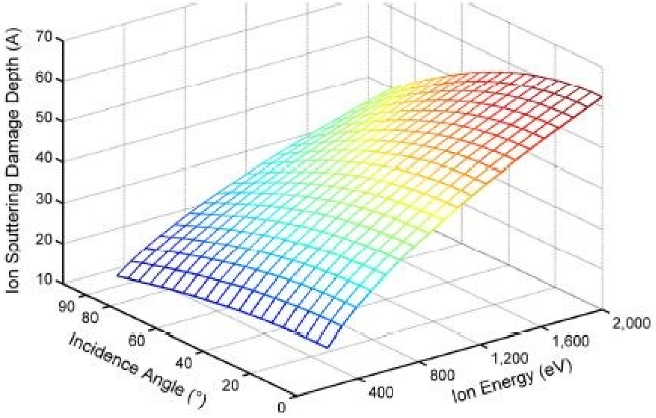

Fig. 3. Simulation of ion sputtering damage depth depending on incidence angle and ion energy [39].

Different energies of Ar ions could be selected for sample processing during ion etching process. Values may vary from several hundreds of eV to almost 1 keV [39]. Low ion energies result in lower material removal rate, but this also ensures preservation [37] or even allows smoothening of initial surface roughness [47]. Impact of energetic ions on substrate surface introduces additional defects like lattice distortion, material densification [39]. It should be also noted, that ion beam based technologies also are used for additional substrate shaping to achieve ultra-precise surfaces [48].

SSD layer can extend as far as 1-100 μm under the surface of polished substrate, depending on the polishing process. In order to increase process efficiency, reactive ion or plasma etching could be used, which involves chemical reaction. In such case, chemical reaction is taking place between working gas and substrate, that leads to the formation of volatile product, which evaporates and is pumped away [49]. Such removal of the surface is much faster comparing to direct surface sputtering, because of the fast evaporation rate of formed volatile products. CHF_3- or CF_4- contained plasma is used for SiO_2/Si etching [50]. The etching then results in such components like SiF_4, CO_2, COF_2 and H_2O. Ar gas is also usually added in order to get plasma more stable and to cool the mixture. Additionally, ion bombarding increases anisotropy of etching process and increases its rate. However, RIE also introduces some drawbacks, like deposited polymer layer, roughening of the surface [51, 52], implanted ions and neutrals and lattice distortion [53], which have to be coped with. Several investigations had already identified suitable process parameters, like equal oxygen and argon ratio within SF_6 gas mixture allowing to maintain initial surface roughness [54]. Study of Sun et al has optimized conditions of plasma generation in order to reduce the etching-induced contamination on FS surface [55]. A change from inductively to capacitive coupled plasma discharge mode allowed to get lower plasma density and much higher ion energy. This helped to prevent fluorocarbon deposition. Also hydrogen was added to CF_4 gas in order to suppress fluorocarbon polymerization and Ar proportion in gas mixture was doubled to enhance effectivity of ion bombardment.

Ion/plasma surface treatment increases laser damage resistance of polished and coated substrates by removing polishing contaminants and SSD. Ar^+ ion beam etching of conventionally polished fused silica substrate increased its LIDT for $\lambda = 266$ nm, 8-9 ns laser pulses 2 times [37]. RF plasma treatment of CLBO ($CsLiB_6O_{10}$) crystal using 100 W power has prolonged surface lifetime under irradiation of $\lambda = 266$ nm pulses more than 10 times up to 160 hours [56]. Increase from 7.84 J/cm^2 to 11.89 J/cm^2 for $\lambda = 308$ nm, 20 ns pulses after 700 nm removal by dielectric barrier discharge Ar plasma treatment was reported [57]. Reactive ion etching (RIE) technology using CHF_3-Ar mixture gas was also successfully combined together with dynamic chemical etching to improve LIDT of FS optics at $\lambda = 355$ nm from initial 22.7 J/cm^2 to 39 J/cm^2 almost without any surface degradation [41]. Another study has shown LIDT ($\lambda = 355$ nm, 7 ns, R-on-1) improvement by 134% using argon ion beam etching process after 800 nm etching [40]. Sun et al investigated RIE (CHF_3-Ar gas) of FS substrates using 1 um, 5 um, 15 um depths and reported increase of LIDT at $\lambda = 355$ nm (3ns) from 4.7 J/cm^2 to 7.3 J/cm^2 [50].

1.2 Ion beam sputtering technology

The first multilayer optical coating by ion beam sputtering technology was produced in 1976 [58, 59]. Very strict requirements, such as total optical losses below 10 ppm, no backscatter and successful performance in aggressive environment for dielectric mirrors of ring laser gyroscope were the main driving forces for foundation of IBS technology. The first successful results raised huge interest of optical coating community in this new emerging coating method.

IBS technology experienced a boom in 1990's, when there was an extensive development of dense wavelength-division multiplexing (DWDM) narrowband filters. Further technological developments in broad beam ion sources, electron sources, fast spectrometers, various sensor and computing technologies allowed to expand this coating technology further. Nowadays it is well established, fully automated and precise method for deposition of the most complex, environmentally resistant coatings with superb optical and mechanical properties.

It is also interesting to note, that prototypes of ion sources, which are the core components of IBS technology, had emerged as a product of NASA's electric propulsion project. This project was dedicated to create ion thrusters for movement of satellites in space and was under execution during period of 1960-1972 [60].

Physical principles of sputtering, main components of modern IBS systems, also properties of IBS deposited layers will be discussed in the following subsections below.

1.2.1 Physical principles of sputtering

David Wei was one of the inventors of ion beam sputtering. He elegantly characterized the basic principle of ion beam sputtering technology, imagining coating process like a gradual deposition of sand in the beach, grain by grain. The main principle of IBS is bombarding material target in vacuum with accelerated and neutralized ions. Sputtering is a result of momentum transfer of an impinging particle to the atoms of the target material. Sputtering process schematically is shown in Fig. 4 [61].

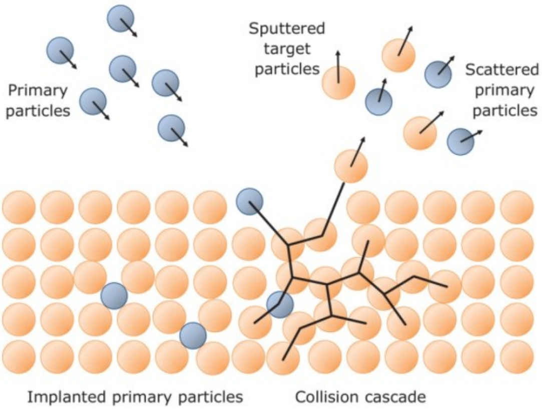

Fig. 4. Scheme of sputtering process [61].

Target atoms leave the surface, if enough energy is transferred by incident ions to overcome the binding forces. Binding energies for different metals varies between 2 eV and 5 eV. Threshold energy E_{th} is the minimum energy, required to cause sputtering. Its typical values are 5-40 eV and depends on several factors, such as mass, atomic number of target atoms and nature of incident atom. For example, sputtering yield of Ta metal using Xe ions is about 50% higher than for Ar ions, but it is almost the same for Ag, Ti metals [62]. Two main sputter regimes are considered – single knock-on and collision cascade. Single knock-on regime occurs when energy of incident ion is in the range of ~40 eV – ~ 1000 eV. Sputtering yield in this case can vary from zero to about ten or more atoms for a single incident ion. Several characteristics for knock-on regime are known [63]:

a) There is linear increase of the sputter yield regarding the increase of incident ion energy;
b) The highest yield is obtained when there is a good match between the mass of incident atoms and target atoms;
c) The sputtering yield increases significantly (~1.5-3 times) while increasing the angle of incidence from normal to ~50 degrees;
d) Number of sputtered atoms also increases linearly with the increase of the ion flux.

If ions have higher energies (1-50 keV), they can initiate collision cascade regime. During this process, ion penetrates beneath the surface and breaks all inner bonds of atoms within the target in a spherical region around the impact zone. This results in even higher yield, but it is not so practical for real applications, because of high voltages needed.

Several comprehensive studies were performed in order to trace how parameters influence different properties of deposited thin films, such as density, refractive index, stoichiometry, surface roughness, microstructure, stress, etc [64, 65].

1.2.2 Main components of IBS system

Main parts of IBS system are shown in Fig. 5 [66]

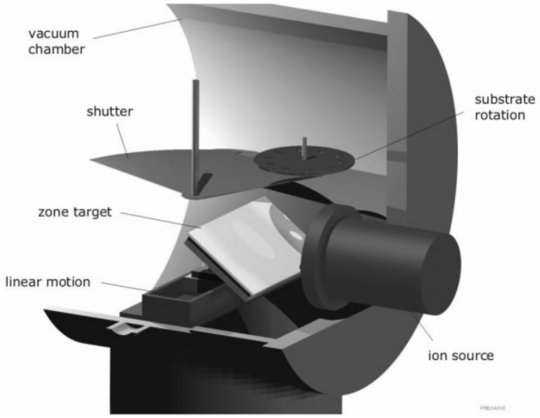

Fig. 5. Main parts of modern IBS coating chamber [66].

Broad beam ion source is the essential part of IBS system. Architecture of broad beam ion source determines the advantages of IBS process comparing to the other sputtering processes, such as diode plasma sputtering. Operation of modern broad beam ion source could be described shortly in the following way [67, 68]. Ion source is filled with the pulse of inert gas, which has some free electrons. Then variable electromagnetic field (usually ~13,56 MHz) is applied, and increases kinetic energy of these free electrons, which induce gas ionization. In this way, self-sustainable plasma is generated and no additional injection of electrons is needed. Some amount of ions move thermally towards extraction system, are accelerated and extracted by multi-aperture grid accelerator system (Fig. 6) [69]. Several grid system allows achieving much higher beam currents comparing with single aperture systems. Beam voltage usually could be set in 600-2000 V range. Ion beam usually is highly collimated - about 95% of ion current in the beam is distributed within a cone of 12° half-angle [70].

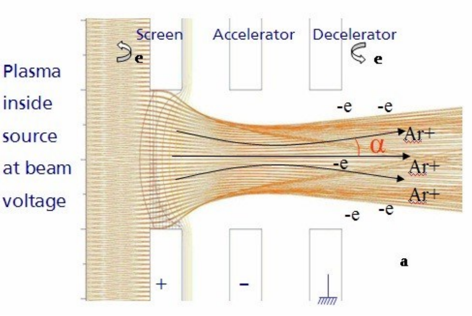

Fig. 6. Schematics of ion extraction grid system for broad beam ion source [69].

Broad beam ion source has many important advantages, because energy, direction and current density might be controlled independently over wide parameter range. Another significant advantage is spatially and electrically isolated ion production. This results in much better control of sputtering environment. Neutralization of extracted ion beam and suppression of undesirable charge accumulation within the chamber is achieved by using neutralizer, which emits electrons.

Another important part of IBS coating plant is material target holding system. Several possible geometries could be used, allowing switching to different materials by using rotation or linear motion. Zone target concept is used for producing material mixtures, as it is described here [66, 71, 72].

All other parts of IBS coating system are common with the other coating systems. These are – pumping, substrate rotation, heating, cooling systems, reactive gas inlet and process monitoring systems. Ion beam sputtering process is very stable and repetitive. Combined with sophisticated optical monitoring systems like broadband monitoring, it allows precise control of forming layers in terms of physical thicknesses and refractive indices [73].

It is also worth to note, that there are modification of IBS technology, so called dual ion beam sputtering technology (DIBS). In this case, additional ion source is used for bombarding growing film with energetic ions. There are several reasons, why such configuration is beneficial for production of superior optical coatings:

1) Cleaning/etching of the substrates before coating to increase coating adhesion or to increase LIDT of transparent optics by removing contaminated subsurface Beilby layer;
2) Modification of other important coating properties like mechanical stress [74-77], surface roughness [75], layer optical properties, LIDT [78], stoichiometry.

1.2.3 Main properties of dielectric coatings prepared by IBS

After IBS technology was established as a very perspective technology, there were several studies comparing it to EBE technology mostly in terms of absorption, scatter [79] and LIDT for UV laser wavelengths. Though initial results demonstrated, that absorption of IBS formed Al_2O_3 and SiO_2 layers was slightly higher, later appeared that by tuning the process [80, 81] and using additional post-processing steps [82], it is possible to achieve fully stoichiometric coatings [81, 83]. Regarding optical scatter, experiments demonstrated much lower losses of IBS prepared dielectric UV mirrors, comparing with samples coated by evaporation technology [79, 84].

Considering LIDT, IBS deposited mirrors using HfO_2/SiO_2 materials showed the same LIDT for 248 nm nanosecond pulses as evaporated coatings [79]. More recent direct comparisons demonstrated, that IBS made dielectric mirrors for 355 nm even outperformed EBE deposited coatings [85]. IBS technology is also considered as an alternative to traditional EBE process for further development of damage resistance optics for such high power systems as Megajoule laser (LMJ) in France [81] or National Ignition Facility (NIF) in United States [86, 87].

Initial and all following works have established the following main properties of thin films prepared by ion beam sputtering:

1) Smaller defect density, comparing to other sputter technologies. Due to relatively low working pressure ($\lesssim 10^{-2}$ Pa), sputtering is performed

in cleaner environment, therefore less residual gas atoms and other impurities could be incorporated within the forming film;
2) Refractive indices of formed layers are close to bulk values [88];
3) Highly homogeneous films [88];
4) High compressive stresses of ~500 - ~1500 MPa. This disadvantage could be suppressed using additional techniques, for example employing additional assisting source, using mixture materials and/or additional thermal post-treatment. These methods are discussed in more details in 1.6.2 subsection;
5) Low porosity films, leading to almost water adsorption-free and spectral shift-free behavior [89-93]. Temperature shift is in the range of 1-10 ppm/°C [94];
6) For the most of the cases, amorphous layer structure [89, 90], leading to extremely low scatter losses. For example, high reflecting mirrors, produced by IBS have demonstrated total losses below 1.6 ppm at 850 nm, which corresponds to R>99.99984% [95]. IBS technology was also used for developing extremely low loss mirrors for such projects as LIGO (Laser Interferometer Gravitational Observatory) and Virgo [74, 96];
7) Very good environmental resistance and stability, including very intense background radiation or space environment [93, 97-100];

There are also other benefits of IBS technology – relatively long maintenance periods, also possibility to deposit coatings on temperature-sensitive substrates.

Main drawbacks of IBS technology, comparing with EBE process, are the following:

1) Inability to produce coatings for DUV range, due to complicated sputtering process of fluorides. The main challenge of such process is to compensate fluorine, which is selectively sputtered from fluoride target, or to add necessary amount of it, if pure metal target is used. Different gases could be used for this purpose, like CF_4, F_2, but serious safety procedures should be implemented due to very high toxicity and corrosive action of fluorine. Several studies demonstrated successful sputtering deposition of fluorides and prototype coatings for DUV-UV spectral range [91, 101-104]. However, according to the thesis author’s knowledge, this technology still is not used commercially for production of optical coatings for DUV range;
2) Much lower production yield and higher cost due to several times slower deposition rates.

1.3 Oxides for UV spectral range

Oxides are widely used materials for dielectric coating production. Choice of suitable material depends on necessary coating properties: spectral performance, resistance to laser pulses, other requirements of its final application. Usually multilayer coating consists of alternating layers of high and low refractive index materials. SiO_2 is the most common used low-refractive index material, while choice of high *n* materials usually includes TiO_2, Nb_2O_5, Ta_2O_5, ZrO_2, HfO_2 and others. In the following subsections, the most common oxides, used for production of optical coatings for UV spectral range, will be reviewed.

1.3.1 HfO_2, Sc_2O_3

HfO_2 has one of the highest bandgap (5.1-6.2 eV [105-107]) between all high refractive index dielectric materials. The same applies to Sc_2O_3 (>5.7 eV [108, 109]). Due to this, both materials are considered as the best candidates to use in multilayer optical coatings dedicated for high power UV lasers [110, 111].

Hafnium oxide prepared by IBS technology has refractive index $n = 2.18$ at 355 nm [112]. Different properties of ion beam sputtered HfO_2 films were examined in several studies. Patel et al investigated refractive index, LIDT, stress properties, stoichiometry and microstructure depending on assist beam and used oxygen flow [113]. Liu et al examined influence of main ion beam source voltage, current, oxygen flow and substrate temperature on optical and stress properties of hafnia [114]. It was found, that background oxygen pressure [81, 115] is one of the key parameters for obtaining low absorbing and high LIDT HfO_2 films. Relation between film absorption, scatter, regarding to ion beam current and starting material (metal versus oxide) was also observed [81]. IBS prepared HfO_2 exhibits amorphous structure [116], which might turn to polycrystalline if additional ion beam assistance is used during the process [113, 117], or additional post deposition thermal treatment is used [82].

Sc_2O_3 thin films prepared by IBS were studied much less extensively, than HfO_2. However, scandia properties were reported in several publications. Refractive index of Sc_2O_3 prepared by DIBS technology was reported $n = 2.025$ at 355 nm in study of Menoni et al [118]. It was also showed, that scandia absorption, stoichiometry and microstructure are influenced by O_2/Ar partial pressure during the coating. Though single-shot LIDT for ps pulses was lower using higher O_2/Ar ratios, differences during multiple shot test were negligible. Another study shown that IBS deposited scandia films had smaller stress, order of magnitude smaller oxygen interstitials density and lower absorption coefficient values while using low O_2 partial pressure and smaller ion beam voltage [119]. Layers also had amorphous structure consisting of ~10 nm size crystallites. Mende et al also investigated potential of Sc_2O_3-SiO_2 mixtures for high power fs applications [120]. Though LIDT using 10000-on-1 test procedure for 355 nm ns pulses decreased, for deposited films with higher scandia content, LIDT using 1-on-1 test and 0.5 ps pulses at 1030 nm was surprisingly constant and was about 1.5 times higher, than for HfO_2-SiO_2 mixture having similar refractive index. These investigations demonstrated promising perspectives to use scandia-silica mixtures to produce high power coatings for ultrashort laser pulse applications, however, no further publications appeared up to the moment of this thesis preparation time.

1.3.2 Al_2O_3

Aluminum oxide is considered as a mid-refractive index material ($n = 1.7$ at 355 nm wavelength). However, due to even higher bandgap (6.5-7.6 eV [107, 121]) than scandia or hafnia, it is combined with SiO_2 layers to produce multilayer stacks having even higher LIDT's [85, 122-126]. As the most IBS produced films, alumina has amorphous structure [80]. However, material has other stable crystalline phases like α, γ, Θ, having different bandgaps [121, 127, 128].

Al_2O_3 was also used to produce mixtures with AlF_3 in search for new laser damage resistant composite materials for femtosecond applications [129].

1.3.3 SiO_2

Due to its physical properties and low cost, silicon dioxide is widely used in almost every multilayer coating as a low refractive index material ($n = 1.55$ at 355 nm [112]). It has very low optical absorption and high bandgap (7.54-8.3 eV [101, 107, 112]). Much research was performed through the years focusing on different optical and physical properties of SiO_2 deposited by different coating technologies [130-133]. Several papers reported about the influence of different IBS process parameters on silica thin film properties [76, 131, 134]. Also post-deposition thermal treatment was investigated in order to suppress film stress and chemical defects [135]. SiO_2 is also widely used as a component to produce mixtures with high refractive index materials to create new materials with tailored optical and LIDT properties [112, 116, 136-138].

1.4 Optical, microstructural and mechanical properties of dielectric material mixtures

Material mixtures gained attention of optical coating community for more than three decades, since it is possible to tune their bandgap, refractive index, microstructure, absorption, etc. Moreover, it was shown, that these properties do not depend linearly on the concentrations of the components. For example, Sahoo et al demonstrated, that mixtures can result in a higher refractive index material, than original pure materials [139]. The first investigations were carried out using electron beam co-evaporation [140], however later sputtering technologies were employed. In the following subsections, different applications of metal oxide mixtures will be reviewed, concentrating on increasing bandgap, LIDT and modification of multilayer coating stress.

1.4.1 Bandgap and LIDT of mixture materials

Extensive investigation of optical and laser damage resistance properties has been performed for different material mixtures, usually focusing on UV spectral range or ultrafast applications. Since material bandgap is one of the crucial parameters determining LIDT of optical coatings, several studies focused on mixing high refractive index (lower bandgap) materials with low refractive index (and high bandgap) materials, like SiO_2 or AlF_3. Research by Gouldieff et al investigated refractive indices and LIDT properties of HfO_2, Al_2O_3 and SiO_2 mixtures deposited by IBS [141]. They found, that density of damaging defects rapidly decreased with increasing bandgap (Fig. 7). Authors also made conclusion, that particularly HfO_2 contributed to high defect density of the mixture where it has been used.

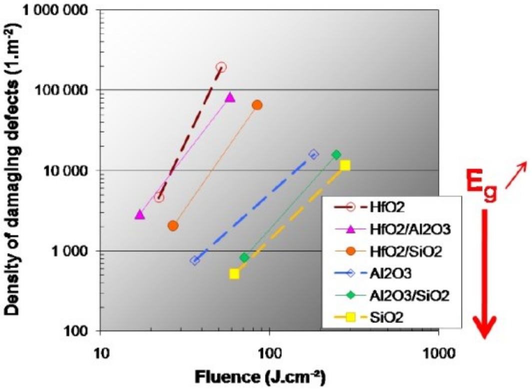

Fig. 7. Density of damaging defects as a function of fluency at λ = 355 nm (8 ns). S-on-1 test, beam waist diameter 50 μm. Pure materials are represented with dash lines, mixtures – using thin solid lines [141].

Also, several researches were conducted regarding application of material mixtures for improving LIDT of multilayer coatings. Mende et al [72] had explored several different designs of HR coatings for 355nm, including HfO_2-ZrO_2, HfO_2-Al_2O_3, HfO_2-SiO_2 mixtures as high refractive index materials. 10000-on-1 test using 7 nanosecond pulses at 100 Hz repetition rate and 220 ± 10 µm beam diameter showed the highest LIDT (~10 J/cm^2) of HfO_2-SiO_2/SiO_2 mirror for 355 nm (Fig. 8).

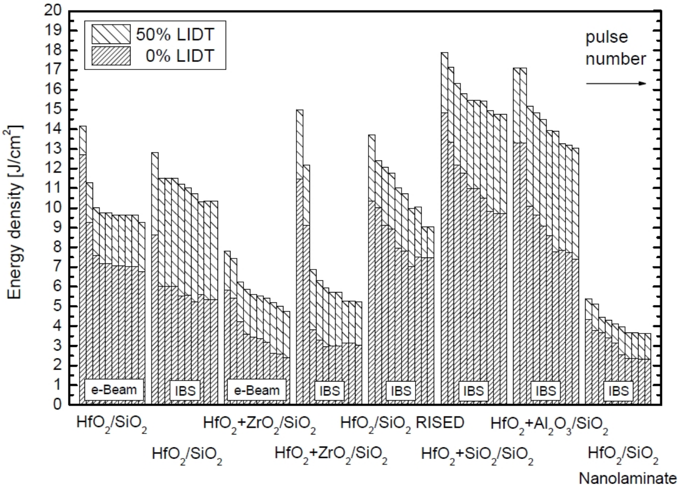

Fig. 8. LIDT 10000-on-1 test results for 355 nm wavelength high reflectors having different structures and materials [72].

Another study by Mende et al [116] had investigated possible application of HfO_2-SiO_2 mixtures for making dichroic mirror and AR coating optimized for 355 nm on LBO crystal. Again, hafnia mixture based coatings demonstrated higher LIDT's comparing to pure material layer stacks. Linear dependency of LIDT on optical bandgap was observed for Al_2O_3-AlF_3 ion beam sputtered single layers using femtosecond pulses at 343 nm wavelength [129]. Mixing high bandgap materials like SiO_2 with high refractive index layers and applying these mixtures in multilayer stacks helps to improve their LIDT properties in UV spectral range. All these studies investigated mixture layers, which were not post-treated additionally. However, it might be still possible to increase LIDT of mixture-based coatings, if employing additional post-deposition thermal treatment. This topic will be addressed by presented thesis results in subsection 3.2.

1.4.2 Microstructural and mechanical properties of mixture layers

Engineering of material mixtures also allows modifying their important mechanical and microstructural properties, like film stress, crystallinity. For example, adding 19% of SiO_2 to TiO_2 material during IBS process induced increase of mixture layer crystallization temperature up to 500 °C comparing with 250 °C for pure TiO_2 layer [142]. Phase diagram for annealed TiO_2- SiO_2 mixture films is presented in Fig. 9.

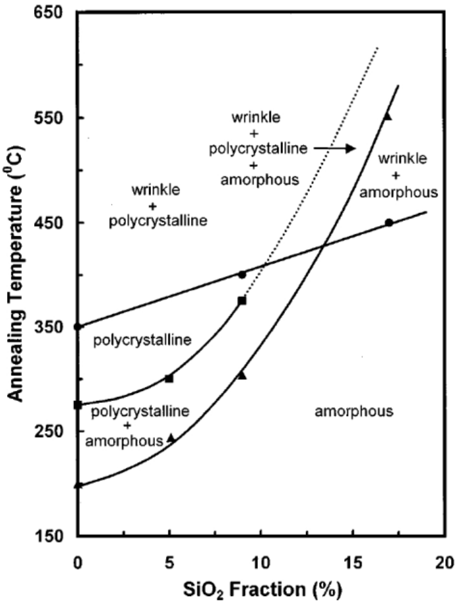

Fig. 9. Phase diagram for annealed TiO_2-SiO_2 mixture films [142].

Lee et al demonstrated increase of crystallization temperature for sputtered TiO_2 mixture by admixing Ta_2O_5 material [143]. Composite of 79%ZrO_2-21%SiO_2, deposited by EBE, exhibited amorphous structure, while pure ZrO_2 layers had mixed monoclinic and tetragonal phases [140]. This study also demonstrated that adding silica helped to increase film density, refractive index, its refractive index stability, also decreased surface roughness and scatter losses.

Material mixtures could also be successfully applied while solving stress compensation issues for multilayer coatings. IBS deposited SiO_2 films exhibits high compressive stress, while most high refractive index materials like Nb_2O_5, Ta_2O_5 and others have smaller compressive stress. These stresses can be suppressed by thermal annealing. However, for SiO_2 films, stress remains compressive even after treatment to 500 °C. Study of Kičas et al has demonstrated successful application of using 8%Nb_2O_5+92%SiO_2 mixture as a low refractive index and 93%Nb_2O_5+7%SiO_2 as a high refractive index material for achieving stress compensated dielectric mirror applying selected thermal annealing (Fig. 10) [144].

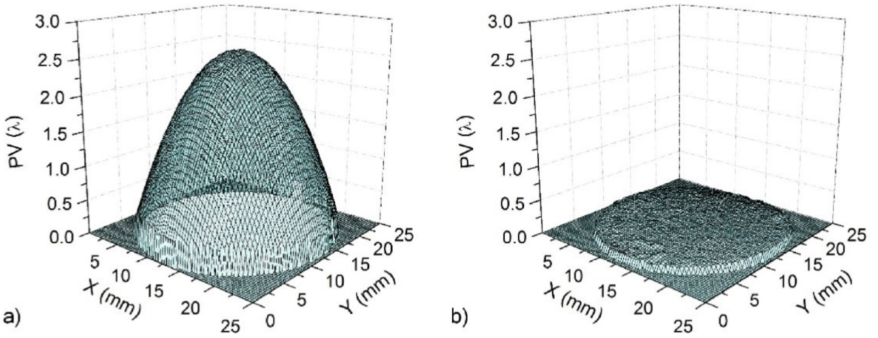

Fig. 10. Surface of deposited mirror (a) and annealed mirror (b), based on Nb_2O_5- SiO_2 mixture materials [144].

Demonstrated mixture approach is suitable for optical coatings used in visible-near infrared spectral range applications. However, niobium oxide is strongly absorbing below ~ 400 nm, so other possible oxide mixtures and optimized annealing temperatures should be identified for development of stress compensated multilayer coatings for UV spectral range. This task is addressed by the thesis in subsection 3.3.

1.5 Optical resistance of dielectric coatings

Laser induced damage of optical coatings was always very active research area. The first studies of dielectric film damage threshold were carried out already in 1965. The maximum achievable power output by laser is usually limited by its optical components (windows, beam splitters, mirrors, output couplers, polarizers, etc.), which are usually coated with interference coatings. Annual Laser Damage symposium in Boulder, USA by SPIE (Society of Photographic Instrumentation Engineers), including annual competitions for LIDT of different coatings, laser pulse duration and other requirements, clearly illustrates importance of optical resistance issue. Complexity of this problem could be illustrated by big scatter of LIDT competition results. LIDTs for 1064 nm HR coatings, based on hafnia/silica materials, were spread by a factor of 20 in 2008 [145], while values for 355 nm mirrors - by factor of ~15 in 2017 [85]. Optical resistance of multilayer coating comprises many different aspects, starting from material science and finishing with the engineering of thin film deposition process.

Fig. 11 shows main processes, phenomena and final outcome of laser damage process [146].

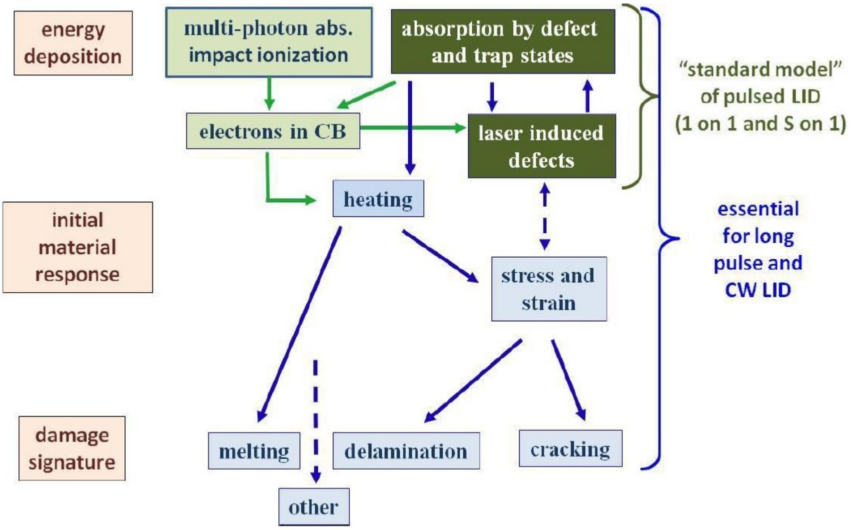

Fig. 11. Processes and phenomena in laser damage of optical materials [146].

Damage process starts from energy deposition within the coating. There are several processes, which couple laser energy into the film – avalanche ionization, multiphoton ionization, tunneling ionization, absorption by impurities. During avalanche ionization, if electron in the conduction band absorbs enough energy, it could ionize additional valence electron. The process could continue and the number of electrons in the conduction band grows exponentially. In this way, absorbing plasma is formed, laser energy is absorbed and damage of the coating occurs. For multiphoton ionization case, electrons move from valence to the conduction band by direct absorption of two or more photons. Material bandgap and laser wavelength defines number of photons, which should be absorbed by valence electron to get to the conduction band. Wider bandgap needs more photons to be absorbed, however, photons of shorter laser wavelengths possess higher energies.

Various defects can also absorb laser pulse energy. On the other hand, pulse train itself could also create defects within the material. These processes induce heating of the material, which could lead to melting or dramatically increased local stress. Finally, coating at the exposed area is damaged. It could melt, delaminate or crack.

1.5.1 Current model of pulsed laser damage

Fig. 12, left part demonstrates main processes involved in laser damage induced by subpicosecond pulses and right part – by longer pulses.

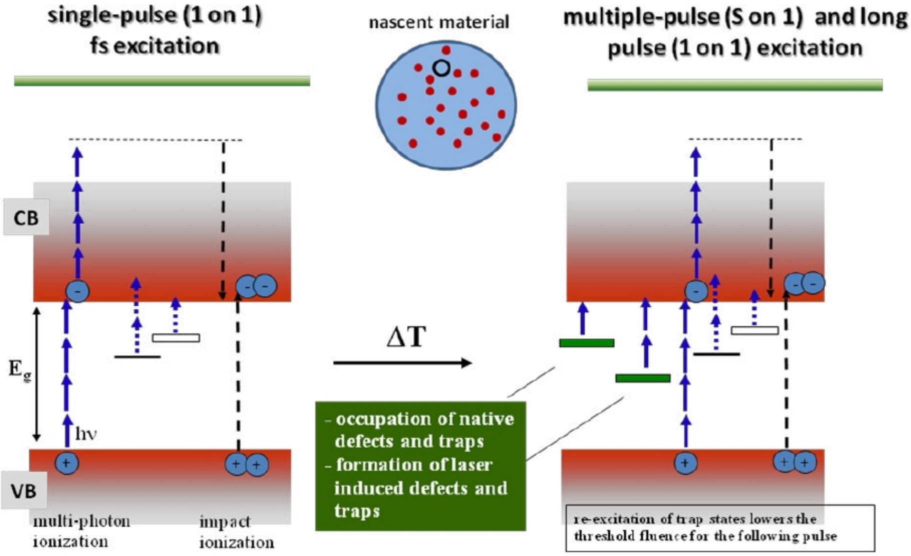

Fig. 12. Processes, involved in laser damage phenomena for different pulse durations and regimes [146].

For short pulse case, electrons are excited to the conduction band (CB) by multi-photon absorption and tunneling. These electrons can further absorb laser energy and when this gain equals band gap energy, resettlement of other valence electrons could occur. Dielectric material suffers breakdown, when CB electron density reaches critical density at which the plasma absorbs all incoming laser energy [147].

Single pulse laser induced damage threshold has a linear dependency on material bandgap for the sub picosecond pulse range:

$$F_{th} = \frac{(c_1 E_{gap} + c_2)\tau_p^{\kappa}}{|F|} \tag{2}$$

Where E_{gap} is bandgap energy, τ_p is pulse duration and F represents the fluency.

Despite many successful investigations of LIDT phenomenon, many important issues still are not addressed, including absent of direct multi-photon absorption coefficient measurements, neglect of band structure, amorphous character of films, etc.

1.5.2 Laser damage in UV spectral range

Photon energies at UV spectral range are quite high – 3.49 eV for 355 nm and 4.66 eV for 266 nm. Therefore, multi-photon (two or three-photon) absorptions plays significant role in damage processes of UV coatings. Several important facts were observed in early investigations of LIDT phenomena [148, 149]:

1) Optical resistance decreases with shorter wavelength, since number of smaller particles, which interacts with the laser pulses, increases;
2) Morphology of 266 nm damages for most oxide films are uniform damage area, while for other wavelengths it comprises individual craters.

1.5.3 Main methods for increasing LIDT of optical coatings

During years of investigation of laser induced damage phenomenon, many techniques were suggested and developed. In the following subsections the most important ones will be shortly reviewed.

1.5.3.1 Suppression of coating defects influence

Absorption due to coating defects is the main factor determining optical resistance to nanosecond lasers pulses. Relation between defects and coating's optical resistance was studied for many years [150]. Concept of "defects" here means several types of defects. They could be simply material particles, or nodules, which reach size of several microns. Also defects could be nanometer size metal clusters within dielectric matrix, or defects within material microstructure, resulting in additional energy levels within material bandgap [151]. Nodules could have classic dome shape, which originates from molten particulate ejection and deposition within forming layer or irregular shape, which is the cause of solid source particle ejection [152]. Irregular shape nodules could also be created due to flaking of coating from mechanical parts of coating chamber. Actually, such defects within the coating can suppress potential LIDT in several ways:

1) Directly absorbing incident energy of laser pulse, if these defects are more absorbing, than surrounding layers [153-156].

2) Drastically increasing electric field intensity within the layer structure of the coating. Numerous studies demonstrated, that electric field intensity could be increased by the defects up to 4 times for nanosecond pulses [157]. This leads to much higher temperature and local stress rise within absorbing regions [158]. Electric field enhancement also depends on nodule dielectric

constant, size and depth within the layer stack. Bigger size nodules, located within outer stack layers amplify electric field much more efficiently.

3) Defects themselves usually are much less susceptible to increase of local stress. It means that when stress around the nodule will reach some threshold value, they will be ejected from the coating structure.

There are several techniques, which could be used for minimizing defect density within the finished coating. For EBE case, metals or oxygen-deficient oxides with better melting properties could be used in order to reduce spitting during the material evaporation [159]. Several studies also have demonstrated planarization technique during DIBS coating process, which involves discrete or simultaneous deposition and etching of the material using secondary ion source [160]. Investigation of artificially engineered and then planarized defects during IBS deposition of dielectric mirrors for 1053 nm wavelength demonstrated 5-20 times higher single shot LIDT comparing with unprocessed samples [161]. The increase for 600-shot LIDT was smaller, but still triple improvement was observed [162].

Defect density of IBS coatings is usually several times lower, than for the coatings deposited by TE or EBE [163]. Several studies were dedicated for investigation of point defects within IBS thin film structure. Langston et al have found that the density of oxygen interstitials of Sc_2O_3 films was lower using smaller ion beam voltages and smaller partial oxygen pressure [119]. This study also demonstrated, that difference between point defect density can be up to 10 times, depending on chosen process parameters.

1.5.3.2 Material engineering

Material bandgap is one of the main factors determining LIDT, especially for UV spectral range. Therefore, there were many attempts to use materials having as high bandgap as possible to achieve necessary spectral and other coating characteristics. High refractive index (H) material has smaller bandgap comparing with low refractive index (L) material. Due to this, mixing H and L materials opens new possibilities to obtain composite material with increased bandgap and intermediate refractive index. Several papers have demonstrated increment of multi pulse LIDT for different pulse duration cases. Jupe et al has demonstrated double increase of LIDT for 150 femtosecond pulses using TiO_2-SiO_2 mixture based mirror comparing to pure material case [164]. Possibility to use material mixtures of variable composition also allows to use so called RISED (refractive index steps down) design, where refractive index is constantly reduced for outer coating layers (Fig. 13) [164].

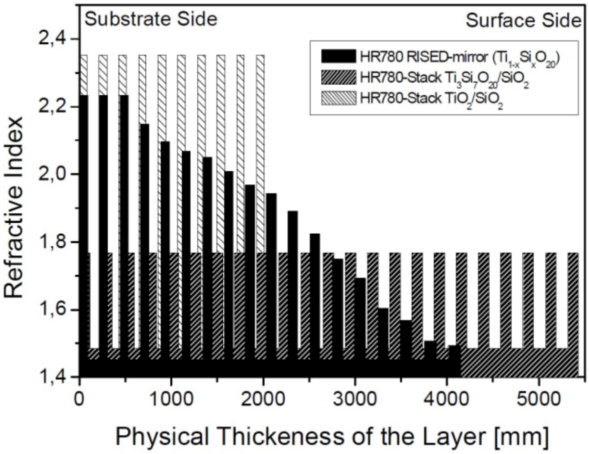

Fig. 13. Refractive index profiles of standard TiO_2/SiO_2, mixture and RISED designs [164].

Success of mixture approach was also proved for nanosecond pulses at UV spectral range. Dielectric and dichroic mirrors for 355 nm, based on HfO_2-SiO_2 mixtures demonstrated 20% - 80% higher LIDT's comparing with pure material coatings [72, 116].

1.5.3.3 Modification of electric field

Thicknesses of coating layers determines electric field intensity distribution of laser radiation within the coating. Classic structure of Bragg mirror, which has all layers of equal optical thicknesses, has maxima of electric field located at layer interfaces. The idea of placing these maxima to the more resistant layers of low refractive index material has emerged already in 1977 [165]. Example of electric field distribution in standard and modified dielectric mirrors is shown in Fig. 14.

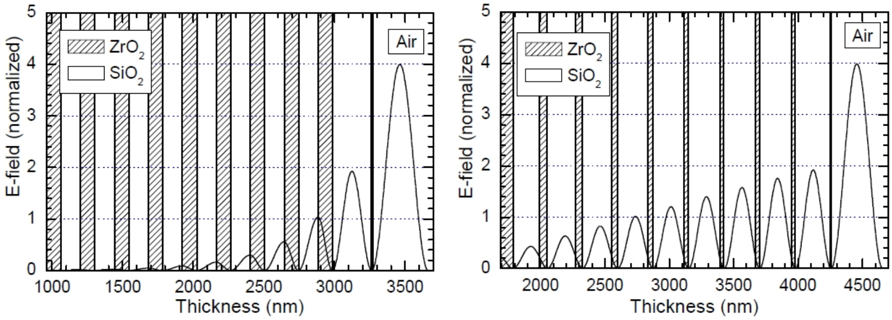

Fig. 14. Electric field intensity distribution within standard and modified layer structures of dielectric mirrors [166].

Optimization of electric field intensity distribution is far more effective method for ultrashort pulse applications, resulting 1.5 - ~2 times increase of LIDT [166]. However, it also helps to improve LIDT of multilayer optical components for ns pulse regime, especially for UV range, where coating material absorption coefficients are higher [167].

1.5.3.4 Post-processing technologies

Laser annealing [168] and conditioning [87, 169-171] also might be used to increase LIDT of deposited optical coatings. During laser annealing, continuous wave (cw) laser radiation is used to reduce coating absorption. Up to 70% of permanent reduction in UV absorption for HfO_2 thin film was registered after 351 nm cw laser annealing, It was proportional to local deposited energy [168]. Within this study, several other interesting phenomena were also revealed: no additional surface modification, indicating that heating of the film produced temperatures below melting point; 25% increase in LIDT (1-on-1 test) was registered for nanosecond pulses and also slight improvement for subpicosecond pulses at 1053 nm. Possible explanation of laser annealing efficiency is depopulating absorbing additional electronic defect-related trap states.

During laser conditioning, optical coating is exposed to smaller laser fluencies than its LIDT. Several conditioning steps could also be used to achieve better results. Different processes take place during this procedure. Gentle nodule ejection from the coating under applied laser exposure is one phenomenon. Another is the improvement of stoichiometry and reduced absorption of exposed area. Laser conditioning could increase LIDT up to 22 times [162].

Thermal annealing is another post-processing method, widely used for improving LIDT properties of deposited coatings. One of the main mechanisms of laser resistance improvements using technique is the repair of stoichiometry [172] of coating material after the deposition, leading to decrease of absorption [173-176]. Increase of LIDT for single EBE hafnia films from 7 J/cm^2 to 13.7 J/cm^2 and for DIBS formed films from 4 J/cm^2 to 9 J/cm^2 at $\lambda = 1064$ nm for single ns laser pulses was demonstrated [175, 176]. Positive effect for multilayer coatings was also shown in several studies. Titania/silica based dielectric mirrors for 1064 nm wavelength had LIDT = 13.1 J/cm^2 after annealing to 400 °C, comparing with LIDT = 5.1 J/cm^2 for as-deposited coatings [177].

1.6 Stress in thin films and optical coatings

Stress in thin films is very important mechanical property, determining its usability, durability and stability. It has been studied since the first investigation of chemically deposited films at 1877. It primarily depends on coating material, deposition process, its parameters like film growth rate, temperature, and on the properties of used substrate. Film stress can be compressive (film expands parallel to the surface) or tensile (film tends to contract parallel to the surface), as it is shown in Fig. 15 [1].

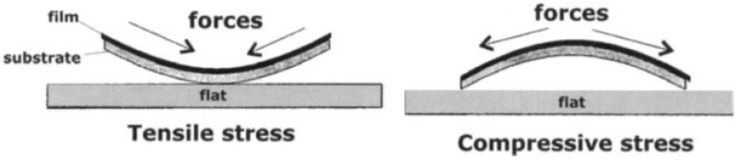

Fig. 15. Stresses in thin films - tensile and compressive [1].

Observed stress consists of three different components:

$$\sigma = \sigma_{ext} + \sigma_{therm} + \sigma_{int} \tag{3}$$

Here σ_{ext} is external stress, which is generated by external forces, σ_{therm} is thermal stress, arising if large difference exists in the thermal expansion coefficients between substrate and film materials. It could occur during deposition process, or during thermal post deposition annealing, for example. Intrinsic film stress σ_{int} is dependent on the film microstructure, and contamination. During growth and possible later annealing of film several processes could happen, which influence stress properties [1]:

- Formation of lattice defects, like lattice disorder, microscopic voids, etc.;
- Differences of the lattice spacing of substrate and film, if epitaxial growth occurs;
- Incorporation of residual or working gas particles, possible chemical reactions;
- Recrystallization processes and phase transformation;
- Changes in the interatomic spacing (emerging of regions of higher and lower density);

Stresses within coated laser optical components are very important, since they affect initial substrate optical surface quality and might lead to degradation of optical component flatness [144] or even its spectral properties

[178, 179]. Deterioration of optical component surface curvature cause optical aberration and pulse wavefront distortion [180]. High compressive stress also could be the reason of coating delamination.

For multilayer coating, total stress is the result of individual layer stresses, weighted by the corresponding thicknesses. The final optical component curvature κ could be written in the following way [181]:

$$\kappa = \frac{6(1-\nu_s)}{E_s h_s^2}[\sigma_1 h_1 + \sigma_2 h_2 + \cdots + \sigma_n h_n] \tag{4}$$

where ν_s is the Poisson ration, E_s the Young's modulus, and h_s substrate thickness.

In the following subsections, main stress mechanisms will be overviewed shortly. In addition, main techniques for its suppression will be discussed, concentrating on films and coatings, deposited by ion beam sputtering technology.

1.6.1 Intrinsic stress mechanisms

Broad variety in experimental results as well as limited knowledge of structural details led to multiple stress models. These usually depend on the kinetic energy of condensing particles.

In evaporation case, incident particles have small kinetic energy. This results in a film, which has voids and consists of columnar microstructure. The origin of its observed tensile stresses could be explained by grain boundary model [182]. Here, column interaction is treated in the same way, like grain interplay in polycrystalline films. Growing columns attract each other, which are counterbalanced by adhesion forces to the substrate surface. It was shown, that elastic strain here is inversely proportional to the final grain size, so large column sizes are associated with low stresses, and small column sizes – with large tensile stresses. It also should be mentioned, that in case of additional thickness growth, recrystallization of the film can occur, resulting in large decrease of the stress.

Thin films, which are formed under conditions that are more energetic, like ion/plasma assisted deposition or sputtering processes, have much higher atom mobility. Energies of condensing particles in this case could reach ~10 eV, which is hundreds times more, comparing to evaporation process. Final film structure has much less voids and achieves density, close to the bulk. Such coatings possess stress, which could be from small tensile to highly compressive. Transition region is dependent on the energy of energetic particles and their ratio to condensing atoms [183, 184]. For highly energetic processes like magnetron sputtering or ion beam sputtering, highly compressive stresses are the result of considerably increased atom density within the available volume. Therefore, expanding forces appear within the film, which result in compressive stress. This mechanism of compressive stress generation is so called atomic “peening” [185-187].

1.6.2 Main stress engineering techniques for IBS coatings

Ion beam sputtered coatings have high compressive stresses [188-190]. There are several in-situ and ex-situ techniques for reducing or even compensating this stress. Modification of IBS process, introducing additional ion assistance – so called DIBS (dual ion beam sputtering) process [191] or changing IBS process parameters allows modifying the stress. It was demonstrated, that bombarding of growing Nb_2O_5 layer by argon and oxygen ion mixture having 550 eV energy has decreased compressive stress from ~230 MPa to ~120 MPa [77]. Another study showed, that it was possible to change stress considerably by using different process parameter values, like partial oxygen pressure, voltage of primary ion source or substrate temperature [114, 119].

Some post-deposition techniques, like thermal treatment, could also be used effectively to reduce or eliminate high compressive stresses [74, 82, 83, 135]. Drawback of this method is that it could not be applied to temperature sensitive substrates. Thermal annealing could also induce crystallization of some materials and respectively – increase roughness and optical scatter loss [142, 192]. Another way for stress reduction involves deposition of additional back coating (usually SiO_2 layer) of necessary thickness after already deposited front side coating. Shortcoming of this approach is that additional coating process is necessary. Both ex-situ techniques are not suitable for compensating stresses if IBS deposition is made on very thin (sub-millimeter) thickness substrates. If thick multilayer coatings are deposited, substrate could be broken down during the process.

One more method to manipulate the stress in IBS optical coatings is to use material mixtures [144, 193, 194]. Material mixture approach also attracted attention of researchers during past decades, because of other benefits like tailoring index of refraction, reducing optical losses, tuning band gap and increasing laser damage performance, which was already described in section 1.4.

2 EXPERIMENTAL TECHNIQUES

2.1 Preparation of experimental samples

2.1.1 Substrate cleaning

Experimental fused silica substrates were cleaned by ultrasonic cleaning machine UCS40 (Optimal Technologies). Typical cleaning procedure consisted of four stages: ultrasonic cleaning in alkali solution for 5 minutes; ultrasonic rinsing in water; then 5 minutes rinsing in deionized water; 5 minutes drying in hot 60 °C temperature air.

2.1.2 Plasma etching of FS substrates

Plasma etching was performed using two different RF plasma sources: PSC 301 (Evatec AG) and IS 300 (CCR GmbH) [195]. PSC 301 has capacitive coupled plasma generation using RF voltage. Plasma density is enhanced with the usage of magnetic fields by coils. It has maximum RF power of 3000 W, ion energy could be changed within range of 100 – 1000 eV, inert or reactive gas could be used. IS 300 plasma source has inductively coupled RF (frequency 13.56 MHz) power to the plasma through a matching network. It has maximum RF power of 3000 W. Beam of the source is quasi-neutral; it contains the same number of ions and electrons. IS 300 achieves high dissociation degree close to 100% of used molecular gasses while it is not dependent on RF power. Ion energy might be chosen in the range of 80-250 eV and is not influenced by RF power, while ion current density is linearly dependent by RF power, and has range of 0.8-1.5 mA/cm^2.

2.1.3 Deposition of samples. Sample annealing.

IBS deposition of experimental films and coatings was performed using ion beam sputtering system IBS-LAB (Cutting Edge Coatings GmbH) (Fig. 16 a).

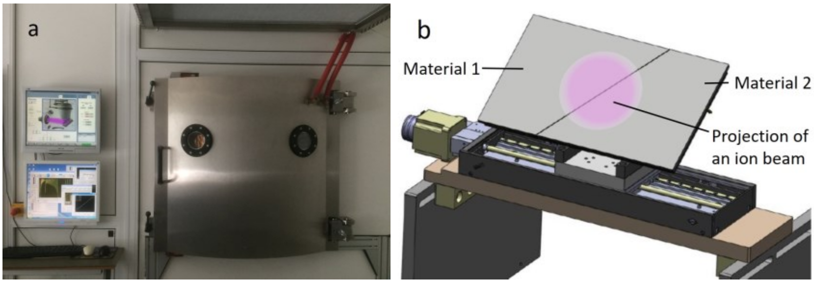

Fig. 16. IBS-Lab sputtering system at FTMC (a). Two material zone target (b) (adapted from [196]).

Initial coating chamber pumping is performed by dry mechanical pump. Installed cryogenic pump allows reaching ~10^{-6} mbar base vacuum. System is equipped with RF plasma source generating Ar^+ ions which are accelerated and extracted to the chamber using three grid system. Two material zone target is installed in the chamber, allowing sputtering of pure material or material mixtures of controlled ratio by moving target regarding to ion beam position (Fig. 16 b). Sputtering targets, used for all experiments are pure metals. To ensure neutralization of ion beam, neutralizer is installed into system chamber and emits electrons. Additional oxygen gas is introduced during the process to ensure oxidation of forming layer during the process. Broadband spectrum control system (range 380 nm – 1600 nm) working in transmittance mode is installed into the chamber. During each rotation of palette, transmittance spectrum of selected test FS sample is measured. Control software constantly fits measured spectrum using optical constants of depositing materials. In such a way, physical thickness of forming layer is determined. All deposition process is performed automatically and layers are terminated when their determined physical thickness reaches values of coating design.

Main operating parameters of IBS system, used for the experiments are summarized in Table 1.

Table 1. Main IBS process parameters used for depositing experimental films and coatings

Parameter	Value
Base pressure	~10^{-3} Pa
Target angle	56-58 deg
Accelerating voltage of primary ion source	1150-1250 V
Focusing voltage of primary ion source	300-350 V
Radio Frequency power	130-140 W
Flow of Ar gas	11 sccm
Flow of background oxygen gas	10-50 sccm
Rotation speed of substrate holder	30 rpm

Deposited thin films and multilayer coatings were also post-annealed using heating furnace SNOL 13/1100 (Umega Group). Annealing procedure consisted of constant heating to target temperature at the rate of 1 °C/min, then keeping target temperature for 60 mins and then cooling down.

2.2 Optical analysis techniques

Optical measurements were performed using spectrophotometer and in-house cavity-ring-down measurement set-up.

2.2.1 Spectrophotometric measurements. Modelling of optical constants

Transmittance measurements of experimental samples were performed using Lambda 950 spectrophotometer (Perkin Elmer). Most of the measurements were done using spectral bandwidth of 1 nm at spectral range of 190 – 1100 nm and for AOI = 0° incident angle.

Single layer transmittance spectra were used for modelling of deposited film optical constants – refractive index, extinction coefficient and layer thickness. Commercial software OptiChar v.8.85 was used for this purpose. This software allows to model dispersion of refractive index and extinction coefficients using selected different models. Program algorithm generates synthetic spectra and compares it to measured spectrum using optimization procedures in order to find the best match. All pure materials and their mixtures in this work were characterized using Cauchy model for refractive index:

$$n(\lambda) = A_1 + \frac{A_2}{\lambda^2} + \frac{A_3}{\lambda^4} \tag{5}$$

where λ is wavelength, n – refractive index, A_1, A_2 and A_3 – coefficients.

Extinction was modelled employing exponential model:

$$\kappa(\lambda) = B_1 \mathrm{e}^{(\frac{B_2}{\lambda} + B_3\lambda)} \tag{6}$$

2.2.2 Cavity-ring-down measurements

Cavity-ring-down technique is used for very low optical loss determination in liquids, bulk materials and thin films. The principle of CRD is trapping of laser pulse in a cavity. In this way, transmitted intensity decreases with time constant τ:

$$\tau = \frac{L}{c((1 - R)} \tag{7}$$

Here, c denotes the speed of light, L is the length of cavity, R is the geometric mean of the reflectivity of all cavity mirrors. The fourth harmonic Nd:YAG laser (Ekspla Co.) generating pulses of repetition rate 15 Hz, pulse duration ~2.2 ns at 266 nm was used for making “in-house” CRD set-up at Optical Coatings Laboratory, in a similar manner as described in [185]. The signal time-decay data from the oscilloscope was used to calculate sample mirror reflectivity. Two identical plano-concave mirrors with a diameter of 25.4 mm and a radius of curvature $r = 1370$ mm were chosen as references in combination with sample HR coatings. Reference mirrors were initially calibrated in the cavity. Their calculated reflectance values were obtained 98.98 ± 0.02% and 98.94 ± 0.02% respectively.

2.2.3 Optical inspection of laser damaged sites

Damaged sites of the coatings were analyzed by optical microscope Olympus BX and Nikon Eclipse LV100 in bright and dark field modes. Different magnification (20x and 50x) objectives were used.

2.3 Analysis of structural, mechanical and LIDT properties

2.3.1 Laser induced damage threshold measurements

Laser induced damage is an irreversible modification of the surface or bulk characteristics of the specimen. LIDT is the energy density of certain duration pulses, which optical component could withstand without suffering the damage. LIDT of experimental samples in this work was measured according to so-called 1-on-1 test. In this case, place in the tested surface is exposed by a single laser shot. Tests were done according to slightly modified method described in ISO 21254-1 procedure [197] with micro-focusing approach, resulting in laser beam spot diameter of ~ 60 µm for 355 nm pulses and ~ 50 µm for 266 nm pulses. LIDT system, which was used for measurements was developed in Optical Coating Laboratory (OCL) at FTMC and is showed in Fig. 17.

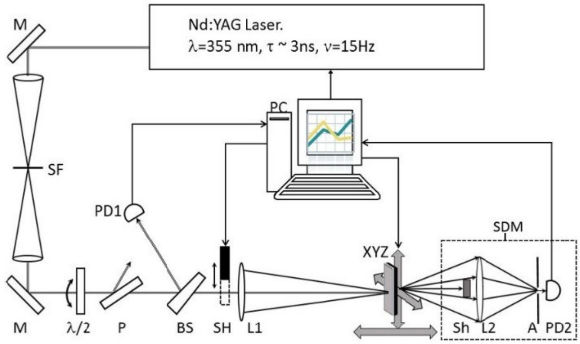

Fig. 17. LIDT in-house system, developed in OCL at FTMC. M – mirrors, PC – control computer, SF – space filter, PD1 – incident beam energy registration photodiode, $\lambda/2$ – phase plate, P – polarizer, BS – beam splitter, SH – beam shutter, L1 – focusing lens, XYZ – motorized sample holder, SDM – scattering detection module: Sh – direct beam path shield, L2 – scattered light collecting lens, A – aperture, PD2 – scattered light registration photodiode.

The third and the fourth harmonic of pulsed (frequency 15 Hz) nanosecond Nd:YAG laser (Ekspla Co.) with one longitudinal mode and Gaussian temporal form was used for LIDT measurements. The space filter (SF) was applied and Gaussian beam shape was formed with pulse duration of ~2.5-3.0 ns. Attenuator, consisting of $\lambda/2$ phase plate and polarizer allowed to change pulse energy without influence to pulse duration, beam shape, etc. Automated program has controlled X-Y direction of motorized sample holder, operated shutter and collected incident and scattered energy data of each pulse. Manual rotating of $\lambda/2$ phase plate allowed control of energy fluency at focused area in wide interval. Calibrated energy meter was used to calculate laser beam energy in damaged area. The beam spot diameter was measured by "knife" method using the same X-Y motorized sample holder with submicron step scanning.

During measurement procedure, several matrices of 144 laser shots using different fluencies were made. Inspection by optical microscope then was performed in dark field mode, and damaged areas were identified. Using obtained data, laser induced damage probability points were calculated, and laser induced damage threshold was determined, where the damage probability of the tested component was zero. Measurement error of LIDT was evaluated to be 10%.

2.3.2 Atomic force microscopy measurements

Surface roughness evaluation of experimental samples was performed using atomic force microscope "Dimension Edge" (Bruker) scans. The AFM probe was used in tapping mode at the resonant frequency. During this process, Van de Waals attractive, short range Coulomb repulsive forces are present, therefore amplitude of the oscillating probe changes according to the surface morphology. Surface roughness was evaluated using term root mean square (RMS):

$$R_q = \sqrt{\frac{1}{N}\sum_{i=1}^{N}(Z_i - Z_{ave})^2} \tag{8}$$

here N is the number of measured surface points, Z_i is the height of i^{th} surface point, Z_{ave} is the average height. Five different surface places of 20 µm × 20 µm size were scanned of each experimental sample to obtain average RMS value.

AFM measurements also were carried out for measuring depth of damaged places of dielectric experimental mirrors. In this case, profiles of measured area scans were analyzed in three different directions, and average depth value was calculated.

2.3.3 X-ray diffraction measurements

XRD analysis of coatings was done collaborating with Department of Characterization of Materials Structure at FTMC. Microstructural properties of experimental coatings were investigated using X-ray diffractometer Smart Lab (Rigaku) equipped with 9 kW rotating Cu anode X-ray tube. Grazing incidence (GIXRD) method was used in 2θ range 20–70°. Phase identification was performed using software package PDXL (Rigaku) and ICDD powder diffraction data-base PDF-4+ (2015 release).

2.3.4 Stress measurements

Residual stress of layers was calculated using Stoney's formula:

$$\sigma = \frac{Et^2}{6(1-\gamma)t_l}\left(\frac{1}{R_1} - \frac{1}{R_0}\right) \tag{9}$$

here E and γ is Young's modulus and Poisson ratio of a substrate, respectively, t and t_l – thickness of substrate, and layer, respectively. R_0 and R_1 are curvature radiuses of uncoated and coated substrate, respectively. For stress evaluation, surface curvatures of the samples were measured in two perpendicular directions by "Dektak 150" profilometer (Veeco), before and after coating process. Layer thickness was determined using modelling of optical parameters, as it was described in 2.2.1 section.

3 RESULTS

The results of the thesis are presented in the following arrangement. Section 3.1 presents and discusses argon and low energy oxygen plasma etching of fused silica substrates, its influence on optical properties and laser damage resistance. In addition, perspectives of plasma treatment technique for development of UV laser damage resistant laser components are examined. Section 3.2 includes investigation of thermal post-deposition treatment of HfO_2-SiO_2 mixture based dielectric mirrors for 266 nm, its influence on coating's microstructural, optical and LIDT properties. Section 3.3 includes high temperature annealing influence analysis on optical, surface and stress properties of HfO_2, Sc_2O_3 and Al_2O_3 binary mixtures, and discuss possibilities of designing stress compensated multilayer coatings for UV spectral range.

3.1 Plasma etching of FS substrates

Fused silica is widely used as a material for production of substrates, which are coated with dielectric coatings in order to make optical components for UV laser beam guidance. Substrate production includes various steps, like grinding, lapping or polishing. These operations create so called Beilby and subsurface damage (SSD) layers, which drastically decrease optical resistance of transparent optical components. This happens due to UV laser radiation absorbing polishing residuals, which are located within Beilby layer and within SSD layer cracks.

Substrate surface treatment using ions or plasma is one of the most promising tools to remove polishing contaminants, since it is non-contact and non-contaminating process, if appropriate process design and parameters are chosen. However, it may also introduce unwanted effects, like surface roughness degradation or additional defects, like lattice distortion, material densification, if high ion energies are used.

Successful removal of absorbing residuals from polished substrate subsurface without sacrificing other important properties is the key factor to develop optical components for UV spectral range with increased laser damage resistance**.**

3.1.1 Argon plasma etching

3.1.1.1 Experimental set-up and design

The first set of polished FS substrates by loose abrasive lapping of the same vendor were etched using Ar plasma in "RADIANCE" sputter cluster platform (Evatec AG), equipped with three magnetron sputter sources and radio frequency (RF) plasma source. Etching procedure was performed at 0.23 Pa argon pressure and using 1 kW of RF power. Substrates were rotated at the rate of 53 rpm. Schematic diagram of plasma etching is shown in Fig. 18. Firstly, calibration procedure was done to estimate etching rate. Three etching procedures on polished FS substrate using the same duration were performed. Then this process was repeated 4 times in 3 days in order to confirm plasma stability and get average values. For evaluation of the etching depth, part of the substrate surface was covered by special mask. In this way, border between etched and non-etched FS surface was created and was measured by profilometer. For every depth determination, 20 scans were done. The maximum measurement error of this technique was evaluated not exceeding 7%. After estimation of etching rate, different surface thicknesses were removed from the FS substrates surface: 20 ± 1.4 nm, 50 ± 3.5 nm, 100 ± 7 nm, 200 ± 14 nm and 400 ± 28 nm.

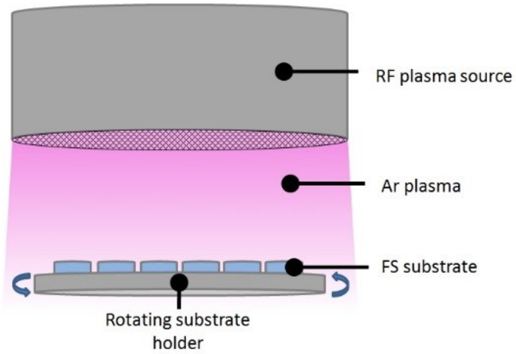

Fig. 18. Scheme of FS substrate Ar plasma etching.

Anti-reflective (AR<0.2%@355 AOI = 0 deg) and polarizing (Pol@355 AOI = 56 deg) coatings for 355 nm wavelength were chosen to deposit on etched and non-etched substrates by the e-beam process. Both coatings has important common feature - almost all laser energy during irradiation goes through the substrate-coating interface. Therefore, etching effect, if positive, should increase coating's LID performance. Reflectance and transmittance spectra of deposited coatings are shown in Fig. 19. EBE of SiO_2 granules and HfO_2 tablets (both from Umicore AG) in O_2 environment was chosen to form selected dielectric coating.

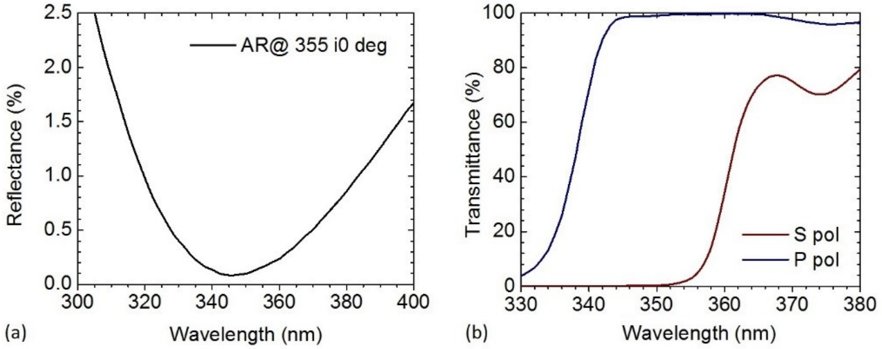

Fig. 19. Reflectance and transmittance spectra of anti-reflective (AR<0.2%@355 AOI = 0 deg) (a) and polarizing (Pol@355 AOI = 56 deg, Tp>95%, Rs>99.5%) (b) coatings deposited on etched and non-etched FS substrates.

The HfO_2 served as high (H) and SiO_2 as low (L) refractive index materials. Both H and L materials had a quarter-wave optical thickness at the reference wavelength of 355 nm, which matches respective physical thicknesses of 43.40 nm (H) and 60.30 nm (L).

Antireflective coating with a layer structure Substrate/0.40H1.29L/Air and polarizing coating with a layer structure Substrate/1.23H0.74L0.93H0.92L0.95H1L(HL)^12_0.77H1.05L0.85H0.68L /Air were deposited. The working pressure and temperature of the substrates were $2 \cdot 10^{-2}$ Pa and 300º C respectively.

3.1.1.2 Optical properties

Optical loss evaluation of etched substrates were performed before coating processes using transmittance measurements. Many authors have noticed significant decrease of transmittance in UV range after exposure to ion flux due to contamination of the surface from filament/grid erosion or other contaminants. Transmittance spectra of FS substrates before and after plasma etching are compared in Fig. 20. Several etching test runs were executed to check for transmittance changes.

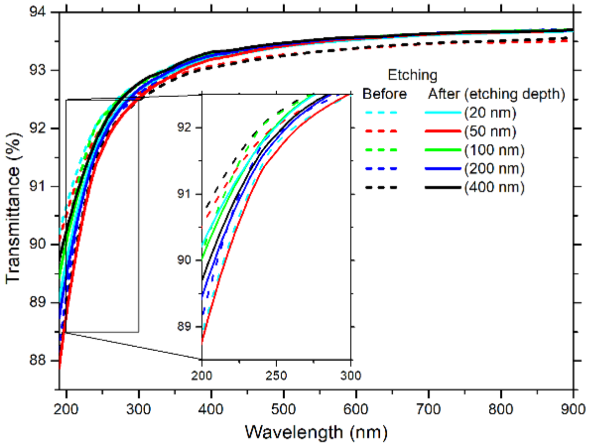

Fig. 20. Comparison of transmittance spectra of individual FS substrates before and after ion etching.

Slightly different transmittances in UV range of non-etched substrates are due to fluctuations of metallic impurities during manufacture process.

Spectrophotometric transmittance measurements have not revealed significant increase of optical loss in etched FS substrates. If there were vanishingly small quantities of photo-absorbing contaminants, for example tungsten (W), which could originate from plasma source grid, this method was not enough sensitive to detect it.

3.1.1.3 Surface and flatness properties

One of the negative side effects of etching smooth and flat surface is degradation of its optical quality, i.e. increasing roughness and decreasing flatness. Comparison of FS surface roughness and flatness values before and after argon plasma etching of different depths is presented in Fig. 21. Measurements have revealed that the roughness of etched samples did not increase comparing to the initial values, within the error margins. Moreover, surface roughness of laser grade optical substrates varied between 0.4 ÷ 0.7 nm (RMS), which is clearly acceptable for laser optics.

Flatness analysis revealed that no significant change in surface flatness after plasma etching procedure occurred.

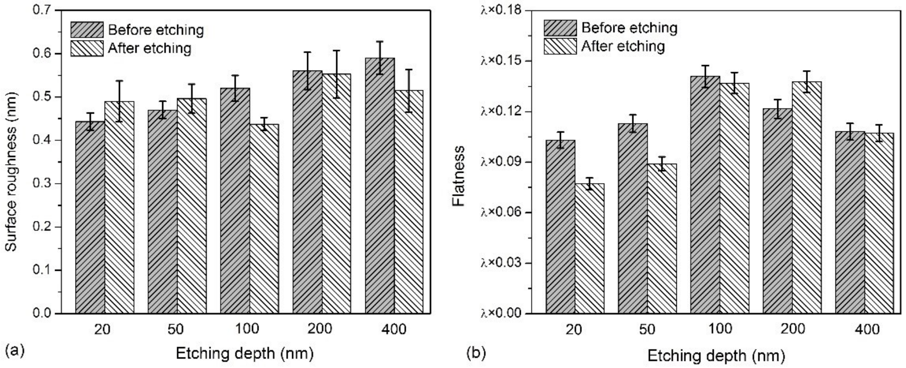

Fig. 21. Comparison of FS surface roughness (a) and flatness (b) values before and after argon plasma etching. Interferometer wavelength $\lambda = 633$ nm.

3.1.1.4 LIDT properties

All etched FS samples had significantly higher (from ~4 to 8 times) laser induced damage threshold than unprocessed ones. Etched to 50 ± 3.5 nm and 100 ± 7 nm depth FS substrates demonstrated the highest laser resistance, resulting in 8 times higher LIDT (1-on-1) for 355 nm wavelength, compared with non-etched ones (Fig. 22). This suggests that the etching depth from around 50 nm to 200 nm, demonstrates the best surface quality (in terms of RMS, flatness, and LIDT). Absolute value of non-etched commercially polished FS substrates varies between 5 J/cm^2 to 22 J/cm^2 and it is dependent on the polishing processes used by different vendors. Due to this, LIDT difference among non-etched and etched substrates can vary as well.

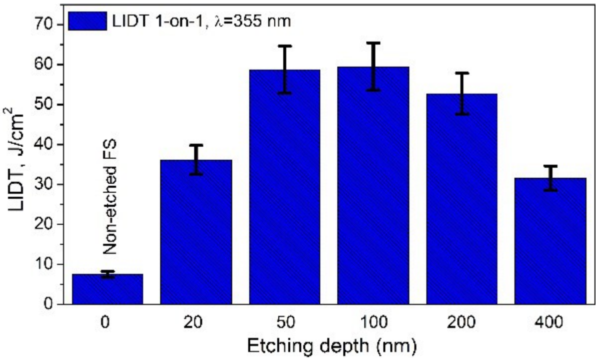

Fig. 22. LIDT comparison of non-etched and argon plasma etched FS substrates.

On the other hand, etching of more than 100 nm resulted in decrease of LIDT. This could be related with increased possible contamination from ion source during longer exposure, because etching of 200 nm and 400 nm took considerably longer (~29 min and ~58 min, respectively), compared to etching the thickness of 100 nm. It is possible to increase etching rate if changing plasma density and energy by increasing RF power. However, etching with considerable higher energy Ar^+ plasma might induce implantation of Ar^+ ions and create additional subsurface defects [198]. In addition, investigation of substrate etching using different operating regimes of this plasma source was not the scope of this thesis.

3.1.1.5 LIDT of etched and coated FS with antireflective and polarizing coatings

Fig. 23 shows measured LID probabilities of antireflective and polarizing coatings, deposited on optimally etched and also on unprocessed FS substrates as well. More than double improvement in optical resistance was registered for both coatings - 2.4 times for AR@ 355 and 2.1 times for Pol@ 355 coating, comparing with similar coatings applied to unprocessed FS substrates.

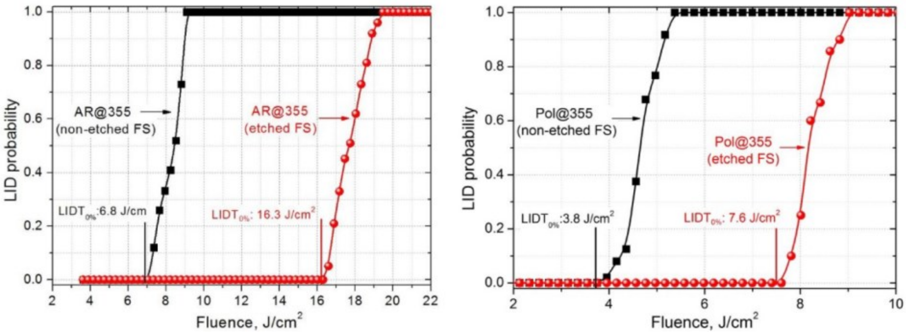

Fig. 23. LID probability curves of AR@355 and Pol@355 coatings, deposited on non-etched and Ar plasma etched substrates.

Characteristic damage morphologies of AR coated components were investigated by optical microscope. From these observations, it is clear that the damage behavior of different samples is significantly different, as shown in Fig. 24.

(a) Increasing laser fluence ⇨

(b)

Fig. 24. Characteristic damage morphologies of non-etched (a) and etched (b) FS substrates, coated with AR@355 coatings. Images at the most left correspond to fluencies slightly above LIDT, while images at the most right correspond to LIDT probability = 1.

The breakdown of AR coatings deposited on non-etched substrates starts from point defects. This phenomenon could be clearly seen while observing sequence of damage sites, exposed with constantly increasing laser fluency. These point defects could be related to polishing particles, embedded within Beilby layer or subsurface damage layer and therefore acting as damage precursors. Damage morphologies of initially etched and then coated FS samples had very few visible point defects. Based on these observations, it may be hypothesized that thermal effects are mostly involved in damage processes of both, etched and non-etched samples due to absorption of laser radiation by these point defects. Bombarding fused silica with Ar^+ ions might still introduce some additional surface damage, by creating atom displacement, and introducing color centers or other lattice defects [198]. Oxygen plasma treatment might be an alternative technique. Moreover, O^+ ions are highly reactive, therefore may also effectively remove organic contaminants [199]. Due to this, low energy oxygen plasma etching of FS substrates was investigated in the next stage.

3.1.2 Oxygen plasma etching

3.1.2.1 Experimental set-up

Another set of FS substrate etching experiment was designed using lower energy (peak below 300 eV) oxygen plasma etching. Experiments were done using radio-frequency (RF) driven Copra IS300 plasma source (CCR Technology GmbH) installed in electron beam deposition plant Vera 1100 (VTD Vakuumtechnik Dresden GmbH). Substrates were placed in the dome at the distance of 40 cm above plasma source extraction grid surface. Etching process was performed without rotation of the substrates. Incident angle of plasma beam to the substrate surface was about 40 deg. Schematic drawing of experimental set-up is shown in Fig. 25.

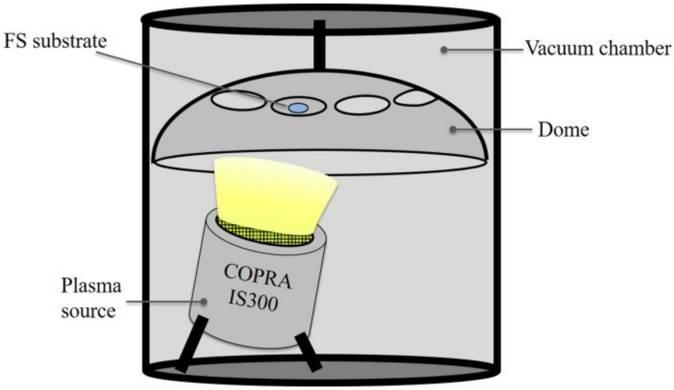

Fig. 25. Schematic drawing of oxygen plasma etching experimental set-up.

Etching depth was evaluated by analyzing surface profile measurement across the border between non-etched (mask covered) and etched substrate area. Each sample was scanned at 3 different places forwards and backwards across the border dividing etched and non-etched zones using profilometer. Average values were used for further analysis. Etching rate was calculated using estimated etching depth and process duration.

Ultrasonic cleaning system was used for substrate cleaning before etching, coating and LIDT measurement procedures.

3.1.2.2 Plasma characterization, etching rates

Plasma ion energy spectra were measured prior to etching experiments using in-house made Faraday cup and are shown in Fig. 26. Faraday cup measures *I-V* characteristics of plasma, which might be differentiated to get plasma ion energy spectrum.

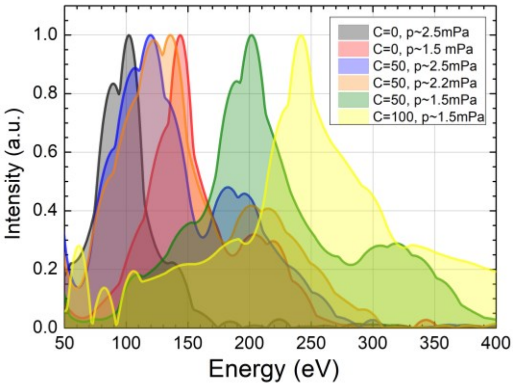

Fig. 26. Measured energy spectra of oxygen plasma using different plasma source parameters

Constant RF = 2500 W power and two different parameters – C parameter (which defines ion energies) and vacuum chamber pressure were varied. Obtained plasma is not mono-energetic, but all spectra have well defined peaks, which positions vary from 100 eV up to 240 eV. Term "plasma ion energy" which is used in further text should be considered as the position of the main peak of plasma energy spectra.

Etching rate for different oxygen plasma ion energies was measured before further experiments of defined etching depths. Fig. 27 shows that obtained etching rate was linearly proportional to plasma ion energy.

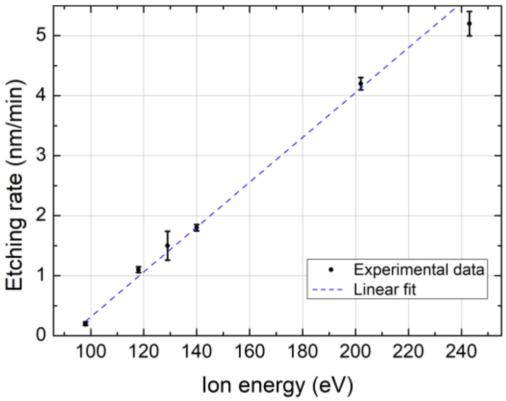

Fig. 27. Etching rate of FS substrate depending on different oxygen plasma ion energies.

3.1.2.3 Surface roughness and LIDT

Several publications have reported negligible amounts of Ce [30] and Fe [25] impurities after removal of more than 100 nm from FS surface. Therefore, initial 250 ± 30 nm thickness was removed using different oxygen plasma ion energies to investigate its possible influence on FS substrate properties.

Measured surface roughness is presented in Fig. 28 (a). Five 20x20 μm size areas at different surface places were scanned for each sample, and averaged values were used for this analysis. It is clear, that FS treatment with oxygen plasma of selected different energies does not change the initial surface smoothness. Fig. 28 (b) shows measured LIDT including non-etched substrate case. Samples treated with 130 eV and 140 eV plasma have demonstrated very high LIDT of 67 ± 3 J/cm^2 and 75 ± 4 J/cm^2 respectively for $\lambda = 355$ nm. These values are very close to the bulk damage values of synthetic fused silica, which in recent research [200] was reported to be 70 - 90 J/cm^2 using 1-on-1 test and 355 nm 9.3 ns pulses. Damage competition of AR coatings for $\lambda = 355$ nm wavelength [201] had revealed the best optical resistance values (raster scanned at 355 nm, 10 Hz, 7.5 ns) of uncoated FS surface not exceeding 50 J/cm^2. Huge improvement in LIDT values over non-etched substrate in this research could be attributed to efficient removal of polishing residuals contamination layer, however further studies including chemical analysis are needed. Etching with more energetic plasma (200 eV, 245 eV) did not provide any optical resistance improvement of the samples. Though process duration was more than 2 times shorter in this case (60 min and 50 min), comparing with 140 eV case, 200 eV and 245 eV energy plasma spectra (Fig. 26) have "tails" of high ion energies (300 – 400 eV). Employing higher energy oxygen plasma could introduce higher sputtering rate of tungsten grid within plasma source. These processes could induce additional contamination on the etched FS surface, which is not possible to remove by standard procedure of ultrasonic cleaning. Another possible mechanism might be implantation of energetic ions, creating defects below the surface [198]. However, more detailed investigations are needed to confirm these hypotheses.

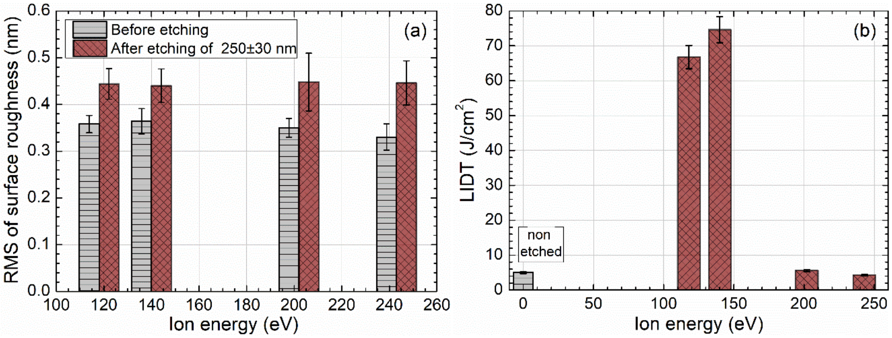

Fig. 28. Surface roughness (a) and LIDT (b) of non-etched and etched FS substrates using different oxygen plasma ion energies.

Possible effect of different etching depths was explored in the next phase of experiments. 140 eV ion energy oxygen plasma, which led to the highest LIDT result in previous set, was used to etch additional depths of 39 ± 4 nm and 543 ± 22 nm. Measured surface roughness values are presented in Fig. 29 (a). No degradation or improvement in surface roughness was registered considering measurement errors. Fig. 29 (b) shows measured LIDT.

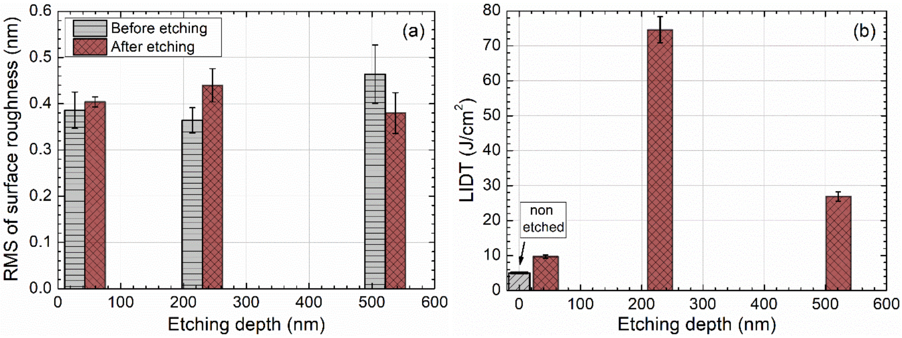

Fig. 29. Surface roughness (a) and LIDT (b) of non-etched and etched FS substrates using 140 eV plasma ion energy and different etching depths.

Removal of 39 ± 4 nm thickness from FS surface has resulted in double increase of damage resistance comparing to non-etched FS sample. The strongest effect was achieved after etching 218 ± 8 nm depth, when LIDT has increased to 75 ± 4 J/cm^2. FS sample with 543 ± 22 nm surface material removal reached 27 ± 1 J/cm^2 LIDT. Etching of just 39 ± 4 nm still could be not enough to remove effectively most of the polishing residuals. Several works support this possible explanation. Shi et al had found significant decrease of polished-induced Fe and Ce contaminants only after etching of 100 nm [40]. Hongjie et al had found 10 times decreased concentration of Fe and Ce after sputtering off the 30 nm thickness of traditional chemo-mechanical polished fused silica sample, but still 100 times smaller concentration was recorded after removal of ~ 60 nm [25]. It is worth to note, that polishing residuals layer thickness could also vary between different substrate manufacturers. It is hard to make direct comparison of obtained 75 ± 4 J/cm^2 result to the other groups, since different LIDT measurement parameters, especially beam diameter, might give different results. Several groups report obtained LIDT of plasma (or ion) etched FS at 355 nm reaching 52.2 J/cm^2 [202], 44 J/cm^2 [37].

3.1.2.4 LIDT of etched and AR coated FS

AR coatings for $\lambda = 355$ nm wavelength were chosen to deposit in order to check low energy oxygen plasma etching effect of coated optical component. Etched (depth of 218 ± 8 nm using 140 eV energy oxygen plasma) and non-etched FS substrates were used in this set of experiments. Two layer design of Al_2O_3 ($d = 52$ nm) and SiO_2 ($d = 58$ nm) layers having reflectance minimum at $\lambda = 355$ nm wavelength was chosen. Coating was deposited using ion beam sputtering coating plant IBS-LAB (Cutting Edge Coatings GmbH). RF generated Ar+ ions sputtered Al/Si zone target. Oxygen gas was introduced into the chamber to ensure oxidation of sputtered aluminum and silicon. Deposited AR coatings were annealed at $T = 300$ °C after the deposition process to complete oxidation and minimize possible absorption losses.

Presented LIDT (1-on-1) of antireflective coatings (Fig. 30) demonstrate the efficiency of plasma etching process. Increase of 3.4 times in LIDT up to 14 ± 0.7 J/cm^2 of plasma treated and AR coated component was recorded.

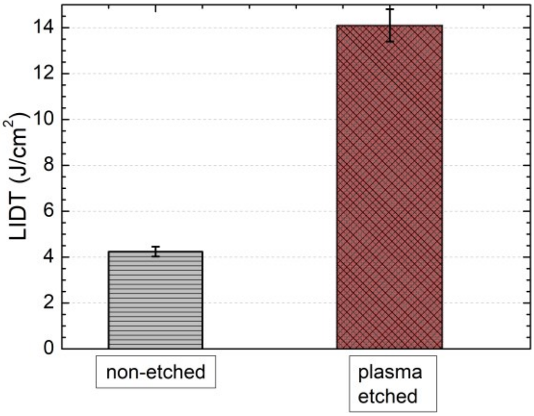

Fig. 30. LIDT of anti-reflective $\lambda = 355$ nm coating deposited on non-etched and oxygen plasma etched (140 eV energy, etching depth $d = 218 \pm 8$ nm) FS substrates.

This improvement is bigger, than Hu et al study [29] reported, where increase of 1.5 times was obtained reaching ~7.2 J/cm^2 (using 8 ns pulses) at 355nm for electron beam evaporated AR coatings on chemically etched FS substrate. Obtained result is also comparable to LIDT of sol-gel coated AR coatings on superpolished and etched FS substrates in study of Li et al, which reported LIDT of 19.5 J/cm^2 using 8 ns pulses [203]. Sol-gel deposition is considered as one of the most efficient coating technologies for production of highly laser damage resistant AR coatings [201]. We believe, that is it possible to achieve even higher optical resistance of AR coated component on plasma etched FS substrate. Careful analysis of our coating process should be performed to identify factors, which limited damage performance of plasma etched and AR coated FS substrates.

3.1.2.5 Damage morphologies

Optical microscope photos of damage site morphologies are presented in Fig. 31. Plasma treated FS substrate case is shown in Fig. 31 (a) and non-etched substrate case – in Fig. 31 (b). Laser energy densities are specified for each damaged site.

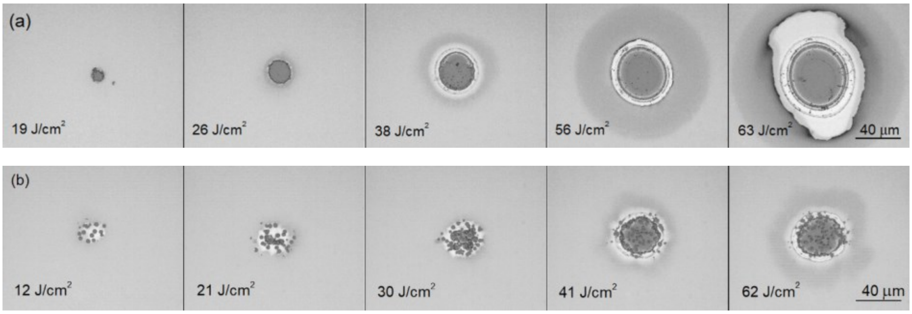

Fig. 31. Damage sites by optical microscope of AR@ 355 nm coatings on etched (a) and non-etched (b) FS substrates.

There is a clear difference in damage morphology of both AR coated components. Laser pulses caused coating layer delamination in etched substrate case, while plasma untreated and AR coated sample suffered multiple pit-like damages, possibly caused by ejection of laser energy absorbing multiple particles.

Fig. 32 shows measured relative distances of damaged sites with respect to coating-substrate interface. Presented values were obtained using AFM scan profile analysis of different laser fluencies damage sites.

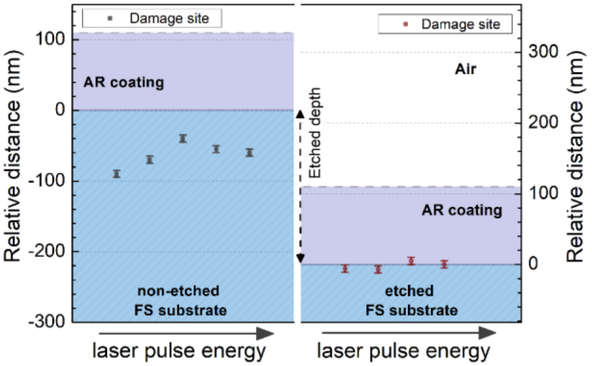

Fig. 32. Comparison of damage site relative distance of AR coated non-etched and etched FS substrates. Coating and substrate interface was considered as a zero level. Laser pulse fluencies of damage sites are increasing from 19 J/cm^2 to 63 J/cm^2 for non-etched substrate case and from 12 J/cm^2 to 62 J/cm^2 for etched case.

Damage was initiated at coating-substrate interface for etched FS case. Non-etched substrate had damages at depths of 40-80 nm below substrate-coating interface, which were caused by existing polishing residuals layer. Recorded damage morphologies by optical microscope and analysis of AFM scan supports evidence of absorbing polishing residuals within thin subsurface layer, which limit the performance of AR coated fused silica. 218 ± 8 nm thickness removal by oxygen plasma etching allowed to increase LIDT of AR coated component 3.4 times.

3.1.2.6 Main results and conclusions

Plasma etching of FS substrates was investigated changing working gas, etching depth and for oxygen plasma case – ion energy. Processing the substrates with argon plasma and removing 50-100 nm depth increased its LIDT 4-8 times without any degradation of optical, surface roughness and flatness properties. Transparent antireflective, also polarizing optical components for $\lambda = 355$ nm were prepared employing optimized FS substrate etching depth, and demonstrated 2.4 and 2.1 increase of LIDT values compared to the coatings of the same deposition process applied on non-etched substrates.

Different low energy oxygen plasma etching was also investigated. Applying 140 eV energy oxygen plasma for etching of 218 ± 8 nm has resulted in the highest 75 ± 4 J/cm^2 LIDT for $\lambda = 355$ nm 3ns laser pulses. Obtained value is close to reported bulk LIDT of fused silica. Surface roughness analysis has shown that application of low energy plasma allowed to preserve initial surface smoothness. Anti-reflective coating for $\lambda = 355$ nm coated on etched FS substrate demonstrated LIDT of 14 ± 0.7 J/cm^2 which was 3.4 times higher comparing with non-etched substrate case.

Inspection of damaged sites has revealed, that not-etched substrate, which was coated with AR coating, suffered ejection and explosion of laser energy absorbing particles, located at the interface of the coating and substrate.

Obtained LIDT improvement demonstrates good possibilities to apply low energy oxygen plasma etching for making high power transparent UV laser optical components.

Results were published in:

- K. Juškevičius, R. Buzelis, **G. Abromavičius** et al., „Argon plasma etching of fused silica substrates for manufacturing high laser damage resistance optical interference coatings,“ Optical Materials Express, **7** (10), 2017.
- **G. Abromavičius**, T. Juodagalvis, R. Buzelis et al., “Oxygen plasma etching of fused silica substrates for high power laser optics”, Applied Surface Science, **453**, 2018.

Also presented in the following conferences:

- **G. Abromavičius**, T. Juodagalvis, R. Buzelis, S. Kičas and R. Drazdys, “Plasma treatment of fused silica substrates for enhancement of resistance to UV laser radiation”, Optical Systems Design, Frankfurt, Germany, 2018.
- **G. Abromavičius**, T. Juodagalvis, R. Buzelis, S. Kičas and R. Drazdys, “Lydyto kvarco optinių pagrindukų ėsdinimo deguonies plazma taikymas formuojant didelės galios lazeriams skirtus optinius komponentus”, Fizinių ir technologijos mokslų tarpdalykiniai tyrimai, Vilnius, Lithuania, 2018.

3.2 HfO_2-SiO_2 mixture based HR coatings

Hafnium oxide is one the most widely used high refractive index materials for development of laser damage resistant optical components for high power UV laser systems. High bandgap (5.6-6.2 eV) is one of the main reasons, which makes HfO_2 so important. Despite this attribute, bandgap could be even more increased, if mixing hafnia with silica. Several investigations already demonstrated high potential of HfO_2-SiO_2 mixture application, resulting in ~70-100% LIDT increase for 355 nm laser ns pulses of multilayer stacks.

There are also various post-deposition treatment methods, such as thermal annealing, oxygen plasma treatment, laser conditioning, which also might help to improve LIDT and other important properties like stoichiometry, reflectance, transmittance, stress of coated components. Thermal post-deposition treatment perhaps is one of the most significant and efficient methods, which is used in the industry, because it is efficient, rather simple and cost-effective.

Ion beam sputtered layers usually are amorphous. However, crystallization might be triggered under thermal annealing at selected temperatures, which are dependent on coating material and layer thicknesses. Also, several studies demonstrate, that HfO_2 bandgap is dependent on its microstructure, being higher for crystalline phases and lower for amorphous. There is a lack of data about laser damage resistance in UV spectral range of annealed single hafnia or hafnia-based multilayer stacks above their crystallization temperature. Moreover, previous studies focused on analyzing single hafnia films. In this section effects of high temperature thermal annealing before and after crystallization onset on properties of different pure hafnia and hafnia-silica mixture-based dielectric mirrors for $\lambda = 266$ nm wavelength are presented. Optical, microstructural, surface properties of high reflectance (HR) coatings are analyzed and discussed, focusing on LIDT properties, which are usually the ultimate goal for HfO_2 and SiO_2 based multilayer stacks.

3.2.1 Experimental set-up

Ion beam sputtering (IBS) coating plant from Cutting Edge Coatings was used for all depositions. Hf and Si zone target was sputtered by Ar^+ ions. Oxygen gas was introduced into the chamber to ensure oxidation of forming layers. No additional substrate heating was used. HfO_2-SiO_2 mixture layers were formed by sputtering intersection zone of two materials at defined target position. Zone target calibration was performed using initial single mixture layer depositions. Mixtures having 82% and 46% content of hafnia as high refractive index materials were chosen for preparing experimental HR coatings. SiO_2 was used as a low refractive index material. It is assumed, that modelling of transmittance spectra using OptiChar could result roughly in 2-3% accuracy of HfO_2 fraction determination within the mixture (for the sake of clarity, in the further text, fractions without stated accuracy will be used). Experimental coatings were deposited on not-etched fused silica substrates of 25.4mm diameter and 5mm thickness. Samples were annealed using heating furnace. $R > 99\%$ at $\lambda = 266$ nm was selected as a target for coating designs.

Other design properties are summarized in Table 2. H and L denotes optical thickness of quarter wavelength at $\lambda = 266$ nm for high and low refractive index material layer, correspondingly.

Table 2. Main properties of experimental mirror designs

Sample name	H material	L material	Structure	Physical thickness of H layer (nm)	Physical thickness of L layer (nm)
Hf_100%	HfO_2	SiO_2	(HL)^12L	29	44
Hf_82%	82%HfO_2+18%SiO_2	SiO_2	(HL)^16L	32	44
Hf_46%	46%HfO_2+54%SiO_2	SiO_2	(HL)^23L	37	44

Initial experiments were dedicated to find annealing temperature enabling crystallization of each different HR coating. As-deposited samples were heated up and kept for 1 h at a target temperature. $T = 300$ °C was chosen as a starting target value. It was gradually increased by 100 °C increments in further annealing tests. Due to different hafnium oxide fractions within the high refractive index material layers, they underwent crystallization at different temperatures. These temperatures further will be denoted as “T_c”. However, one should keep in mind that these were not accurate crystallization temperatures and crystallization appeared within T_c−100 °C and T_c range. After initial set of annealing experiments, three sets of samples were annealed at three different temperatures: T_c−200 °C; T_c and T_c+100 °C. Exact annealing temperature values were different for each coating case and are presented in (Table 3).

Table 3. Selected annealing temperatures of mirror coatings

Sample name	T_c−200 °C	T_c	T_c +100 °C
Hf_100%	400	600	700
Hf_82%	700	900	1000
Hf_46%	800	1000	1100

3.2.2 Microstructural and surface properties

Scatter properties of multilayer coatings can be affected by grain size, crystallinity and surface roughness [204]. XRD spectra of experimental mirrors are shown in Fig. 33. All as-deposited coatings were amorphous.

Annealed to $T = 600$ °C pure hafnia based samples demonstrated crystalline phase of cubic hafnia having cell edges $a = b = c = 0.5$ nm and angles $\alpha = \beta = \gamma = 90°$. Considerably higher temperatures ($T = 900$ °C for Hf_82% and $T = 1000$ °C for Hf_46% mirror) were necessary to get onset of crystallization for hafnia-silica mixture-based mirrors. Hafnia based coatings demonstrated different crystalline phase while comparing to the most other research. Pure monoclinic phase of ion beam sputtered hafnia was reported in several works [82, 116, 173]. For different coating technologies pure monoclinic [205-207] or mixed phase [208, 209] of monoclinic and cubic hafnia phase was registered.

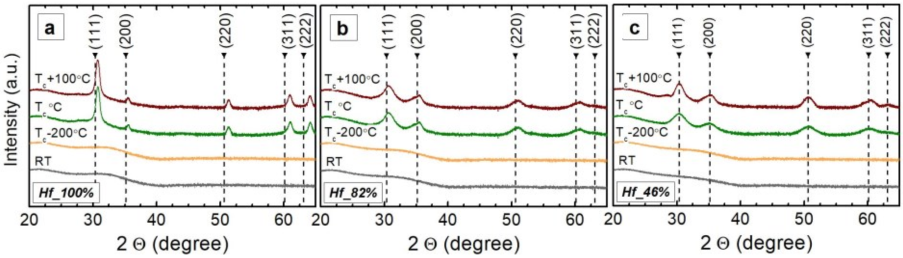

Fig. 33. XRD spectra of deposited (RT) and annealed HR coatings (a) – (c). Exact temperature values are presented in Table 3.

Determined crystallite sizes from XRD spectra are shown in Fig. 34.

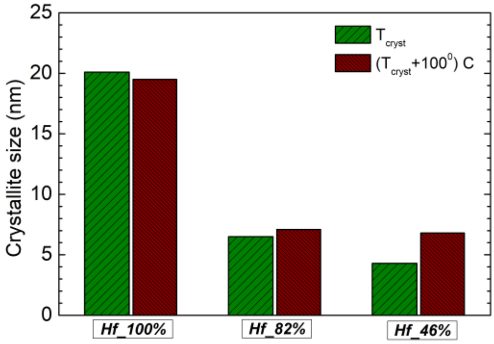

Fig. 34. Crystallite sizes of annealed HR coatings, based on pure hafnia and two different hafnia-silica mixtures as a high refractive index materials. Exact temperature values are presented in Table 3.

Crystallite size of about 20 nm was determined for both T_c and T_c+100 °C annealed Hf_100% coatings. Similar sizes between 14.2 nm [208] and 17 nm [210] are reported in other studies. Presence of silica fraction within hafnia layers strongly suppressed size of formed crystallites within mixture layers of Hf_82% mirror down to 6.8 nm and to 4.3 nm of Hf_46% mirror. Annealing at higher T_c+100 °C temperature increased the crystallite sizes to ~7 nm for both mirrors. Smaller crystallite size of annealed mixture layers is beneficial for UV multilayer coating applications, because it should result in lower bulk scatter. Surface roughness RMS values of all experimental mirrors are shown in Fig. 35 and typical AFM scans of amorphous deposited and polycrystalline annealed coatings are presented in Fig. 36.

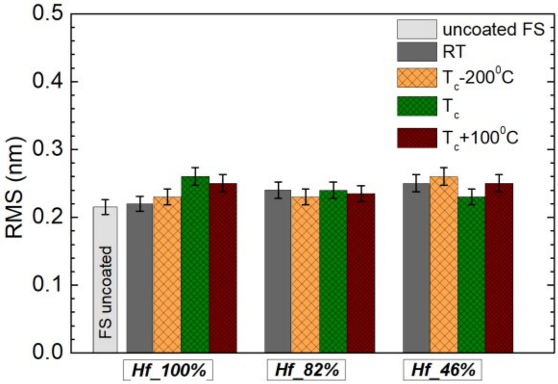

Fig. 35. RMS of deposited (RT) and annealed mirror surface roughness, determined by AFM scans. Exact temperature values are presented in Table 3.

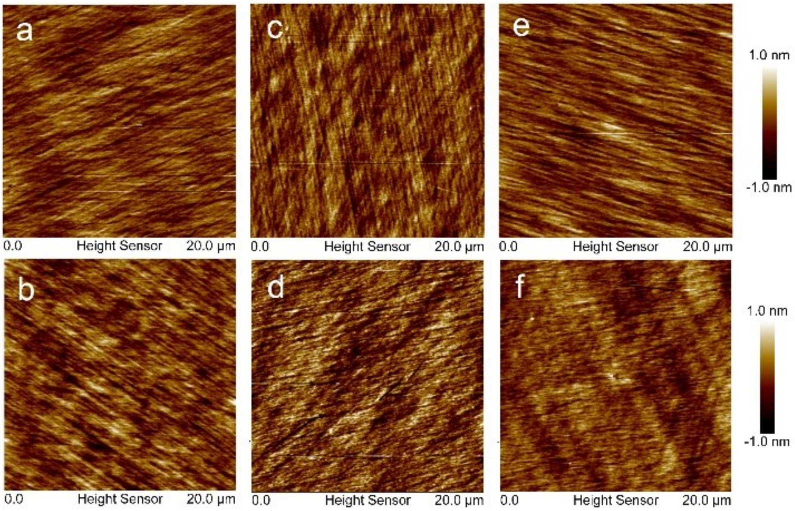

Fig. 36. Surface topography AFM scans of deposited Hf_100% (a), Hf_82% (c), Hf_46% (e), and annealed at T_c Hf_100% (b), Hf_82% (d), Hf_46% (f) coatings. Exact temperature values are presented in Table 3.

None of the annealed coatings showed degradation of initial surface smoothness despite transition from amorphous to polycrystalline phase of high refractive index layers, since all RMS values were within error range.

AFM scans also demonstrate that initial surface texture (polishing traces) is preserved even after crystallization. Initially, these substrates were not etched. Obtained phenomenon might be the result of SiO_2 layer overcoat, which remained amorphous after all thermal treatments of the samples.

3.2.3 Optical properties

Transmittance spectra of experimental mirrors are shown in Fig. 37.

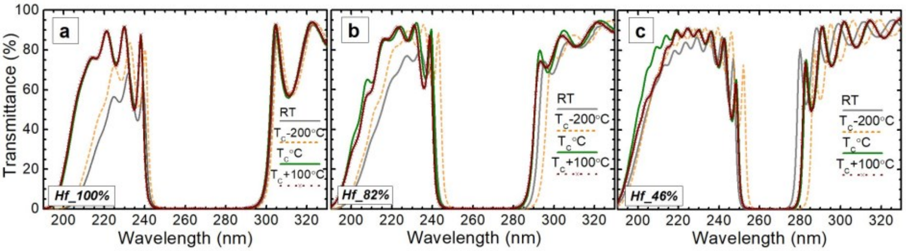

Fig. 37. Transmittance spectra of deposited (RT) and annealed HR coatings Exact annealing temperature values are presented in Table 3.

All coating spectra share similar trends while increasing annealing temperature. Baking the samples to T_c–200 °C already resulted in increase of transmittance at shorter wavelength (~210-230 nm) range. Decreased absorption of deposited coating material due to stoichiometry improvement is the main cause, as it was revealed in several works [82, 172, 177, 211]. All samples annealed to T_c showed rapid increase of UV transmittance at ~200-230 nm range. Hf_100% coating demonstrated the biggest increase from $T = 10\%$ to $T = 70\%$ at $\lambda = 210$ nm after the baking. Extinction coefficient of annealed at 500 °C SiO_2 for $\lambda = 220$ nm is negligible ($k = 2\cdot10^{-4}$) comparing to as-deposited HfO_2 ($k = 2\cdot10^{-2}$). Therefore, the main cause of transmittance increase could be attributed to changes within hafnia or hafnia-silica mixture layers after annealing, respectively. These layers underwent phase transition from amorphous to crystalline cubic phase, resulting in material bandgap increase. Bandgap increase of hafnia thin films after crystallization was reported in several works [206, 208, 209].

Measured reflectance of experimental dielectric mirrors at $\lambda = 266$ nm is shown in Fig. 38.

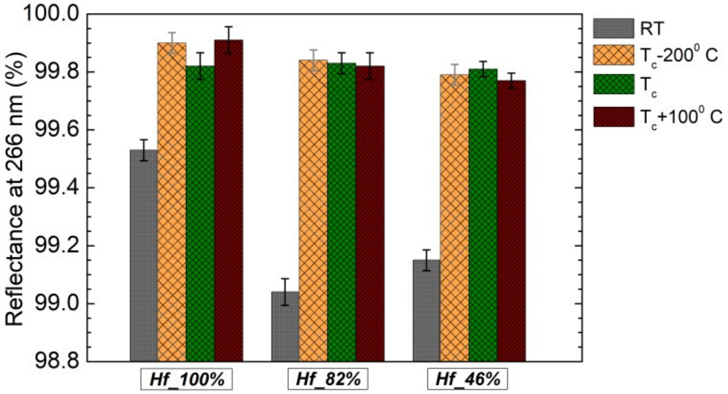

Fig. 38. Reflectance at $\lambda = 266$ nm of deposited (RT) and annealed HR coatings. Exact temperature values are presented in Table 3.

Annealing to T_c−200 °C has increased the reflectance by 0.4% - 0.8% for all 3 different mirror coatings and reached 99.8% - 99.9% values. Decreased absorption of high refractive index material layers within multilayer stack is the main cause of this change. However, remaining losses still consist of scatter and residual absorption. Thermal treatment at higher temperatures T_c and T_c+100 °C did not introduce any reflectance changes. Conservation of reflectance values also imply, that occurred crystallinity within hafnia and hafnia-silica mixture layers did not have considerable impact on scatter properties of these coatings. Another possible explanation might be that induced slight scatter losses were “compensated” by even more reduced absorption after annealing to higher temperatures of T_c and T_c+100 °C. However, additional investigations are needed to clarify this phenomenon. The highest reflectance of 99.91 ± 0.04% at $\lambda = 266$ nm can be obtained by annealing hafnia-based coating at T_c−200 °C.

3.2.4 LIDT properties

Laser induced damage tests (1-on-1) are presented in Fig. 40. Dielectric mirror Hf_46% had the highest optical resistance of 2.0 ± 0.2 J/cm^2 between as-deposited samples due to higher expected bandgap and lower extinction values of 46%HfO_2+54%SiO_2 mixture layers. Several studies also revealed increased damage resistances for single ion beam sputtered mixture layers [141] as well as for multilayer coatings [72, 116]. Similar trend among different coatings remained also using annealing all of them at T_c−200 °C temperatures. Hf_100% coating annealed at T_c showed almost double increase in LIDT from 2.2 ± 0.2 J/cm^2 to 4.3 ± 0.4 J/cm^2. It reached the resistance properties of similarly treated Hf_82% coating. Measured reflectance (Fig.

38) did not indicate any additional absorption decrease after Hf_100% treatment to T_c. Therefore, increased effective bandgap of hafnia layers due to reduction of defect absorption tail after crystallization might be the most probable reason of this considerable LIDT increase. Optical resistance of the other two different hafnia-silica mixture-based mirrors also increased by 20–40% after annealing at T_c. LIDT of coatings, annealed to post-crystallization temperatures T_c+100 °C, remained unchanged within error bars. This could be also related to increased effective bandgap of mixture layer after crystallization, however further studies are needed to obtain better insight about this phenomenon. The highest LIDT of 5.5 ± 0.6 J/cm^2 was measured for Hf_46% coating annealed at T_c+100 °C.

Despite the lack of multiple pulse resistance tests, obtained results demonstrate interesting potential of high temperature annealing above crystallization point of hafnia-silica mixture-based coatings.

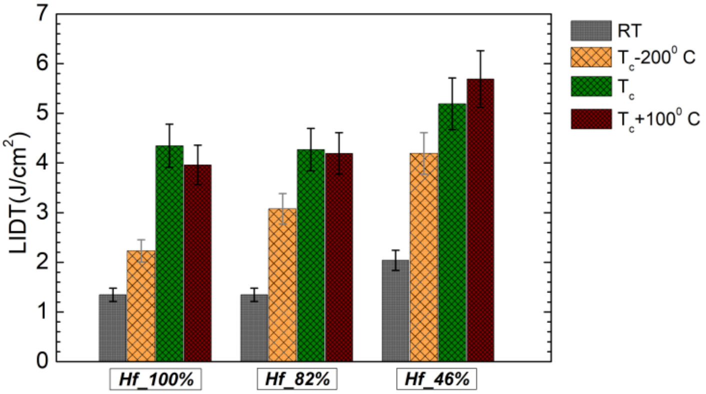

Fig. 39. LIDT (test 1-on-1) at $\lambda = 266$ nm of deposited (RT) and annealed HR coatings. Exact annealing temperature values are presented in Table 3.

3.2.5 Damage morphologies

Damage morphologies of Hf_100% and Hf_46% coatings are presented in Fig. 40. Results of damages using fluencies 4%-7% above threshold values are shown in Fig. 40 pictures a, e, c and g. Craters observed after exposure of the coatings using considerably higher energies (21-29% above LIDT) pulses, are presented in Fig. 40 b, f, d and h. There is a clear distinction between pure hafnia and $46\%HfO_2+54\%SiO_2$ mixture-based coating damage morphologies. Damage of Hf_100% coating was initiated by micron size defects, while for Hf_42% mirror delamination occurred using slightly higher energies than its LIDT. In addition, there are clear differences in morphology between annealed amorphous and annealed polycrystalline version of the same coating if using ~30% higher fluencies. This effect is much more pronounced for Hf_100% mirror case. Surface of damaged amorphous coating crater (Fig. 40b) is smooth while the bottom surface of the crater for crystalline coating shows granular structure (Fig. 40d). Crater bottom of Hf_42% mirror is very smooth, its edge is sharp and defined (Fig. 40f). After crystallization roughness of crater bottom slightly increased and its edge became irregular (Fig. 40h).

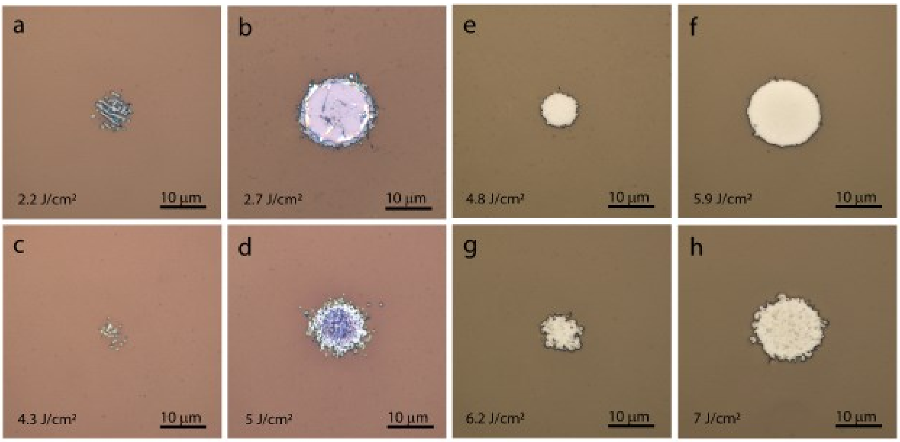

Fig. 40. Damage morphologies for different pulse fluencies of Hf_100% mirror, annealed at T_c-200 °C (a), (b); at T_c (c), (d) and Hf_46% mirror annealed at T_c-200 °C (e), (f); at T_c (g), (h). Exact annealing temperature values are presented in Table 3.

Areas that were damaged by slightly higher (8–10%) pulse fluencies than LIDT were also scanned by AFM in order to measure their depth. Cross section measurements were performed in 3 different directions. In this way, average value of crater depth was evaluated. Fig. 41e shows obtained damage locations within Hf_100% annealed amorphous (short dash line) and annealed polycrystalline (dash line) coatings and normalized electrical field distribution within seven outermost coating layers. Damaged area depths of annealed amorphous Hf_100% mirror coincides with the second interface of HfO_2 and SiO_2, where there is a maximum of the electric field. Observed submicron size separated microcrater morphology indicates, that damage is possibly initiated by nanometric range Hf metal absorbing clusters, as it was discussed in several works [156, 212, 213]. In a similar manner, Hf_42% case is presented in Fig. 41f. Damage morphology of annealed amorphous as well as polycrystalline Hf_42% coatings suggest, that nanocluster absorbers might be absent in this case and layers delaminate around the third SiO_2/HfO_2-SiO_2 mixture interface. This finding is unexpected, since electric field intensity has the minimum here.

At this point, currently there is no possible explanation for this result – understanding this phenomenon requires additional investigation.

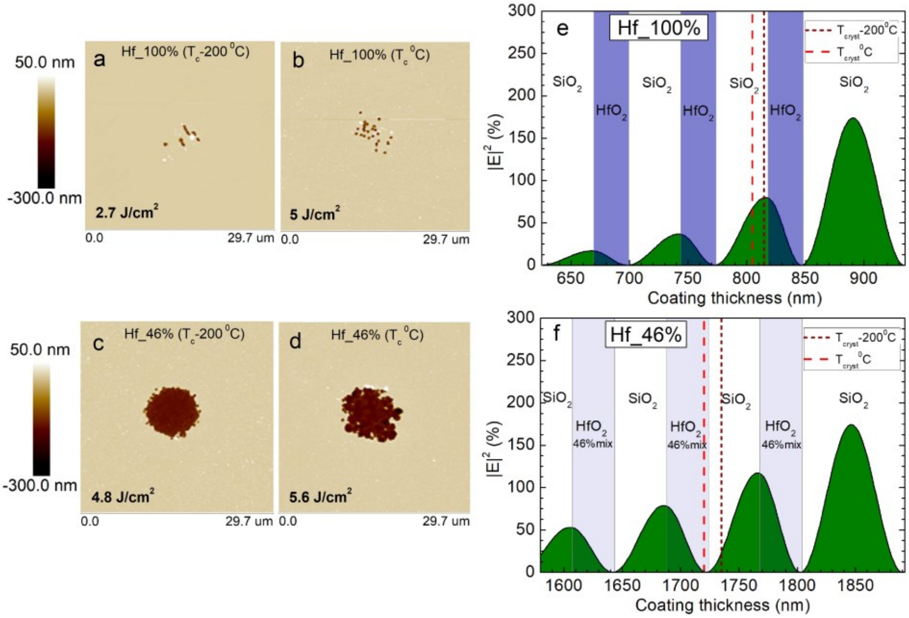

Fig. 41. Damage morphologies of annealed experimental Hf_100% and Hf_46% mirrors exposed by fluencies, which are 7–17% above relevant LIDT. Annealed at T_c-200 °C and amorphous Hf_100% (a), annealed at T_c and polycrystalline Hf_100% (b). Annealed at T_c-200 °C and amorphous Hf_46% (c), annealed at T_c and polycrystalline (d). Schematic drawing of crater depth measurement is presented at (a), low right. Damage locations for Hf_100% annealed amorphous (short dash line) and annealed polycrystalline (dash line) coatings with normalized electrical field distribution within outer coating layers (e). Damage locations for annealed Hf_46% coatings (f). Exact annealing temperature values are presented in Table 3.

3.2.6 Main results and conclusions

Dielectric mirrors for $\lambda = 266$ nm wavelength were prepared by ion beam sputtering technology based on different high refractive index materials - pure hafnia and two different hafnia-silica mixtures with 82% and 46% hafnia content, respectively. Analysis of high temperature annealed coatings properties has revealed several important points.

Preservation of coatings' initial surface roughness was determined even after its high refractive index layer transition from amorphous to polycrystalline cubic phase. Annealing at high temperatures considerably improved optical properties for all coatings. Increase of reflectance up to 99.91 ± 0.04% was measured for HfO_2/SiO_2 mirrors after annealing at 500 °C and still maintaining amorphous structure of high refractive index layers. Also, considerable increase of transmittance at ~200–240 nm range of all HR coatings was obtained after triggering crystallization. This phenomenon might be successfully exploited, while designing other types of coatings, like beamsplitters, etc.

Annealing of the mirrors at the selected temperatures resulting in hafnia based layers crystallization has improved coating LIDTs more than 2.5 times for mixture-based coatings and more than 3 times for HfO_2/SiO_2 coating. Annealed at 1100 °C $(46\%HfO_2+54\%SiO_2)/SiO_2$ mirror had the highest optical resistance of 5.5 ± 0.6 J/cm^2.

Obtained results demonstrate great potential of high temperature annealing above crystallization point of hafnia-silica mixture-based coatings for considerable LIDT and optical property improvement at UV spectral range.

Results were published in:

- **G. Abromavičius**, S. Kičas, R. Buzelis, "High temperature annealing effects on spectral, microstructural and laser damage resistance properties of sputtered HfO_2 and HfO_2-SiO_2 mixture-based UV mirrors", Optical Materials **95**, 2019.

Also presented in the following conferences:

- **G. Abromavičius**, S. Kičas, "Post-deposition annealing of ion beam sputtered dielectric mirrors based on hafnia-silica mixtures", Advanced Materials and Technologies, Palanga, Lithuania, 2018.
- **G. Abromavičius**, S. Kičas, "Optical and surface properties of HfO_2-SiO_2 mixture based UV mirrors", Open Readings, Vilnius, 2018.

3.3 Stress, optical and surface properties of high temperature annealed HfO_2, Sc_2O_3 and Al_2O_3 binary mixture thin films

Ion beam sputtering (IBS) allows depositing bulk-like complex multilayer optical coatings with low optical losses, precise and stable spectral characteristics. However, high compressive stress is one of the main drawbacks of ion beam sputtered coatings. Deposited coating deforms the substrate and leads to degradation of final optical component flatness. Such deteriorated element causes optical aberration and pulse wavefront distortion. Several in-situ and ex-situ techniques could be used to control or reduce obtained stress. These include adjustments of process parameters, deposition of compensating back side coating, using thermal post-deposition treatment, or also using material mixtures to avoid unnecessary crystallization, which might occur after baking the coating. Crystallization of coatings, having high number of thick layers and transparent to laser pulses might be undesirable because of higher scatter losses, which might be even more pronounced for UV range applications.

Choice of materials for IBS coating deposition in UV spectral range is relatively limited. Mainly oxide materials are used - HfO_2, Sc_2O_3 and Al_2O_3 as a high refractive index materials and SiO_2 - as a low refractive index material. In this section, optical, surface and stress properties of ion beam sputtered HfO_2, Sc_2O_3 and Al_2O_3 binary mixtures, having different mixing ratios, were investigated using post-deposition annealing up to 900°C. Possible applications for designing stress compensated amorphous multilayer coatings for UV spectral range are discussed.

3.3.1 Experimental set-up

The same IBS coating chamber and similar substrate cleaning procedure was used, as in investigation of 266 nm dielectric mirrors (Section 3.2). FS substrates, having 25.4 mm diameter and 1 mm thickness were used for the experiments. Linear translation stage performed necessary shifting of material zone target with respect to ion beam position for HfO_2-Al_2O_3, Sc_2O_3-Al_2O_3 and HfO_2-Sc_2O_3 mixture deposition (Fig. 42).

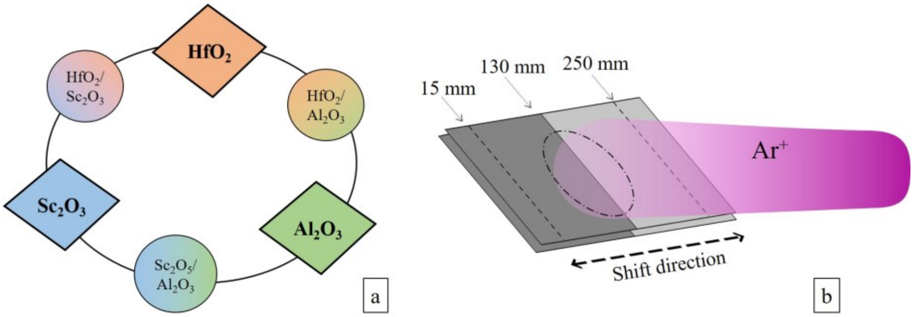

Fig. 42. Set of sample materials and their mixtures (a). Sample film deposition using sputtering of zone target. Schematic representation of different (15 mm, 130 mm and 250 mm) target positions (b).

Samples rotated at 30 rpm ensuring homogeneous material intermixing in the layer structure. No additional heating of substrates were used, so sputtering process was performed at a temperature of approximately ~50 °C.

Physical thickness was controlled using broadband transmittance optical monitoring. Optical thickness of the samples were chosen to be 7 QWOT at 355 nm.

Deposited coatings were annealed in air at selected temperatures. Annealing procedure consisted of several stages. Temperature was raised linearly at the rate of 1 °C/min starting from room temperature, until target temperature was reached. Samples then were kept at constant baking temperature for one hour. Finally, cooling down to room temperature was reached simply turning off the furnace.

Optical parameters were determined assuming homogeneous single layer model. Good agreement between measured and model spectra was observed in all cases. Accuracy of refractive index determination was assumed to be not worse than 0.5%, according to performed analysis by Tikhonravov et al [214].

Volumetric fractions of materials in mixture films were estimated using effective medium theory (EMT) according to Bruggemann's formula in low absorption spectral zone [215]. For HfO_2-Sc_2O_3 mixtures, volumetric fractions were not calculated, because different mixture ratios resulted in almost similar transmittance spectra due to very close refractive index values of these pure materials. However, deposition rates of hafnia and scandia are very similar, so approximate fractions within mixture could be evaluated by the position of the zone target (Table 4).

Table 4. Approximate material fractions within HfO_2-Sc_2O_3 mixtures depending on zone target position.

Target position (mm)	HfO_2 fraction (%)	Sc_2O_3 fraction (%)
15	100	0
100	~70	~30
130	~50	~50
160	~30	~70
250	0	100

Stoney's formula [144, 216] was applied to calculate the residual stress of layers. Substrate curvature was measured before coating, after coating and after each annealing stage using profilometer. Measurements were performed in two perpendicular directions and averaged values were used in further calculations. Tensile stress was considered as a negative and compressive stress - as a positive.

For surface roughness measurements, three 20×20 μm size areas at different places were scanned using AFM probe and average values were used for analysis.

3.3.2 Optical properties of as-deposited films

Measured transmittance spectra, determined dispersions of refractive index and extinction coefficients of prepared HfO_2-Al_2O_3, Sc_2O_3-Al_2O_3 and HfO_2-Sc_2O_3 mixture and pure materials are presented in Fig. 43. For the sake of simplicity, only the percentage of higher n material within the mixture will be denoted further.

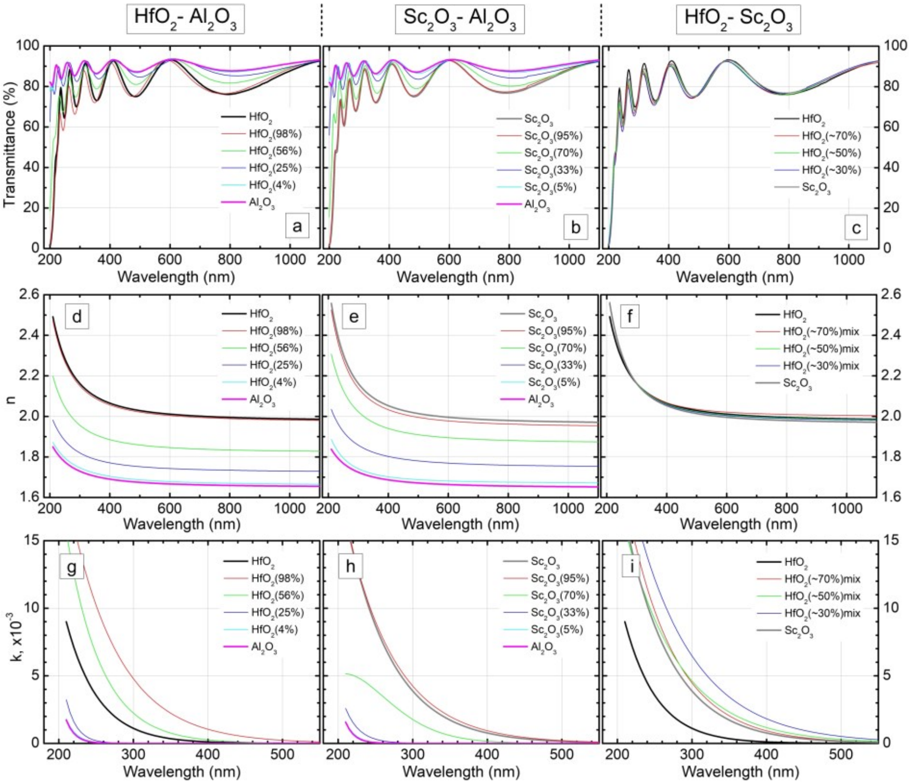

Fig. 43. Transmittance spectra (a, b, c), refractive index (d, e, f) and extinction coefficient (g, h, i) dispersions of deposited HfO_2-Al_2O_3, Sc_2O_3-Al_2O_3, HfO_2-Sc_2O_3 mixture and pure material thin films.

For hafnia-scandia mixture case, refractive index values of all samples are very close each other. Refractive indices of other pairs were dependent on volumetric fraction and were located between higher and lower refractive index of pure materials. Several material mixture-related studies also reported similar trends [129, 142, 217]. Extinction coefficients of several mixture layers in all cases were higher than for pure materials. Optimal oxygen flow is considerably different for sputter deposition of pure alumina, hafnia or scandia. For mixture film deposition, necessary oxygen flow values were calculated using simple interpolation of pure materials values. It is very likely, that used O_2 flow during deposition of composite materials was non-optimal. However, optimization of reactive gas flow during the process was not the main scope of this work.

3.3.3 Optical and surface properties after thermal annealing

Ion beam sputtered material layers are initially amorphous, and can change their phase to polycrystalline after annealing at higher temperatures [82]. Therefore, before analyzing influence of annealing to optical, surface and stress properties of mixture layers, critical annealing temperature ranges, which trigger layer crystallization will be discussed. Many studies demonstrated, that surface roughness of crystalline thin film is considerably higher comparing to amorphous one [86, 218-220]. Evolution of surface roughness root mean square (RMS) was analyzed, while increasing the annealing temperature. Fig. 44a shows, that for pure hafnia and HfO_2 (98%) mixture layers such phase change temperature (T_c) was between 500 °C and 600 °C, while for Al_2O_3 it was 800 °C $< T_c \leq$ 900 °C.

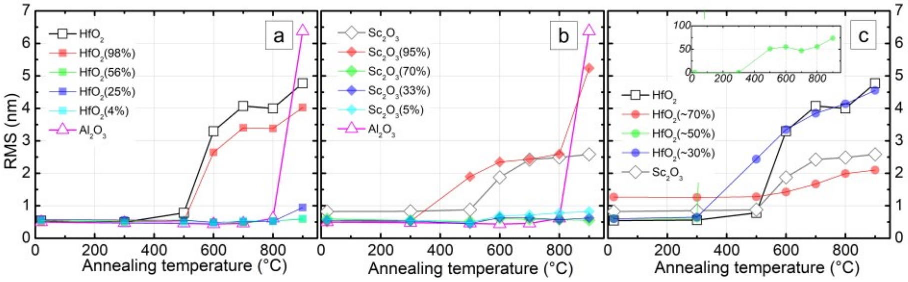

Fig. 44. Surface roughness evolution after thermal annealing to selected temperatures of HfO_2-Al_2O_3 (a), Sc_2O_3- Al_2O_3 (b) and HfO_2-Sc_2O_3 (c) mixture thin films.

It is important to note, that other hafnia-alumina mixtures - HfO_2 (25%), HfO_2 (56%) and HfO_2 (4%) did not show similar behavior and they remained amorphous or at least polycrystalline with very small crystallite sizes. These results are in line with investigations of hafnium aluminate formed by pulsed laser deposition, which showed crystallization temperature exceeding 900 °C [221]. Pure scandia underwent phase transition within 500 °C $< T_c \leq$ 600 °C range (Fig. 44 b). Adding 5% of Al_2O_3 to scandia film has downshifted T_c to 300 °C $< T_c \leq$ 500 °C, while other intermediate Sc_2O_3-Al_2O_3 mixtures did not change their surface roughness until annealing at 900 °C. The situation was completely different for hafnia-scandia films. HfO_2 (~70%)-Sc_2O_3 mixture already had higher initial roughness, which may indicate polycrystalline structure. Its surface roughness slightly increased with the rise of annealing temperature. Other HfO_2-Sc_2O_3 mixtures demonstrated phase transition temperatures at ranges 300 °C $< T_c \leq$ 500 °C and 500 °C $< T_c \leq$ 600 °C. Over all, they are much less stable under influence of medium temperatures comparing to other binary mixtures, discussed previously.

Fig. 45 a, b, c shows changes in refractive indices at 355 nm, while Fig. 45 d, e, f - defined wavelength $\lambda_{0.001}$.

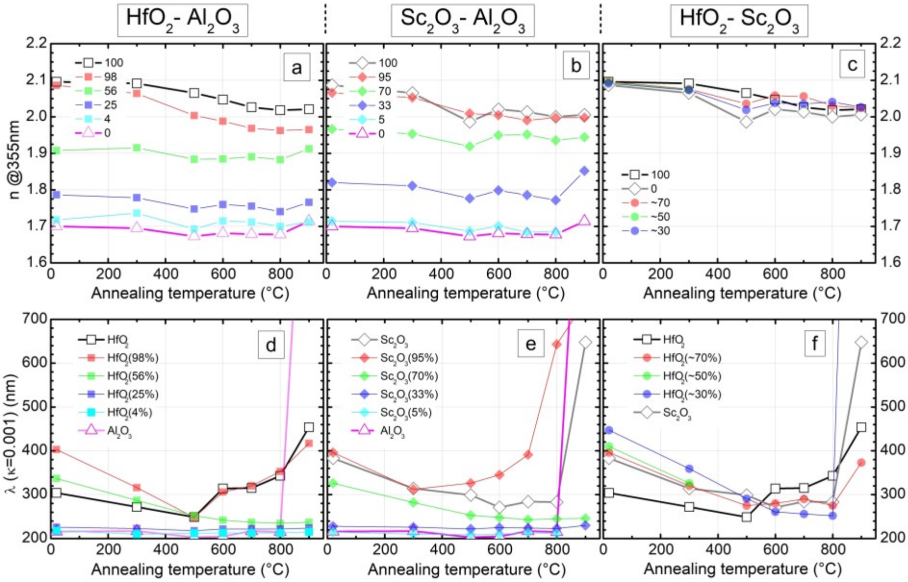

Fig. 45. Refractive index and λ ($k = 0.001$) evolution after thermal annealing to selected temperatures of HfO_2-Al_2O_3 (a, d), Sc_2O_3-Al_2O_3 (b, e) and HfO_2-Sc_2O_3 (c, f) mixture thin films.

We define this wavelength by $k = 0.001$ criterion, which is met, when extinction coefficient is increasing going from longer to shorter wavelengths. Decrease of $\lambda_{0.001}$ means, that extinction at $\lambda > \lambda_{0.001}$ wavelengths decreased to 0.001 value, which means, that the film became less absorbing and more transparent. As it was stated in experimental set-up section, accuracy of refractive index determination should not be worse than 0.5%, which equals to $\Delta n = 0.01$ for $n = 2$.

Refractive indices of pure hafnia and HfO_2 (98%) mixture (Fig. 45a) decreased for higher annealing temperatures up to 700 °C. For intermediate mixture case, refractive index remained more or less the same, and pure alumina showed increase of refractive index after phase change at $800\ °C < T_c \leq 900\ °C$. Fig. 45d demonstrate, that extinction of pure hafnia and its mixtures having 98% and 56% hafnia content was constantly decreasing while annealing until 500 °C. This could be attributed to increased oxidation and stoichiometry of deposited layers, as it was reported by several investigations [172, 173, 222]. We found higher extinction for the same mixture layers annealed at 600 °C, which perhaps is the result of increased optical scatter after crystallization, having in mind also considerably increased surface roughness (Fig. 44 a). All other hafnia-alumina mixtures demonstrated slightly decreasing or constant extinction until the annealing at the highest 900 °C point. Pure Al_2O_3 also suffered drastically increased extinction after heating above 800 °C, due to scatter, resulting by phase change to crystalline structure, as it was reported in several works [223, 224].

Refractive index of pure Sc_2O_3 decreased after initial annealing. However, after crystallization at $500\ °C < T_c \leq 600\ °C$ it increased ant then slight decrease was further observed. Mixture with 5% of alumina slightly decreased with the annealing, while other Sc_2O_3-Al_2O_3 mixtures followed the same trend, as pure scandia. Extinction of Sc_2O_3 decreased with annealing, even after crystallization. That might mean, that small crystallites were present within polycrystalline material and did not contribute to optical scatter loss, which dramatically rose after annealing at 900 °C. Sc_2O_3 (95%) mixture underwent phase change after treating at 500 °C, and extinction constantly increased while annealing further to higher temperatures. Intermediate mixtures demonstrated constantly decreasing or unchanged extinction.

Refractive indices of HfO_2-Sc_2O_3 mixtures followed intermediate trends between their pure counterpart materials until 500 °C annealing. However, using 700 °C annealing, *n* of HfO_2 (~70%)-Sc_2O_3 slightly exceeded values of mixture constituents. Extinction of composite films was bigger than hafnia and scandia. After annealing at 600 °C, extinction of HfO_2mix (160mm) became the smallest of all samples. HfO_2 (~50%)-Sc_2O_3 after 500 °C treatment suffered phase change with hugely increased surface roughness, leading to big optical losses. Due to this, there are no extinction data points presented for this mixture above 300 °C. Annealing at 900 °C increased extinction for all samples, and this could not be related just due to scatter losses, because roughness remained almost unchanged or even reduced for HfO_2 (~70%)-Sc_2O_3 case.

Analysis of HfO_2, Al_2O_3 and Sc_2O_3 mixture optical properties changes using thermal annealing showed, that refractive indices values were in between constituent materials, while extinction coefficients of some samples was bigger, than for pure materials. More rapid changes of both optical constants during annealing were correlated with increase in surface roughness increment, which most possibly is related to changes from amorphous to crystalline change. There are particular ratio of corresponding components in HfO_2-Al_2O_3 and Sc_2O_3-Al_2O_3 mixture cases, which do not suffer extinction increase in UV spectral range even after annealing at temperatures as high as 800-900 °C.

3.3.4 Stress properties under thermal annealing

Fig. 46 shows residual stresses of deposited and post-annealed samples.

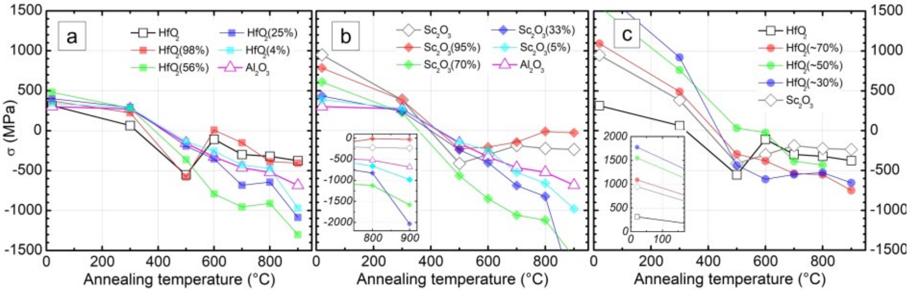

Fig. 46. HfO_2-Al_2O_3 (a), Sc_2O_3-Al_2O_3 (b) and HfO_2-Sc_2O_3 (c) mixture film stress evolution with the increase of annealing temperature.

Pure hafnia and hafnia mixture doped with 2% alumina content demonstrated rapid decrease of stress by $\Delta\sigma = 600$ MPa after crystallization by annealing at 600 °C (Fig. 46a). The most interesting behavior was observed for HfO_2 (56%) and HfO_2 (25%) mixture films. Their compressive stresses were bigger by $\Delta\sigma \sim 150$-200 MPa, than for pure constituents. Tensions became tensile after the next annealing step at 500 °C. Even more, for the next two baking steps (600 °C and 700 °C), their tensile stresses further increased, especially for HfO_2 (56%) mixture. Peculiar changes of tension amplitude is clearly seen after 900 °C annealing.

Stresses of deposited Sc_2O_3-Al_2O_3mixtures (Fig. 46b) were distributed among pure material values. After annealing at 500 °C, stresses of pure scandia and Sc_2O_3 (95%) mixture films became tensile. However, after baking at 600 °C, they shifted towards zero values. Other mixtures also showed change from compressive to tensile stresses, which further increased after higher temperature treatment.

All deposited HfO_2- Sc_2O_3 mixtures show higher compressive stresses than pure materials. Initial values were reduced after annealing, but after treating at T > 600 °C, further changes in tensile stress values remain small.

Changes of ion beam sputtered SiO_2 film stress after annealing are presented in Kičas et al work [144]. Annealed SiO_2 has the following stresses at corresponding temperatures: ~380 MPa (400 °C), and ~225 MPa (500 °C). For standard Bragg dielectric mirrors, low-*n* SiO_2 layers are thicker, than high-*n* layers. The actual difference depends on refractive index difference among the stack materials. Therefore, to release total stress of such coatings by thermal treatment, high refractive index material should achieve higher tensile stress value, than remaining compressive stress by SiO_2 layers. According to presented stress and optical properties change dynamics under thermal annealing of presented high refractive index binary mixtures, the following combinations could be used to design stress-compensated multilayer coatings for UV spectral range:

a) HfO_2(56%)- Al_2O_3(44%) ($\sigma = -360$ MPa, $T = 500$ °C), annealing of HR coating at 450 °C < T < 500 °C);

b) Sc_2O_3(70%)-Al_2O_3(30%) ($\sigma = -560$ MPa, $T = 500$ °C), annealing of HR coating at 400 °C < T < 500 °C);

c) HfO_2 (~70%)-Sc_2O_3(~30%) ($\sigma = -295$ MPa, $T = 500$ °C), annealing of HR coating at 450 °C < T < 500 °C).

The last hafnia-scandia mixture also has additional benefit having the highest refractive index of all listed candidates, however, slightly higher extinction value implies, that additional experiments depositing and analyzing multilayer coatings are necessary to determine optimal selection of the best mixture.

However, further experiments, implementing multilayer stress compensated coating were not possible, since available ion beam sputtering equipment had just two material target. Therefore, deposition of alternating layers of selected binary mixture and SiO_2 was not possible.

3.3.5 Main results and conclusions

Binary mixture films of common high refractive index material for UV spectral range - HfO_2, Sc_2O_3 and Al_2O_3 were deposited by IBS technology. Changes of their optical, surface and stress properties were analyzed with respect of thermal annealing up to 900 °C. HfO_2(56%)-Al_2O_3(44%), Sc_2O_3(70%)-Al_2O_3(30%) and selected HfO_2-Sc_2O_3 mixture were identified as possible candidates to achieve stress compensated multilayer coatings for UV range without sacrificing optical and low surface roughness (and consequently optical scatter) properties. However, further iteration of experiments should be designed to refine precise annealing temperatures of multilayer coatings to obtain total stress close to zero.

Results are submitted for publication in:

- **G. Abromavičius**, T. Juodagalvis, "Mechanical stress, optical and surface properties of high temperature annealed HfO_2, Sc_2O_3 and

Al_2O_3 binary mixture thin films deposited by ion beam sputtering", submitted to Optical Materials.

MAIN RESULTS AND CONCLUSIONS

1) Processing fused silica substrates with argon plasma and removing 50-100 nm of substrate material significantly increased its LIDT without any degradation of optical, surface roughness and flatness properties. Transparent antireflective, polarizing optical coatings for $\lambda = 355$ nm, applied on etched substrates, demonstrated more than 2 times higher LIDT values compared to the similar coatings applied on non-etched substrates.

2) Applying 140 eV energy oxygen plasma for etching of fused silica substrate to 220 ± 10 nm depth has resulted in 75 ± 4 J/cm^2 LIDT for $\lambda = 355$ nm 3ns laser pulses. Anti-reflective coating for $\lambda = 355$ nm applied on etched FS substrate demonstrated LIDT of 14 ± 0.7 J/cm^2 which was 3.4 times higher comparing with non-etched substrate case. Obtained LIDT improvements demonstrate good possibilities to apply low energy oxygen plasma etching for making high power transparent UV laser optical components.

3) Triggering crystallization of HfO_2 and HfO_2-SiO_2 mixture layers within dielectric mirror structure by high temperature annealing led to improvement of reflectance and UV transmittance properties, without inducing surface roughness deterioration.

4) Annealed at 1100 °C (46%HfO_2+54%SiO_2)/SiO_2 mirror had the highest optical resistance of 5.5 ± 0.6 J/cm^2 for 266 nm laser pulses. Demonstrated novel approach of high temperature annealing and inducing crystallization of hafnia-silica mixture-based coatings shows good perspectives to develop multilayer optical coatings for UV spectral range having high optical resistance.

5) By combining appropriate thermal annealing and selected binary mixtures of HfO_2, Sc_2O_3 and Al_2O_3, it is possible to create stress-compensated multilayer coatings for UV spectral range.

BIBLIOGRAPHY

[1] N. Kaiser, H.K. Pulker, Optical Interference Coatings, Springer, Berlin, 2003.
[2] T.H. Maiman, Stimulated optical radiation in ruby, (1960).
[3] A.J. Glass, A.H. Guenther, Laser induced damage of optical elements–a status report, Appl. Opt., 12 (1973) 637-649.
[4] A.F. Turner, Ruby laser damage thresholds in evaporated thin films and multilayer coatings, Damage in Laser Materials: 1971, 356 (1971) 119-123.
[5] E. Ritter, Deposition of oxide films by reactive evaporation, Journal of Vacuum Science Technology, 3 (1966) 225.
[6] G. HASS, Preparation, Structure, and Applications of Thin Films of Silicon Monoxide and Titanium Dioxide, Journal of the American Ceramic Society, 33 (1950) 353-360.
[7] W.R. Grove, On the electro-chemical polarity of gases, in: Abstracts of the Papers Communicated to the Royal Society of London, The Royal Society London, 1854, pp. 168-169.
[8] J.E. Greene, Tracing the 5000-year recorded history of inorganic thin films from ~3000 BC to the early 1900s AD, Applied Physics Reviews, 1 (2014) 041302.
[9] H.F. Fruth, Cathode sputtering, a commercial application, Physics, 2 (1932) 280-286.
[10] H.R. Kaufman, Technology of ion beam sources used in sputtering, Journal of Vacuum Science and Technology, 15 (1978) 272-276.
[11] W.R. Mickelsen, H.R. Kaufman, Electrostatic thrusters for space propulsion, present and future, Journal of the British Interplanetary Society, 19 (1963) 319-337.
[12] F.R. Flory, Thin films for optical systems, CRC Press, New York, 1995.
[13] P.A. Franken, A.E. Hill, C.W. Peters, G. Weinreich, Generation of Optical Harmonics, Physical Review Letters, 7 (1961) 118-119.
[14] N.G. Basov, V.A. Danilychev, Y.M. Popov, D.D. Khodkevich, Laser operating in the vacuum region of the spectrum by excitation of liquid xenon with an electron beam, The Journal of Experimental and Theoretical Physics Letters, 12 (1970) 473-474.
[15] X. Ye, J. Huang, H. Liu, F. Geng, L. Sun, X. Jiang, W. Wu, L. Qiao, X. Zu, W. Zheng, Advanced Mitigation Process (AMP) for Improving Laser Damage Threshold of Fused Silica Optics, Scientific Reports, 6 (2016) 31111.
[16] M. Pfiffer, J.-L. Longuet, C. Labrugère, E. Fargin, B. Bousquet, M. Dussauze, S. Lambert, P. Cormont, J. Néauport, Characterization of the Polishing-Induced Contamination of Fused Silica Optics, Journal of the American Ceramic Society, 100 (2017) 96-107.
[17] D.W. Camp, M.R. Kozlowski, L.M. Sheehan, M.A. Nichols, M. Dovik, R.G. Raether, I.M. Thomas, Subsurface damage and polishing compound

affect the 355-nm laser damage threshold of fused silica surfaces, in: Laser-Induced Damage in Optical Materials: 1997, SPIE, 1998, pp. 9.

[18] N. Bloembergen, Role of Cracks, Pores, and Absorbing Inclusions on Laser Induced Damage Threshold at Surfaces of Transparent Dielectrics, Appl. Opt., 12 (1973) 661-664.

[19] F.Y. Génin, A. Salleo, T.V. Pistor, L.L. Chase, Role of light intensification by cracks in optical breakdown on surfaces, J. Opt. Soc. Am. A, 18 (2001) 2607-2616.

[20] P.P. Hed, D.F. Edwards, J.B. Davis, Subsurface damage in optical materials: Origin, measurement and removal: Summary, ; Lawrence Livermore National Lab., CA (USA), 1988.

[21] X. Liu, B. Zhang, Grinding of nanostructural ceramic coatings: damage evaluation, International Journal of Machine Tools and Manufacture, 43 (2003) 161-167.

[22] H.K. Tönshoff, T. Friemuth, In-process dressing of fine diamond wheels for tool grinding, Precision Engineering, 24 (2000) 58-61.

[23] L.f.L.E. (LLE), Subsurface damage in microgrinding optical glasses, in: LLE Review 73, 1997, pp. 45-49.

[24] S.G. Beilby, Aggregation and flow of solids, Macmillan and Co, London, 1921.

[25] L. Hongjie, H. Jin, Y. Xin, S. Laixi, W. Fengrui, F. Geng, J. Xiaodong, W. Wu, Z. Wanguo, Residual impurities on fused silica surface processed by different technics and their effects on laser induced damage at 355 nm Optoelectronics and Advanced materials - Rapid Communications, 9 (2015) 1406-1410.

[26] M.R. Kozlowski, J. Carr, I.D. Hutcheon, R.A. Torres, L.M. Sheehan, D.W. Camp, M. Yan, Depth profiling of polishing-induced contamination on fused silica surfaces, in: Laser-Induced Damage in Optical Materials: 1997, SPIE, 1998, pp. 11.

[27] X. Jiang, Y. Liu, H. Rao, S. Fu, Improve the laser damage resistance of fused silica by wet surface cleaning and optimized HF etch process, in: SPIE/SIOM Pacific Rim Laser Damage: Optical Materials for High-Power Lasers, SPIE, 2013, pp. 9.

[28] J. Neauport, L. Lamaignere, H. Bercegol, F. Pilon, J.C. Birolleau, Polishing-induced contamination of fused silica optics and laser induced damage density at 351 nm, Opt. Express, 13 (2005) 10163-10171.

[29] G. Hu, S. Shao, M. Yang, J. Shao, Y. Zhao, K. Yi, Z. Fan, Influence of subsurface defects on 355 nm laser damage resistance of monolayer and multilayer coatings, in: Laser Damage Symposium XLI: Annual Symposium on Optical Materials for High Power Lasers, SPIE, 2009, pp. 7.

[30] L. Hongjie, H. Jin, W. Fengrui, Z. Xinda, Y. Xin, Z. Xiaoyan, S. Laixi, J. Xiaodong, S. Zhan, Z. Wanguo, Subsurface defects of fused silica optics and laser induced damage at 351 nm, Opt. Express, 21 (2013) 12204-12217.

[31] Z. Zheng, X. Zu, X. Jiang, X. Xiang, J. Huang, X. Zhou, C. Li, W. Zheng, L. Li, Effect of HF etching on the surface quality and laser-induced damage of fused silica, Optics & Laser Technology, 44 (2012) 1039-1042.
[32] P.E. Miller, T.I. Suratwala, J.D. Bude, T.A. Laurence, N. Shen, W.A. Steele, M.D. Feit, J.A. Menapace, L.L. Wong, Laser damage precursors in fused silica, in: Laser Damage Symposium XLI: Annual Symposium on Optical Materials for High Power Lasers, SPIE, 2009, pp. 14.
[33] J. Neauport, C. Ambard, P. Cormont, N. Darbois, J. Destribats, C. Luitot, O. Rondeau, Subsurface damage measurement of ground fused silica parts by HF etching techniques, Opt. Express, 17 (2009) 20448-20456.
[34] T.I. Suratwala, P.E. Miller, J.D. Bude, W.A. Steele, N. Shen, M.V. Monticelli, M.D. Feit, T.A. Laurence, M.A. Norton, C.W. Carr, L.L. Wong, HF-Based Etching Processes for Improving Laser Damage Resistance of Fused Silica Optical Surfaces, Journal of the American Ceramic Society, 94 (2011) 416-428.
[35] J.A. Menapace, B. Penetrante, D. Golini, A.F. Slomba, P.E. Miller, T.G. Parham, M. Nichols, J. Peterson, Combined advanced finishing and UV-laser conditioning for producing UV-damage-resistant fused-silica optics, in: Boulder Damage, SPIE, 2002, pp. 13.
[36] R.M. Brusasco, B.M. Penetrante, J.E. Peterson, S.M. Maricle, J.A. Menapace, UV-laser conditioning for reduction of 351-nm damage initiation in fused silica, in: Boulder Damage, SPIE, 2002, pp. 8.
[37] T. Kamimura, S. Akamatsu, M. Yamamoto, I. Yamato, H. Shiba, S. Motokoshi, T. Sakamoto, T. Jitsuno, T. Okamoto, K. Yoshida, Enhancement of surface-damage resistance by removing subsurface damage in fused silica, in: XXXV Annual Symposium on Optical Materials for High Power Lasers: Boulder Damage Symposium, SPIE, 2004, pp. 6.
[38] K. Juškevičius, R. Buzelis, G. Abromavičius, R. Samuilovas, S. Abbas, A. Belosludtsev, R. Drazdys, S. Kičas, Argon plasma etching of fused silica substrates for manufacturing high laser damage resistance optical interference coatings, Opt. Mater. Express, 7 (2017) 3598-3607.
[39] M. Xu, F. Shi, L. Zhou, Y. Dai, X. Peng, W. Liao, Investigation of laser-induced damage threshold improvement mechanism during ion beam sputtering of fused silica, Opt. Express, 25 (2017) 29260-29271.
[40] F. Shi, Y. Zhong, Y. Dai, X. Peng, M. Xu, T. Sui, Investigation of surface damage precursor evolutions and laser-induced damage threshold improvement mechanism during Ion beam etching of fused silica, Opt. Express, 24 (2016) 20842-20854.
[41] L. Sun, J. Huang, T. Shao, X. Ye, Q. Li, X. Jiang, W. Wu, L. Yang, W. Zheng, Effects of combined process of reactive ion etching and dynamic chemical etching on UV laser damage resistance and surface quality of fused silica optics, Opt. Express, 26 (2018) 18006-18018.

[42] R. Catrin, J. Neauport, D. Taroux, P. Cormont, C. Maunier, S. Lambert, Magnetorheological finishing for removing surface and subsurface defects of fused silica optics, in, SPIE, 2014, pp. 7.
[43] K. Juškevičius, R. Buzelis, S. Kičas, T. Tolenis, R. Drazdys, G. Batavičiūtė, E. Pupka, L. Smalakys, A. Melninkaitis, Investigation of subsurface damage impact on resistance of laser radiation of fused silica substrates, in: SPIE Laser Damage, SPIE, 2013, pp. 9.
[44] F. Shi, Y. Shu, Y. Dai, X. Peng, S. Li, Magnetorheological elastic super-smooth finishing for high-efficiency manufacturing of ultraviolet laser resistant optics, in, SPIE, 2013, pp. 10.
[45] D. Flamm, F. Frost, D. Hirsch, Evolution of surface topography of fused silica by ion beam sputtering, Applied Surface Science, 179 (2001) 95-101.
[46] W. Liao, Y. Dai, X. Xie, L. Zhou, Microscopic morphology evolution during ion beam smoothing of Zerodur® surfaces, Opt. Express, 22 (2014) 377-386.
[47] F. Frost, R. Fechner, B. Ziberi, D. Flamm, A. Schindler, Large area smoothing of optical surfaces by low-energy ion beams, Thin Solid Films, 459 (2004) 100-105.
[48] T. Arnold, G. Böhm, R. Fechner, J. Meister, A. Nickel, F. Frost, T. Hänsel, A. Schindler, Ultra-precision surface finishing by ion beam and plasma jet techniques—status and outlook, Nuclear Instruments and Methods in Physics Research Section A: Accelerators, Spectrometers, Detectors and Associated Equipment, 616 (2010) 147-156.
[49] V.M. Donnelly, A. Kornblit, Plasma etching: Yesterday, today, and tomorrow, Journal of Vacuum Science & Technology A, 31 (2013) 050825.
[50] L. Sun, H. Liu, J. Huang, X. Ye, H. Xia, Q. Li, X. Jiang, W. Wu, L. Yang, W. Zheng, Reaction ion etching process for improving laser damage resistance of fused silica optical surface, Opt. Express, 24 (2016) 199-211.
[51] S.-T. Jung, H.-S. Song, D.-S. Kim, Y.-H. Song, T.-H. Kim, H.-S. Kim, Inductively coupled plasma etching of Ge-doped boron-phosphosilicate glass for planar lightwave circuit devices, Journal of Non-Crystalline Solids, 259 (1999) 191-197.
[52] D.Y. Choi, J.H. Lee, D.S. Kim, S.T. Jung, Formation of plasma induced surface damage in silica glass etching for optical waveguides, Journal of Applied Physics, 95 (2004) 8400-8407.
[53] A.J. van Roosmalen, Review: dry etching of silicon oxide, Vacuum, 34 (1984) 429-436.
[54] Y. Tian, W. Liu, L. Hang, Influence of Oxygen Flow Rate on the Variation of Surface Roughness of Fused Silica during Plasma Polishing Process, Physics Procedia, 18 (2011) 107-111.
[55] L. Sun, T. Shao, Z. Shi, J. Huang, X. Ye, X. Jiang, W. Wu, L. Yang, W. Zheng, Ultraviolet Laser Damage Dependence on Contamination Concentration in Fused Silica Optics during Reactive Ion Etching Process, Materials (Basel, Switzerland), 11 (2018).

[56] T. Kamimura, M. Yoshimura, Y. Mori, T. Sasaki, K. Yoshida, Effect of RF Plasma Etching on Surface Damage in CsLiB6O10 Crystal, Japanese Journal of Applied Physics, 38 (1999) L181-L183.
[57] C. Gerhard, D. Tasche, N. Munser, H. Dyck, Increase in nanosecond laser-induced damage threshold of sapphire windows by means of direct dielectric barrier discharge plasma treatment, Opt. Lett., 42 (2017) 49-52.
[58] a.t.L.S. D.T. Wei; A. W. Lauderback, Inc., Method for fabricating multilayer optical films, in, United States, 1989.
[59] D.T. Wei, Ion beam interference coating for ultralow optical loss, Appl. Opt., 28 (1989) 2813-2816.
[60] K.H. (NASA), Dr. Harold R. Kaufman, in, pp. Center researcher Harold Kaufman has the rare distinction of inventing an experimental spaceflight hardware system that has not only been demonstrated in testing but is being flown in space today.
[61] C. Bundesmann, H. Neumann, Tutorial: The systematics of ion beam sputtering for deposition of thin films with tailored properties, Journal of Applied Physics, 124 (2018) 231102.
[62] M. Ohring, Materials Science of Thin Films, 2 ed., Academic Press, 2002.
[63] K. Seshan, Handbook of thin-film deposition processes and techniques, 2nd ed., Noyes Publications, New York, USA, 2002.
[64] C. Bundesmann, T. Lautenschläger, D. Spemann, A. Finzel, E. Thelander, M. Mensing, F. Frost, Systematic investigation of the properties of TiO2 films grown by reactive ion beam sputter deposition, Applied Surface Science, 421 (2017) 331-340.
[65] C. Bundesmann, T. Lautenschläger, E. Thelander, D. Spemann, Reactive Ar ion beam sputter deposition of TiO2 films: Influence of process parameters on film properties, Nuclear Instruments and Methods in Physics Research Section B: Beam Interactions with Materials and Atoms, 395 (2017) 17-23.
[66] M. Jupé, M. Lappschies, L. Jensen, K. Starke, D. Ristau, Laser-induced damage in gradual index layers and Rugate filters, SPIE, 2007.
[67] H. Bassner, R. Killinger, H. Leiter, J. Müller, Development steps of the RF-ion thrusters RIT, in: 27th International Electric Propulsion Conference, 2001, pp. 01-105.
[68] A. Bulit, J.P. Luna, J.G. Del Ámo, B. Lotz, D. Feili, H. Leiter, Experimental Investigation on the Influence of the Facility Background Pressure on the Plume of the RIT-4 Ion Engine, in: Proceedings of the 32nd International Electric Propulsion Conference, IEPC-2011-028, Wiesbaden, Germany, 2011.
[69] https://www.azom.com/article.aspx?ArticleID=7533.
[70] M.F. Closs, Numerical modelling and optimisation of radio-frequency ion thrusters, in: Aerospace Engineering, Bundeswehr University Munich, Munich, 2001, pp. 135.

[71] M. Lappschies, B. Görtz, D. Ristau, Optical monitoring of rugate filters, in: Advances in Optical Thin Films II, International Society for Optics and Photonics, 2005, pp. 59631Z.

[72] M. Mende, L.O. Jensen, H. Ehlers, W. Riggers, H. Blaschke, D. Ristau, Laser-induced damage of pure and mixture material high reflectors for 355nm and 1064nm wavelength, in: SPIE Optical Systems Design, SPIE, 2011, pp. 11.

[73] K. Starke, T. Grosz, M. Lappschies, D. Ristau, Rapid prototyping of optical thin film filters, SPIE, 2000.

[74] R.P. Netterfield, M. Gross, F.N. Baynes, K.L. Green, G.M. Harry, H. Armandula, S. Rowan, J. Hough, D.R. Crooks, M.M. Fejer, Low mechanical loss coatings for LIGO optics: progress report, in: Advances in Thin-Film Coatings for Optical Applications II, International Society for Optics and Photonics, 2005, pp. 58700H.

[75] S.G. Yoon, Y.T. Kim, H.K. Kim, M.J. Kim, H.M. Lee, D.H. Yoon, Comparision of residual stress and optical properties in Ta2O5 thin films deposited by single and dual ion beam sputtering, Materials Science and Engineering: B, 118 (2005) 234-237.

[76] C. Bundesmann, I.-M. Eichentopf, S. Mändl, H. Neumann, Stress relaxation and optical characterization of TiO2 and SiO2 films grown by dual ion beam deposition, Thin Solid Films, 516 (2008) 8604-8608.

[77] E. Çetinörgü, B. Baloukas, O. Zabeida, J.E. Klemberg-Sapieha, L. Martinu, Mechanical and thermoelastic characteristics of optical thin films deposited by dual ion beam sputtering, Appl. Opt., 48 (2009) 4536-4544.

[78] M. Cosar, A. Ozhan, G. Aydogdu, Improving the laser damage resistance of oxide thin films and multilayers via tailoring ion beam sputtering parameters, Applied Surface Science, 336 (2015) 34-38.

[79] J. Kolbe, H. Kessler, T. Hofmann, F. Meyer, H. Schink, D. Ristau, Optical properties and damage thresholds of dielectric UV/VUV coatings deposited by conventional evaporation, IAD, and IBS, in: Laser-Induced Damage in Optical Materials: 1991, International Society for Optics and Photonics, 1992, pp. 221-236.

[80] J.P. Nair, I. Zon, M. Oron, R. Popovitz-Biro, Y. Feldman, I. Lubomirsky, Stoichiometry control during deposition by ion beam sputtering, Journal of applied physics, 92 (2002) 4784-4790.

[81] A. Fornier, D. Bernardino, O. Lam, J. Neauport, F. Dufour, B.R. Schmitt, J.-M. Mackowski, High-laser-damage-threshold HfO2/SiO2 mirrors manufactured by sputtering process, in: Third International Conference on Solid State Lasers for Application to Inertial Confinement Fusion, SPIE, 1999, pp. 9.

[82] M. Bischoff, T. Nowitzki, O. Voß, S. Wilbrandt, O. Stenzel, Postdeposition treatment of IBS coatings for UV applications with optimized thin-film stress properties, Appl. Opt., 53 (2014) A212-A220.

[83] Q. Lv, M. Huang, S. Zhang, S. Deng, F. Gong, F. Wang, Y. Pan, G. Li, Y. Jin, Effects of Annealing on Residual Stress in Ta2O5 Films Deposited by Dual Ion Beam Sputtering, Coatings, 8 (2018) 150.
[84] J. Ferre-Borrull, A. Duparre, E. Quesnel, Roughness and light scattering of ion-beam-sputtered fluoride coatings for 193 nm, Appl. Opt., 39 (2000) 5854-5864.
[85] R.A. Negres, C.J. Stolz, M.D. Thomas, M. Caputo, 355-nm, nanosecond laser mirror thin film damage competition, SPIE, 2017.
[86] C.J. Stolz, F.Y. Genin, M.R. Kozlowski, D. Long, R. Lalazari, Z. Wu, P.-K. Kuo, Influence of microstructure on laser damage threshold of IBS coatings, in: Laser-Induced Damage in Optical Materials: 1995, SPIE, 1996, pp. 9.
[87] C.J. Stolz, J. Adams, M.D. Shirk, M.A. Norton, T.L. Weiland, Engineering meter-scale laser resistant coatings for the near IR, SPIE, 2005.
[88] D. Ristau, W. Arens, S. Bosch, A. Duparre, E. Masetti, D. Jacob, G. Kiriakidis, F. Peiro, E. Quesnel, A.V. Tikhonravov, UV-optical and microstructural properties of MgF 2-coatings deposited by IBS and PVD processes, in: Advances in Optical Interference Coatings, International Society for Optics and Photonics, 1999, pp. 436-446.
[89] M. Cevro, Ion-beam and dual-ion-beam sputter deposition of tantalum oxide films, Optical Engineering, 34 (1995) 596.
[90] M. Cevro, G. Carter, Ion beam sputtering and dual ion beam sputtering of titanium oxide films, Journal of Physics D: Applied Physics, 28 (1995) 1962.
[91] E. Quesnel, M. Berger, J. Cigna, D. Duca, C. Pelle, F. Pierre, Near-UV to IR optical characterization of YF 3 thin films deposited by evaporation and ion beam processes, in: Developments in Optical Component Coatings, International Society for Optics and Photonics, 1996, pp. 366-373.
[92] B. Görtz, D. Ristau, E. Quesnel, G. Ravel, M. Trovó, M. Danailov, IBS deposition of dense fluoride coatings for the vacuum ultraviolet free electron laser, in: Advances in Optical Thin Films II, International Society for Optics and Photonics, 2005, pp. 59630I.
[93] L. Jensen, M. Jupé, H. Mädebach, H. Ehlers, K. Starke, D. Ristau, W. Riede, P. Allenspacher, H. Schroeder, Damage threshold investigations of high-power laser optics under atmospheric and vacuum conditions, SPIE, 2007.
[94] D. Ristau, T. Gross, Ion beam sputter coatings for laser technology, SPIE, 2005.
[95] G. Rempe, R. Thompson, H.J. Kimble, R. Lalezari, Measurement of ultralow losses in an optical interferometer, Opt. Lett., 17 (1992) 363-365.
[96] F. Beauville, D. Buskulic, R. Flaminio, F. Marion, A. Masserot, L. Massonnet, B. Mours, F. Moreau, J. Ramonet, E. Tournefier, The VIRGO large mirrors: a challenge for low loss coatings, Classical and Quantum Gravity, 21 (2004) S935.

[97] S. Guenster, H. Blaschke, D. Ristau, M. Danailov, M. Trovo, A. Gatto, N. Kaiser, F. Sarto, D. Flori, F. Menchini, Radiation resistance of single- and multilayer coatings against synchrotron radiation, SPIE, 2004.
[98] M.E. Couprie, D. Garzella, M. Billardon, Optical cavities for UV free electron lasers, Nuclear Instruments and Methods in Physics Research Section A: Accelerators, Spectrometers, Detectors and Associated Equipment, 358 (1995) 382-386.
[99] D. Garzella, M.E. Couprie, T. Hara, L. Nahon, M. Brazuna, A. Delboulbé, M. Billardon, Mirror degradation and heating in storage ring FELs, Nuclear Instruments and Methods in Physics Research Section A: Accelerators, Spectrometers, Detectors and Associated Equipment, 358 (1995) 387-391.
[100] S. Becker, A. Pereira, P. Bouchut, F. Geffraye, C. Anglade, Laser-induced contamination of silica coatings in vacuum, SPIE, 2007.
[101] J. DiJon, E. Quesnel, B. Rolland, P. Garrec, C. Pelle, J. Hue, High-damage-threshold fluoride UV mirrors made by ion-beam sputtering, in: Laser-Induced Damage in Optical Materials: 1997, International Society for Optics and Photonics, 1998, pp. 406-417.
[102] E. Quesnel, L. Dumas, D. Jacob, F. Peiró, Optical and microstructural properties of MgF 2 UV coatings grown by ion beam sputtering process, Journal of Vacuum Science & Technology A: Vacuum, Surfaces, and Films, 18 (2000) 2869-2876.
[103] D. Jacob, F. Peiro, E. Quesnel, D. Ristau, Microstructure and composition of MgF2 optical coatings grown on Si substrate by PVD and IBS processes, Thin Solid Films, 360 (2000) 133-138.
[104] T. Yoshida, K. Nishimoto, K. Sekine, K. Etoh, Fluoride antireflection coatings for deep ultraviolet optics deposited by ion-beam sputtering, Appl. Opt., 45 (2006) 1375-1379.
[105] M.C. Cheynet, S. Pokrant, F.D. Tichelaar, J.-L. Rouvière, Crystal structure and band gap determination of HfO2 thin films, Journal of Applied Physics, 101 (2007) 054101.
[106] H. Takeuchi, D. Ha, T.-J. King, Observation of bulk HfO 2 defects by spectroscopic ellipsometry, Journal of Vacuum Science & Technology A: Vacuum, Surfaces, and Films, 22 (2004) 1337-1341.
[107] M. Mero, J. Liu, A. Sabbah, J.C. Jasapara, K. Starke, D. Ristau, J.K. McIver, W.G. Rudolph, Femtosecond pulse damage and predamage behavior of dielectric thin films, SPIE, 2003.
[108] D. Grosso, P. Sermon, Scandia optical coatings for application at 351 nm, Thin Solid Films, 368 (2000) 116-124.
[109] G. Liu, Y. Jin, H. He, Z. Fan, Effect of substrate temperatures on the optical properties of evaporated Sc2O3 thin films, Thin Solid Films, 518 (2010) 2920-2923.

[110] F. Rainer, W. Lowdermilk, D. Milam, T.T. Hart, T. Lichtenstein, C. Carniglia, Scandium oxide coatings for high-power UV laser applications, Appl. Opt., 21 (1982) 3685-3688.
[111] S. Tamura, S. Kimura, Y. Sato, H. Yoshida, K. Yoshida, Laser-damage threshold of Sc2O3/SiO2 high reflector coatings for a laser wavelength of 355 nm, Thin solid films, 228 (1993) 222-224.
[112] L.O. Jensen, M. Mende, H. Blaschke, D. Ristau, D. Nguyen, L. Emmert, W. Rudolph, Investigations on SiO2/HfO2 mixtures for nanosecond and femtosecond pulses, in: Laser Damage Symposium XLII: Annual Symposium on Optical Materials for High Power Lasers, SPIE, 2010, pp. 10.
[113] D. Patel, Y. Wang, M. Larotonda, J. Lovewell, J. Jensen, K.J. Hsiao, E. Krous, J.J. Rocca, C.S. Menoni, F. Tomasel, S. Kholi, P. McCurdy, Assessing the impact of atomic oxygen in the damage threshold and stress of Hafnia films grown by ion beam sputter deposition, in: Boulder Damage Symposium XXXVIII: Annual Symposium on Optical Materials for High Power Lasers, SPIE, 2007, pp. 8.
[114] H. Liu, Y. Jiang, L. Wang, J. Leng, P. Sun, K. Zhuang, Y. Ji, X. Cheng, H. Jiao, Z. Wang, B. Wu, Correlation between properties of HfO2 films and preparing parameters by ion beam sputtering deposition, Appl. Opt., 53 (2014) A405-A411.
[115] P. Langston, D. Patel, B. Regan, A. Curtis, B. Luther, A. Markosyan, R. Route, M. Fejer, J. Rocca, C. Menoni, Influence of oxygen pressure variations on the optical properties of ion beam sputtered metal oxide coatings, in: Frontiers in Optics, Optical Society of America, 2011, pp. JWA25.
[116] M. Mende, L.O. Jensen, H. Ehlers, S. Bruns, M. Vergöhl, P. Burdack, D. Ristau, Applying hafnia mixtures to enhance the laser-induced damage threshold of coatings for third-harmonic generation optics, in: SPIE Laser Damage, SPIE, 2012, pp. 8.
[117] G. Tian, S. Wu, K. Shu, L. Qin, J. Shao, Influence of deposition conditions on the microstructure of oxides thin films, Applied surface science, 253 (2007) 8782-8787.
[118] C.S. Menoni, E.M. Krous, D. Patel, P. Langston, J. Tollerud, D.N. Nguyen, L.A. Emmert, A. Markosyan, R. Route, M. Fejer, Advances in ion beam sputtered Sc 2 O 3 for optical interference coatings, in: Laser-Induced Damage in Optical Materials: 2010, International Society for Optics and Photonics, 2010, pp. 784202.
[119] P.F. Langston, E. Krous, D. Schiltz, D. Patel, L. Emmert, A. Markosyan, B. Reagan, K. Wernsing, Y. Xu, Z. Sun, R. Route, M.M. Fejer, J.J. Rocca, W. Rudolph, C.S. Menoni, Point defects in Sc2O3 thin films by ion beam sputtering, Appl. Opt., 53 (2014) A276-A280.
[120] M. Mende, S. Schrameyer, H. Ehlers, D. Ristau, L. Gallais, Laser damage resistance of ion-beam sputtered Sc2O3/SiO2 mixture optical coatings, Appl. Opt., 52 (2013) 1368-1376.

[121] E.O. Filatova, A.S. Konashuk, Interpretation of the changing the band gap of Al2O3 depending on its crystalline form: connection with different local symmetries, The Journal of Physical Chemistry C, 119 (2015) 20755-20761.

[122] A. Starke, H. Schink, J. Kolbe, J. Ebert, Laser-induced damage thresholds and optical constants of ion-plated and ion-beam-sputtered Al2O3 and HfO2 coatings for the ultraviolet, in: Optical Thin Films and Applications, International Society for Optics and Photonics, 1990, pp. 299-305.

[123] J. Zhang, X. Bu, B. Ma, H. Jiao, X. Cheng, Z. Wang, Research on the mechanical stability of high laser resistant coatings on lithium triborate crystal, Appl. Opt., 56 (2017) C117-C122.

[124] N. Kaiser, H. Uhlig, U. Schallenberg, B. Anton, U. Kaiser, K. Mann, E. Eva, High damage threshold Al2O3SiO2 dielectric coatings for excimer lasers, Thin Solid Films, 260 (1995) 86-92.

[125] L.L. Snead, K.J. Leonard, G.E. Jellison, M. Sawan, T. Lehecka, Irradiation Effects on Dielectric Mirrors for Fusion Power Reactor Application, Fusion Science and Technology, 56 (2009) 1069-1077.

[126] M.L. Grilli, F. Menchini, A. Piegari, D. Alderighi, G. Toci, M. Vannini, Al2O3/SiO2 and HfO2/SiO2 dichroic mirrors for UV solid-state lasers, Thin Solid Films, 517 (2009) 1731-1735.

[127] E.O. Filatova, A.S. Konashuk, F. Schaefers, V.V. Afanas' ev, Metallization-induced oxygen deficiency of γ-Al2O3 layers, The Journal of Physical Chemistry C, 120 (2016) 8979-8985.

[128] S. Toyoda, T. Shinohara, H. Kumigashira, M. Oshima, Y. Kato, Significant increase in conduction band discontinuity due to solid phase epitaxy of Al2O3 gate insulator films on GaN semiconductor, Applied Physics Letters, 101 (2012) 231607.

[129] M. Mende, I. Balasa, H. Ehlers, D. Ristau, D.-b. Douti, L. Gallais, M. Commandré, Relation of optical properties and femtosecond laser damage resistance for Al2O3/AlF3 and Al2O3/SiO2 composite coatings, Appl. Opt., 53 (2014) A383-A391.

[130] L. Gallais, H. Krol, J.-Y. Natoli, M. Commandre, M. Cathelinaud, L. Roussel, M. Lequime, C. Amra, Laser damage resistance of silica thin films deposited by electron beam deposition, ion assisted deposition, reactive low voltage ion plating and dual ion beam sputtering, Thin Solid Films, 515 (2007) 3830-3836.

[131] L. Wang, Y. Jiang, C. Jiang, H. Liu, Y. Ji, F. Zhang, R. Fan, D. Chen, Effect of oxygen flow rate on microstructure properties of SiO2 thin films prepared by ion beam sputtering, Journal of Non-Crystalline Solids, 482 (2018) 203-207.

[132] T. Yamane, N. Nagai, S.-i. Katayama, M. Todoki, Measurement of thermal conductivity of silicon dioxide thin films using a 3ω method, Journal of applied physics, 91 (2002) 9772-9776.

[133] H. Liu, Y. Jiang, D. Liu, S. Li, X. Yang, Y. Ji, Y. Cui, Thermal effect on microstructure vibration of SiO2 thin films, Vibrational Spectroscopy, 96 (2018) 101-105.
[134] M. Alvisi, G. De Nunzio, M.R. Perrone, A. Rizzo, S. Scaglione, L. Vasanelli, Influence of the assisting-ion-beam parameters on the laser-damage threshold of SiO2 films, Thin Solid Films, 338 (1999) 269-275.
[135] H. Liu, L. Wang, Y. Jiang, S. Li, D. Liu, Y. Ji, F. Zhang, D. Chen, Study on SiO2 thin film modified by post hot isostatic pressing, Vacuum, 148 (2018) 258-264.
[136] M. Lappschies, M. Jupé, D. Ristau, Extension of ion beam sputtered oxide mixtures into the UV spectral range, in: Optical Interference Coatings, Optical Society of America, 2007, pp. TuA7.
[137] O. Stenzel, S. Wilbrandt, M. Schürmann, N. Kaiser, H. Ehlers, M. Mende, D. Ristau, S. Bruns, M. Vergöhl, M. Stolze, M. Held, H. Niederwald, T. Koch, W. Riggers, P. Burdack, G. Mark, R. Schäfer, S. Mewes, M. Bischoff, M. Arntzen, F. Eisenkrämer, M. Lappschies, S. Jakobs, S. Koch, B. Baumgarten, A. Tünnermann, Mixed oxide coatings for optics, Appl. Opt., 50 (2011) C69-C74.
[138] R. Rauhut, K. Nehls, L. Mechold, Characterization of HfO2-SiO2 rugate multilayers deposited by ion beam sputtering, in: SPIE Laser Damage, SPIE, 2014, pp. 6.
[139] N.K. Sahoo, S. Thakur, R.B. Tokas, Achieving superior band gap, refractive index and morphology in composite oxide thin film systems violating the Moss rule, Journal of Physics D: Applied Physics, 39 (2006) 2571-2579.
[140] A. Feldman, E.N. Farabaugh, W.K. Haller, D.M. Sanders, R.A. Stempniak, Modifying structure and properties of optical films by coevaporation, Journal of Vacuum Science & Technology A, 4 (1986) 2969-2974.
[141] C. Gouldieff, F. Wagner, L. Jensen, M. Mende, J.-Y. Natoli, D. Ristau, Oxide mixtures for UV coatings, in: SPIE Laser Damage, SPIE, 2012, pp. 9.
[142] S. Chao, W.-H. Wang, M.-Y. Hsu, L.-C. Wang, Characteristics of ion-beam-sputtered high-refractive-index TiO2-SiO2 mixed films, J. Opt. Soc. Am. A, 16 (1999) 1477-1483.
[143] C.-C. Lee, C.-J. Tang, TiO2-Ta2O5 composite thin films deposited by radio frequency ion-beam sputtering, Appl. Opt., 45 (2006) 9125-9131.
[144] S. Kičas, U. Gimževskis, S. Melnikas, Post deposition annealing of IBS mixture coatings for compensation of film induced stress, Opt. Mater. Express, 6 (2016) 2236-2243.
[145] C.J. Stolz, M.D. Thomas, A.J. Griffin, BDS thin film damage competition, in: Laser-Induced Damage in Optical Materials: 2008, International Society for Optics and Photonics, 2008, pp. 71320C.
[146] W. Rudolph, L. Emmert, Z. Sun, D. Patel, C. Menoni, Laser damage in dielectric films: What we know and what we don't, in: Laser-Induced Damage

in Optical Materials: 2013, International Society for Optics and Photonics, 2013, pp. 888516.

[147] B.C. Stuart, M.D. Feit, S. Herman, A. Rubenchik, B. Shore, M. Perry, Nanosecond-to-femtosecond laser-induced breakdown in dielectrics, Physical review B, 53 (1996) 1749.

[148] T. Walker, A. Guenther, P. Nielsen, Pulsed laser-induced damage to thin-film optical coatings-part I: experimental, IEEE Journal of Quantum Electronics, 17 (1981) 2041-2052.

[149] T. Walker, A. Guenther, P. Nielsen, Pulsed laser-induced damage to thin-film optical coatings - Part II: Theory, IEEE Journal of Quantum Electronics, 17 (1981) 2053-2065.

[150] D. Milam, R. Bradbury, M. Bass, The role of inclusions and linear absorption in laser damage to dielectric mirrors, NBS Laser Induced Damage in Opt. Mater, 1973 p 124-132(SEE N 74-20083 11-16), (1973).

[151] A.S. Foster, F.L. Gejo, A. Shluger, R.M. Nieminen, Vacancy and interstitial defects in hafnia, Physical Review B, 65 (2002) 174117.

[152] C.J. Stolz, R.J. Tench, M.R. Kozlowski, A. Fornier, Comparison of nodular defect seed geometries from different deposition techniques, in: 27th Annual Boulder Damage Symposium: Laser-Induced Damage in Optical Materials: 1995, International Society for Optics and Photonics, 1996, pp. 374-383.

[153] Z. Wu, C.J. Stolz, S.C. Weakley, J.D. Hughes, Q. Zhao, Damage threshold prediction of hafnia–silica multilayer coatings by nondestructive evaluation of fluence-limiting defects, Appl. Opt., 40 (2001) 1897-1906.

[154] M. Zhu, K. Yi, D. Li, X. Liu, H. Qi, J. Shao, Influence of SiO2 overcoat layer and electric field distribution on laser damage threshold and damage morphology of transport mirror coatings, Optics Communications, 319 (2014) 75-79.

[155] J. Dijon, G. Ravel, B. Andre, Thermomechanical model of mirror laser damage at 1.06 um: II. Flat bottom pits formation, SPIE, 1999.

[156] J. DiJon, T. Poiroux, C. Desrumaux, Nano absorbing centers: a key point in the laser damage of thin films, SPIE, 1997.

[157] J.F. DeFord, M.R. Kozlowski, Modeling of electric-field enhancement at nodular defects in dielectric mirror coatings, in: Optical Materials for High Power Lasers, SPIE, 1993, pp. 18.

[158] R.H. Sawicki, C.C. Shang, T.L. Swatloski, Failure characterization of nodular defects in multilayer dielectric coatings, in: Laser-Induced Damage in Optical Materials: 1994, SPIE, 1995, pp. 11.

[159] R. Chow, S. Falabella, G.E. Loomis, F. Rainer, C.J. Stolz, M.R. Kozlowski, Reactive evaporation of low-defect density hafnia, Appl. Opt., 32 (1993) 5567-5574.

[160] C.J. Stolz, J.E. Wolfe, P.B. Mirkarimi, J.A. Folta, J.J. Adams, M.G. Menor, N.E. Teslich, R. Soufli, C.S. Menoni, D. Patel, Defect insensitive 100 J/cm2 multilayer mirror coating process, SPIE, 2013.

[161] C.J. Stolz, J.E. Wolfe, J.J. Adams, M.G. Menor, N.E. Teslich, P.B. Mirkarimi, J.A. Folta, R. Soufli, C.S. Menoni, D. Patel, High laser-resistant multilayer mirrors by nodular defect planarization, Appl. Opt., 53 (2014) A291-A296.
[162] C.J. Stolz, J.E. Wolfe, P.B. Mirkarimi, J.A. Folta, J.J. Adams, M.G. Menor, N.E. Teslich, R. Soufli, C.S. Menoni, D. Patel, Substrate and coating defect planarization strategies for high-laser-fluence multilayer mirrors, Thin Solid Films, 592 (2015) 216-220.
[163] C.J. Stolz, J.R. Taylor, Damage threshold study of ion-beam-sputtered coatings for a visible high-repetition laser at LLNL, SPIE, 1993.
[164] M. Jupé, M. Lappschies, L. Jensen, K. Starke, D. Ristau, Improvement in laser irradiation resistance of fs- dielectric optics using silica mixtures, SPIE, 2007.
[165] J.H. Apfel, Optical coating design with reduced electric field intensity, Appl. Opt., 16 (1977) 1880-1885.
[166] G. Abromavicius, R. Buzelis, R. Drazdys, A. Melninkaitis, V. Sirutkaitis, Influence of electric field distribution on laser-induced damage threshold and morphology of high-reflectance optical coatings, in: Boulder Damage Symposium XXXIX: Annual Symposium on Optical Materials for High Power Lasers, SPIE, 2007, pp. 8.
[167] Z. Meiqiong, S. Jianda, Temperature fields of 355 nm HR coatings based on the interface absorption model, Journal of Physics D: Applied Physics, 41 (2008) 045306.
[168] LLE, Near-Ultraviolet Absorption Annealing in HfO2 Thin Films Subjected to Continuous-Wave Laser Irradiation, in: M. Bartczys (Ed.) LLE Review, LLE, 2014, pp. 135-138.
[169] M.R. Kozlowski, Large area laser conditioning of dielectiic thin film mirrors, SPIE, 1990.
[170] F. Dai, W. Shi, B. Yang, W. Huang, Study on Laser Conditioning Parameters of HfO2/SiO2 Mul tilayer Mirrors, Advances in Materials Physics and Chemistry, 7 (2017) 242.
[171] C.J. Stolz, L.M. Sheehan, S.M. Maricle, S. Schwartz, J. Hue, Laser conditioning methods of hafnia-silica multilayer mirrors, SPIE, 1999.
[172] C. Xu, H. Dong, L. Yuan, H. He, J. Shao, Z. Fan, Investigation of annealing effects on the laser-induced damage threshold of amorphous Ta2O5 films, Optics & Laser Technology, 41 (2009) 258-263.
[173] H. Liu, Y. Jiang, L. Wang, S. Li, X. Yang, C. Jiang, D. Liu, Y. Ji, F. Zhang, D. Chen, Effect of heat treatment on properties of HfO2 film deposited by ion-beam sputtering, Optical Materials, 73 (2017) 95-101.
[174] L. Wang, H. Liu, Y. Jiang, X. Yang, D. Liu, Y. Ji, F. Zhang, D. Chen, Effects of hot-isostatic pressing and annealing post-treatment on HfO2 and Ta2O5 films prepared by ion beam sputtering, Optik - International Journal for Light and Electron Optics, 142 (2017) 33-41.

[175] C. Wang, Y. Jin, D. Zhang, J. Shao, Z. Fan, A comparative study of the influence of different post-treatment methods on the properties of HfO2 single layers, Optics & Laser Technology, 41 (2009) 570-573.
[176] D. Zhang, C. Wang, P. Fan, X. Cai, G. Liang, J. Shao, Z. Fan, Influence of substoichiometer on the laser-induced damage characters of HfO2 thin films, Applied Surface Science, 255 (2009) 4646-4649.
[177] J. Yao, J. Shao, H. He, Z. Fan, Effects of annealing on laser-induced damage threshold of TiO2/SiO2 high reflectors, Applied Surface Science, 253 (2007) 8911-8914.
[178] G.J. Ockenfuss, R.E. Klinger, Ultra-low-stress thin-film interference filters, Appl. Opt., 45 (2006) 1364-1367.
[179] S.L. Prins, A.C. Barron, W.C. Herrmann, J.R. McNeil, Effect of stress on performance of dense wavelength division multiplexing filters: optical properties, Appl. Opt., 43 (2004) 626-632.
[180] D.J. Reiley, R.A. Chipman, Coating-induced wave-front aberrations: on-axis astigmatism and chromatic aberration in all-reflecting systems, Appl. Opt., 33 (1994) 2002-2012.
[181] G. Abadias, E. Chason, J. Keckes, M. Sebastiani, G.B. Thompson, E. Barthel, G.L. Doll, C.E. Murray, C.H. Stoessel, L. Martinu, Review Article: Stress in thin films and coatings: Current status, challenges, and prospects, Journal of Vacuum Science & Technology A, 36 (2018) 020801.
[182] Y. Pauleau, Residual stresses in physically vapor-deposited thin films, in: H. Singh Nalwa (Ed.) Handbook of Thin Films, Academic Press, Burlington, 2002, pp. 455-522.
[183] D.W. Hoffman, M.R. Gaerttner, Modification of evaporated chromium by concurrent ion bombardment, Journal of Vacuum Science and Technology, 17 (1980) 425-428.
[184] J.J. Cuomo, J.M.E. Harper, C.R. Guarnieri, D.S. Yee, L.J. Attanasio, J. Angilello, C.T. Wu, R.H. Hammond, Modification of niobium film stress by low-energy ion bombardment during deposition, Journal of Vacuum Science and Technology, 20 (1982) 349-354.
[185] F.M. D'Heurle, J.M.E. Harper, Note on the origin of intrinsic stresses in films deposited via evaporation and sputtering, Thin Solid Films, 171 (1989) 81-92.
[186] H. Windischmann, Intrinsic stress in sputter-deposited thin films, Critical Reviews in Solid State and Materials Sciences, 17 (1992) 547-596.
[187] H. Windischmann, An intrinsic stress scaling law for polycrystalline thin films prepared by ion beam sputtering, Journal of applied physics, 62 (1987) 1800-1807.
[188] C.-J. Tang, C.-C. Jaing, K.-S. Lee, C.-C. Lee, Residual stress in Ta2O5-SiO2 composite thin-film rugate filters prepared by radio frequency ion-beam sputtering, Appl. Opt., 47 (2008) C167-C171.

[189] R. Thielsch, A. Gatto, N. Kaiser, Mechanical stress and thermal-elastic properties of oxide coatings for use in the deep-ultraviolet spectral region, Appl. Opt., 41 (2002) 3211-3217.

[190] O. Stenzel, M. Schürmann, S. Wilbrandt, N. Kaiser, A. Tünnermann, M. Mende, H. Ehlers, D. Ristau, S. Bruns, M. Vergöhl, W. Riggers, M. Bischoff, M. Held, Optical and mechanical properties of oxide UV coatings, prepared by PVD techniques, in: SPIE Optical Systems Design, SPIE, 2011, pp. 10.

[191] E. Randel, A. Davenport, A. Markosyan, R. Bassiri, M.M. Fejer, C.S. Menoni, Ultra-low Stress SiO2 Ion Beam Deposition Coatings, in: Optical Interference Coatings Conference (OIC) 2019, Optical Society of America, Santa Ana Pueblo, New Mexico, 2019, pp. WC.5.

[192] W.-H. Wang, S. Chao, Annealing effect on ion-beam-sputtered titanium dioxide film, Opt. Lett., 23 (1998) 1417-1419.

[193] Z. Qiao, Y. Pu, H. Liu, K. Luo, G. Wang, Z. Liu, P. Ma, Residual stress and laser-induced damage of ion-beam sputtered Ta2O5/SiO2 mixture coatings, Thin Solid Films, 592 (2015) 221-224.

[194] B.J. Pond, J.I. DeBar, C.K. Carniglia, T. Raj, Stress reduction in ion beam sputtered mixed oxide films, Appl. Opt., 28 (1989) 2800-2805.

[195] C. Technology, in.

[196] C.E.C. GmbH, Operation Manual Deposition System "IBS@LAB", Cutting Edge Coatings GmbH, Hannover, Germany, 2009.

[197] I.O.f. Standardization, Lasers and laser-related equipment -- Determination of laser-induced damage threshold of optical surfaces -- Part 1: 1-on-1 test, in, International Organization for Standardization, 2000.

[198] Z. Yan, W. Liao, Y. Zhang, X. Xiang, X. Yuan, Y. Wang, F. Ji, W. Zheng, L. Li, X. Zu, Optical characterization and laser damage of fused silica optics after ion beam sputtering, Optik, 125 (2014) 756-760.

[199] H.Y. Peng, M. Devarajan, T.T. Lee, Comparison of argon and oxygen plasma treatments on LED chip bond pad for wire bond application, Int. J. Sci. Eng. Res, 5 (2014) 908-912.

[200] J. Huang, H. Liu, F. Wang, X. Ye, L. Sun, X. Zhou, Z. Wu, X. Jiang, W. Zheng, D. Sun, Influence of bulk defects on bulk damage performance of fused silica optics at 355 nm nanosecond pulse laser, Opt. Express, 25 (2017) 33416-33428.

[201] C.J. Stolz, M. Caputo, A.J. Griffin, M.D. Thomas, BDS thin film UV antireflection laser damage competition, in: Laser-Induced Damage in Optical Materials: 2010, International Society for Optics and Photonics, 2010, pp. 784206.

[202] K. Guo, Y. Wang, R. Chen, M. Zhu, K. Yi, H. He, J. Shao, Effects of ion beam etching of fused silica substrates on the laser-induced damage properties of antireflection coatings at 355 nm, Optical Materials, 90 (2019) 172-179.

[203] X. Li, M. Gross, K. Green, B. Oreb, J. Shen, Ultraviolet laser-induced damage on fused silica substrate and its sol-gel coating, Opt. Lett., 37 (2012) 2364-2366.
[204] S. Schiller, G. Beister, W. Sieber, G. Schirmer, E. Hacker, Influence of deposition parameters on the optical and structural properties of TiO2 films produced by reactive d.c. plasmatron sputtering, Thin Solid Films, 83 (1981) 239-245.
[205] M.F. Al-Kuhaili, S.M.A. Durrani, I.A. Bakhtiari, M.A. Dastageer, M.B. Mekki, Influence of hydrogen annealing on the properties of hafnium oxide thin films, Materials Chemistry and Physics, 126 (2011) 515-523.
[206] J.-W. Park, D.-K. Lee, D. Lim, H. Lee, S.-H. Choi, Optical properties of thermally annealed hafnium oxide and their correlation with structural change, Journal of Applied Physics, 104 (2008) 033521.
[207] N.-W. Pi, M. Zhang, J. Jiang, A. Belosludtsev, J. Vlček, J. Houška, E.I. Meletis, Microstructure of hard and optically transparent HfO2 films prepared by high-power impulse magnetron sputtering with a pulsed oxygen flow control, Thin Solid Films, 619 (2016) 239-249.
[208] Y. Xie, Z. Ma, Y. Su, Y. Liu, L. Liu, H. Zhao, J. Zhou, Z. Zhang, J. Li, E. Xie, The influence of mixed phases on optical properties of HfO2 thin films prepared by thermal oxidation, Journal of Materials Research, 26 (2011) 50-54.
[209] M. Modreanu, J. Sancho-Parramon, O. Durand, B. Servet, M. Stchakovsky, C. Eypert, C. Naudin, A. Knowles, F. Bridou, M.F. Ravet, Investigation of thermal annealing effects on microstructural and optical properties of HfO2 thin films, Applied Surface Science, 253 (2006) 328-334.
[210] M. Vargas, N.R. Murphy, C.V. Ramana, Structure and optical properties of nanocrystalline hafnium oxide thin films, Optical Materials, 37 (2014) 621-628.
[211] Q. Du, W. Wang, S. Li, D. Zhang, W. Zheng, Effects of substrate temperature on the structural, optical and resistive switching properties of HfO2 films, Thin Solid Films, 608 (2016) 21-25.
[212] S. Papernov, Mechanisms of near-ultraviolet, nanosecond-pulse–laser damage in HfO2/SiO2-based multilayer coatings, Chin. Opt. Lett., 11 (2013) 010703-310709.
[213] S. Papernov, A.W. Schmid, Correlations between embedded single gold nanoparticles in SiO2 thin film and nanoscale crater formation induced by pulsed-laser radiation, Journal of Applied Physics, 92 (2002) 5720-5728.
[214] A.V. Tikhonravov, M.K. Trubetskov, G.W. DeBell, On the accuracy of optical thin film parameter determination based on spectrophotometric data, in: Advanced Characterization Techniques for Optics, Semiconductors, and Nanotechnologies, International Society for Optics and Photonics, 2003, pp. 190-200.
[215] T. Tolenis, M. Gaspariūnas, M. Lelis, A. Plukis, R. Buzelis, A. Melninkaitis, Assessment of effective-medium theories of ion-beam sputtered

Nb_2O_5–SiO_2 and ZrO_2–SiO_2 mixtures, Lithuanian Journal of Physics, 54 (2014).

[216] G.G. Stoney, The tension of metallic films deposited by electrolysis, Proceedings of the Royal Society of London. Series A, Containing Papers of a Mathematical and Physical Character, 82 (1909) 172-175.

[217] X. Fu, M. Commandré, L. Gallais, M. Mende, H. Ehlers, D. Ristau, Laser-induced damage in composites of scandium, hafnium, aluminum oxides with silicon oxide in the infrared, Appl. Opt., 53 (2014) A392-A398.

[218] J. Wang, R.L. Maier, H. Schreiber, Crystal phase transition of HfO_2 films evaporated by plasma-ion-assisted deposition, Appl. Opt., 47 (2008) C189-C192.

[219] J. Gao, G. He, B. Deng, D.Q. Xiao, M. Liu, P. Jin, C.Y. Zheng, Z.Q. Sun, Microstructure, wettability, optical and electrical properties of HfO_2 thin films: Effect of oxygen partial pressure, Journal of Alloys and Compounds, 662 (2016) 339-347.

[220] C. Xu, Y. Qiang, Y. Zhu, T. Zhai, L. Guo, Y. Zhao, J. Shao, Z. Fan, Laser-induced damage threshold at different wavelengths of Ta_2O_5 films annealed over a wide temperature range, Vacuum, 84 (2010) 1310-1314.

[221] X.Y. Qiu, Q.M. Liu, F. Gao, L.Y. Lu, J.-M. Liu, Room-temperature weak ferromagnetism of amorphous $HfAlO_x$ thin films deposited by pulsed laser deposition, Applied Physics Letters, 89 (2006) 242504.

[222] Y. Zhao, Y. Wang, H. Gong, J. Shao, Z. Fan, Annealing effects on structure and laser-induced damage threshold of Ta_2O_5/SiO_2 dielectric mirrors, Applied Surface Science, 210 (2003) 353-358.

[223] V. Edlmayr, M. Moser, C. Walter, C. Mitterer, Thermal stability of sputtered Al_2O_3 coatings, Surface and Coatings Technology, 204 (2010) 1576-1581.

[224] S. Jakschik, U. Schroeder, T. Hecht, M. Gutsche, H. Seidl, J.W. Bartha, Crystallization behavior of thin ALD-Al_2O_3 films, Thin Solid Films, 425 (2003) 216-220.

SANTRAUKA

SANTRUMPŲ SĄRAŠAS

AFM	Atominių jėgų mikroskopas, **A**tomic **F**orce **M**icroscope
AR	Skaidrinanti (danga), **AntiR**eflective
CRD	Gestančio impulso rezonatoriuje (metodas) **C**avity **R**ing **D**own
EBE	Elektronpluoštis garinimas, **E**lectron **B**eam **E**vaporation
FS	Lydytas kvarcas, **F**used **S**ilica
HR	Aukšto atspindžio (danga), **H**igh **R**eflective
H	Aukšto lūžio rodiklio, **H**igh refractive index
IBS	Jonapluoštis dulkinimas, **I**on **B**eam **S**puttering
L	Žemo lūžio rodiklio, **L**ow refractive index
LID	Lazeriu indukuota pažaida, **L**aser **I**nduced **D**amage
LIDT	Lazeriu indukuotas pažaidos slenkstis, **L**aser **I**nduced **D**amage **T**hreshold
RMS	Standartinis nuokrypis, **R**oot **M**ean **S**quared
T	Pralaidumas, **T**ransmittance
UV	Ultravioleto (spektrinis ruožas), **U**ltra**v**iolet
XRD	Rentgeno spindulių difrakcijos analizė, **X**-**R**ay **D**iffraction

Įvadas

Optinės interferencinės dangos yra naudojamos daugumoje optinių sistemų, pradedant nuo akinių lęšių ir baigiant sudėtingiausiomis lazerinėmis sistemomis. Tyrimai šioje srityje prasidėjo jau nuo pat R. Maiman lazerio sukūrimo 1960 metais [2]. Viena iš labiausiai tiriamų ir tobulinamų optinių dangų savybių tapo atsparumas lazerio spinduliuotei. 1969 metais Boulderyje (JAV) buvo pradėtas organizuoti kasmetinis simpoziumas „Lazerio indukuota pažaida optinėse medžiagose“, kuris vyksta ligi šiol. Konferencijos metu optinių dangų, medžiagų ir lazerinių sistemų tyrėjų bendruomenė dalinasi naujausiomis žiniomis ir tyrimų pasiekimais medžiagų, plonų sluoksnių lazerinės pažaidos modeliavimo, matavimo bei tobulinimo srityse. Taip pat yra aptariamos kitos svarbios dangų savybės ir jų sąveika, tokios kaip mikrostruktūra, mechaniniai įtempiai, optiniai nuostoliai, atsparumas ultratrumpiems impulsams ir t.t.

Pirmieji optiniai pagrindukai buvo padengti plonais metalo sluoksniais jau XIX a. naudojant garinimo bei kondensacijos metodus, o XX a. viduryje metalų oksidų sluoksniai buvo formuojami naudojant reaktyvaus garinimo technologiją. Sudėtingesnių dengimo procesų, tokių kaip magnetroninis dulkinimas, ar dulkinimas jonų pluoštu (IBS – *ion beam sputtering*) technologijų užuomazgos siekia 1852 m., kai Velso fizikas W.R. Grove suformavo geležies oksido sluoksnį ant sidabro plokštelės. Iki 1932 metų jau buvo paskelbta daugiau nei šimtas publikacijų, susijusių su plonų sluoksnių ir optinių dangų tyrimais, taip pat jau buvo pradėta sluoksnių nusodinimo dulkinimo būdu sistemų komercinė gamyba. Jau tada buvo pastebėta, jog dulkinimo būdu suformuotos dangos pasižymėjo geresne adhezija, mechaniniu patvarumu, buvo ilgaamžiškesnės nei dangos, nusodintos iš tirpalo ar galvazinavimo būdu. Modernių IBS sistemų prototipai atsirado 1975 m., kai plataus pluošto jonų šaltiniai buvo pritaikyti plonų sluoksnių nusodinimui [10]. Šie šaltiniai buvo sukurti 1960 m. vystant jonų pluoštų varomųjų jėgų sistemas kosmoso taikymams [11]. Viena iš esminių priežasčių, nulėmusių jonapluoščio dulkinimo proceso panaudojimą optinių dangų formavimui buvo dielektrinių veidrodžių, pasižyminčių labai mažais optiniais nuostoliais, poreikis konstruojant lazerinius giroskopus. Nors IBS proceso metu pasiekiama sluoksnių formavimo sparta buvo maža, tačiau jis tuo pačiu pasižymėjo maža tarša, taip pat neatsirasdavo dangų pažeidimai dėl elektrinių iškrovų, bei buvo galima formuoti dangas be papildomo optinių pagrindukų kaitinimo. Pagrindiniai pranašumai, lyginant su tuo metu egzistuojančiomis dengimo technologijomis buvo amorfinė sluoksnių struktūra, maži optiniai nuostoliai, mažas porėtumas, labai geras atsparumas aplinkos poveikiui. Didelis šio proceso stabilumas bei efektyvi proceso kintamųjų kontrolė įgalino sėkmingai formuoti tokias sudėtingas dangas, kaip interferenciniai filtrai, čirpuoti veidrodžiai ir pan. Dėl visų aukščiau išvardintų privalumų, IBS technologija šiuo metu yra plačiai pripažinta ir naudojama precizinių optinių dangų formavimui, pasižyminčių dideliu stabilumu, ilgaamžiškumu, atsparumu lazerinei spinduliuotei, skirtų naudoti tiek įprastose, tiek ekstremaliose aplinkose, tokiose kaip kosminė erdvė. Nepaisant to, nuolatinis lazerinių sistemų tobulinimas kelia vis naujus, sudėtingesnius reikalavimus optinėms dangoms, nuo kurių iš esmės priklauso visos lazerio ar optinės sistemos parametrai ir jos funkcionavimas. IBS technologija turi tokių trūkumų, kaip dideli mechaniniai įtempiai suformuotose dangose. Įtempiai keičia optinių komponentų plokštiškumą, o tai gali tapti nepageidaujamų lazerio pluošto iškraipymų lazerinėse sistemose priežastimi.

P. Franken ir kolegos naudodami rubino lazerį, pirmą kartą pademonstravo lazerinę spinduliuotę ultravioletiniame (UV) spektriniame ruože (λ = 347nm). 1966 m. buvo jau diskutuojama apie galimybes panaudoti inertinių dujų žadinimą norint generuoti fundamentaliąją lazerinę spinduliuotę UV diapazone. Eksperimentiškai tai buvo pademonstruota 1970 metais, sukuriant eksimerinį lazerį. Šiuo metu lazerinė UV spinduliuotė yra naudojama įvairiose srityse, tokiose kaip litografija, elektronika, mikroapdirbimas, biomedicina, spektroskopija, chemija ir pan. Dėl ženkliai didesnės fotonų energijos trumpesnių bangų ruože, tokie lazerio impulsai suteikia tokių naujų unikalių galimybių, kaip efektyvesnė sąveika su medžiaga, geresnis pluošto fokusavimas. Tačiau, tuo pačiu tai kelia papildomų iššūkių naudojamų lazerinių komponentų charakteristikoms bei ilgaamžiškumui.

Disertacijoje dėmesys yra skiriamas keletui JD technologija suformuotų dielektrinių dangų, skirtų UV spektriniam ruožui, aspektų. Visų pirma, yra tiriamas lydyto kvarco pagrindukų, kurie yra neatsiejama UV diapazonui skirtų optinių komponentų dalis, plazminis ėsdinimas, bei jo pritaikymas didinant skaidrių optinių komponentų atsparumą lazerio spinduliuotei. Antra, yra tiriamos metalo oksido mišinių panaudojimo daugiasluoksnių optinių dangų struktūroje kombinavimo galimybės kartu su atkaitinimu aukštose temperatūrose, sukeliančiose pokyčius sluoksnių mikrostruktūroje, siekiant pagerinti dangų optines bei atsparumo 266 nm lazerio spinduliuotei. Trečia, yra tiriama dvikomponenčių HfO_2, Sc_2O_3 ir Al_2O_3 mišinių savybių pokyčiai nuo jų sudėties bei atkaitinimo plačiame temperatūrų ruože, ieškant potencialių kombinacijų, tinkamų daugiasluoksnių dangų UV diapazone su kompensuotais įtempiais formavimui.

Disertacijos darbo tikslas

Išplėsti jonapluoščio dulkinimo būdu suformuotų optinių dangų panaudojimo galimybes UV spektriniame ruože, optimizuojant pagrindukų paviršiaus plazminį apdirbimą, medžiagų mišinių dulkinimo technologijas, suformuotų dangų terminio atkaitinimo procesus.

Sprendžiami uždaviniai

1. Padidinti pagrindukų optinį atsparumą UV lazerinei spinduliuotei pritaikius ėsdinimą argono plazma ir nepabloginant jų paviršiaus charakteristikų.
2. Sukurti pagrindukų paviršiaus modifikavimo ir paruošimo didelio atsparumo optinių dangų dengimui metodiką, naudojant mažų energijų deguonies plazmą.
3. Padidinti HfO_2 ir skirtingų HfO_2-SiO_2 mišinių pagrindu suformuotų aukšto atspindžio dangų atsparumą lazerinei UV spinduliuotei, optimizuojant terminio atkaitinimo procesą.
4. Ištirti dvikomponenčių HfO_2, Sc_2O_3 ir Al_2O_3 mišinių sluoksnių optines, paviršiaus savybes, mechaninius įtempius, bei jų kitimą naudojant atkaitinimą plačiame temperatūrų ruože ir įvertinti šios metodikos taikymo galimybes daugiasluoksnių dangų UV diapazonui su kompensuotais įtempiais kūrimui.

Darbo mokslinis naujumas ir praktinė svarba

Mokslinis naujumas

1. Pirmą kartą buvo tiriamas lydyto kvarco pagrindukų ėsdinimas mažų jonų energijų deguonies plazma, keičiant ėsdinimo gylį ir plazmos jonų energijas. Taikant nustatytas optimalias vertes, buvo pademonstruotas ženklus ėsdinto FS pagrinduko paviršiaus lazerio indukuotos pažaidos slenksčio padidinimas, kurio vertės yra palyginamos su tūriniu LIDT.
2. Pademonstruotas ženklus dielektrinių veidrodžių 266 nm bangos ilgiui LIDT bei optinių savybių pagerinimas panaudojus hafnio-silicio oksidų mišinių bei aukštų temperatūrų atkaitinimą, lemiantį šių sluoksnių kristalizaciją.
3. Nustatyta, jog atitinkamos sudėties HfO_2, Sc_2O_3 ir Al_2O_3 dvikomponenčiai mišiniai, panaudojus atitinkamas atkaitinimo temperatūras, yra tinkami sukurti daugiasluoksnes dangas UV

spektriniam diapazonui su kompensuotais įtempiais bei sumažintais optiniais nuostoliais.

Praktinė svarba

1. Išvystyta lydyto kvarco pagrindukų ėsdinimo argono bei deguonies plazma metodika, padedanti sukurti didelio optinio atsparumo skaidrius optinius komponentus, skirtus didelės galios UV lazerinėms sistemoms. Dalis tyrimų buvo atliekama bendradarbiaujant su UAB Altechna Coatings, rezultatai yra naudojami optinių komponentų gamybos procese.
2. Pademonstruotas aukštos temperatūros atkaitinimo, indukuojančio HfO_2-SiO_2 mišinių sluoksnių kristalizaciją, efektyvumas, leidžiantis daugiau nei 2 kartais padidinti 266nm lazerio spinduliuotei skirtų dielektrinių veidrodžių LIDT, taip pat išlaikant didelius atspindžio koeficientus. Nustatytos galimos HfO_2-Al_2O_3, Sc_2O_3-Al_2O_3 ir HfO_2-Sc_2O_3 dvikomponenčių mišinių sudėtys ir atkaitinimo temperatūros, leidžiančios vystyti kompensuotų įtempių daugiasluoksnes dangas UV spektriniam ruožui su sumažintais optiniais nuostoliais. Šios žinios ypatingai svarbios Lietuvos lazerinių optinių dangų gamintojams projektuojant ir gaminant optinius komponentus UV diapazonui.

Ginamieji teiginiai

1. Taikant optimizuotą lydyto kvarco pagrindukų paviršiaus ėsdinimą argono plazma, žymiai padidinamas jų atsparumas lazerinei UV (355 nm) spinduliuotei, nepabloginus jų paviršiaus optinių charakteristikų.
2. Mažų energijų deguonies plazmos taikymas lydyto kvarco pagrindukų paruošimui ir modifikavimui prieš dengiant optines dangas padidina suformuotų optinių komponentų atsparumą nanosekundiniams UV (355 nm) lazerio impulsams 2-3 kartus.
3. Optimizuoto atkaitinimo proceso taikymas HfO_2 ir HfO_2-SiO_2 mišinių pagrindu suformuotiems aukšto atspindžio optiniams komponentams padidina jų atsparumą UV (266 nm) lazerio spinduliuotei 2.5-3 kartus.
4. Keičiant dvikomponenčių HfO_2, Sc_2O_3 ir Al_2O_3 mišinių sudėtį bei atkaitinimo temperatūras, suformuojami reikalingo dydžio įtempių sluoksniai, tinkami daugiasluoksnių optinių dangų UV spektriniam diapazonui su kompensuotais įtempiais projektavimui ir gamybai.

Aprobacija

Mokslinės publikacijos, tiesiogiai susijusios su disertacijos tema (žurnaluose, referuojamuose CA WoS duomenų bazėje)

1. K. Juškevičius, R. Buzelis, **G. Abromavičius**, S. Abbas, A. Belosludtsev, R. Drazdys, S. Kičas, “Argon plasma etching of fused silica substrates for manufacturing high laser damage resistance optical interference coatings,“ Optical Materials Express, **7** (10), 2017.
2. **G. Abromavičius**, T. Juodagalvis, R. Buzelis, K. Juškevičius, R. Drazdys, S. Kičas, “Oxygen plasma etching of fused silica substrates for high power laser optics”, Applied Surface Science, **453**, 2018.
3. **G. Abromavičius**, S. Kičas, R. Buzelis, “High temperature annealing effects on spectral, microstructural and laser damage resistance properties of sputtered HfO_2 and HfO_2-SiO_2 mixture-based UV mirrors”, Optical Materials **95**, 2019.
4. **G. Abromavičius**, T. Juodagalvis, “Mechanical stress, optical and surface properties of high temperature annealed HfO_2, Sc_2O_3 and Al_2O_3 binary mixture thin films deposited by ion beam sputtering”, pateikta į Optical Materials.

Kitos mokslinės publikacijos

1. **G. Abromavičius**, N. Kyžas, A. Belosludtsev “Oxygen plasma etching of YAG crystals”, Proc. SPIE, Advances in Optical Thin Films VI, **10691**, 2018.
2. **G. Abromavičius**, L. Grinevičiūtė, R. Buzelis, S. Kičas, A. Melninkaitis, E. Pupka, T. Tolenis, “High LIDT mirrors for 355nm wavelength based on combined ion beam sputtering and glancing angle deposition technique”, Proc. SPIE, Laser-Induced Damage in Optical Materials, **10447**, 2017.
3. A. Melninkaitis, L Grinevičiūtė, **G. Abromavičius**, L. Mažulė, L. Smalakys, E. Pupka, M. Ščiuka, R. Buzelis, S. Kičas, T. Tolenis, “Next-generation all-silica coatings for UV applications”, Proc. SPIE, Laser-Induced Damage in Optical Materials, **10447**, 2017.
4. **G. Abromavičius**, R. Buzelis, R. Drazdys, K. Juškevičius, S. Kičas, T. Tolenis, J. Mirauskas, M. Ščiuka, V. Sirutkaitis, A. Melninkaitis, “Optical resistance and spectral properties of anti-reflective coatings

deposited on LBO crystals by ion beam sputtering”, Lithuanian Journal of Physics, **51** (4), 2011.

5. K. Starke, L. O. Jensen, M. Jupé, D. Ristau, **G. Abromavičius**, K. Juškevičius, R. Buzelis, R. Drazdys, “Investigation in oxide mixture coatings with adapted gradient index profiles”, Proc. SPIE, Laser-Induced Damage in Optical Materials, **7504**, 2009.
6. **G. Abromavičius**, R. Buzelis, R. Drazdys, A. Melninkaitis, V. Sirutkaitis. “Influence of electric field distribution on laser induced damage threshold and morphology of high reflectance optical coatings”, Proc. SPIE, Laser-Induced Damage in Optical Materials, **6720**, 2007.
7. **G. Abromavičius**, R. Buzelis, R. Drazdys, A. Melninkaitis, D. Mikšys, V. Sirutkaitis, A. Skrebutėnas, “Improvement of optical properties and radiation resistance of optical coatings based on Nb_2O_5 and Ta_2O_5”, Proc. SPIE, Advanced Optical Materials, Technologies, and Devices, **6596**, 2007.
8. A. Melninkaitis, D. Mikšys, V. Sirutkaitis, **G. Abromavičius,** R. Buzelis, R. Drazdys, “Laser-induced damage threshold measurements of high reflecting dielectric layers”, Proc. SPIE, Advanced Optical Materials, Technologies, and Devices, **6596**, 2007.
9. **G. Abromavičius**, R. Buzelis, R. Drazdys, A. Melninkaitis, D. Miksys, V. Sirutkaitis, A. Skrebutėnas, R. Juškėnas, A. Selskis, “The microstructure and LIDT of Nb_2O_5 and Ta_2O_5 optical coatings”, Proc. SPIE, Laser-Induced Damage in Optical Materials, **6403**, 2006.
10. **G. Abromavičius**, R Buzelis, R. Drazdys, R. Grigonis, A. Melninkaitis, D. Mikšys, T. Rakickas, V. Sirutkaitis, A. Skrebutėnas, R. Juškėnas, A. Selskis, “Influence of ion-assisted deposition on laser-induced damage threshold and microstructure of optical coatings”, Proc. SPIE, Laser-Induced Damage in Optical Materials, **5991**, 2006.
11. A. Melninkaitis, D. Mikšys, T. Balčiūnas, V. Sirutkaitis, A. Skrebutėnas, R. Buzelis, R. Drazdys, **G. Abromavičius**, “Effect of substrate temperature and ion assistance on nanosecond laser-induced damage threshold in high reflection dielectric coatings”, Proc. SPIE, Laser-Induced Damage in Optical Materials, **5991**, 2006.
12. A. Melninkaitis, M. Maciulevičius, T. Rakickas, D. Mikšys, R. Grigonis, V. Sirutkaitis, A. Skrebutėnas, R. Buzelis, R. Drazdys, **G. Abromavičius**, “Comparison of optical resistance of ion assisted deposition and standard electron beam deposition methods for high

reflectance dielectric coatings", Proc. SPIE, Advances in Optical Thin Films II, **5963**, 2005.

Pranešimai konferencijose, tiesiogiai susiję su disertacijos tema

1. **G. Abromavičius**, T. Juodagalvis, R. Buzelis, S. Kičas and R. Drazdys, "Plasma treatment of fused silica substrates for enhancement of resistance to UV laser radiation", Optical Systems Design, Frankfurt, Germany, 2018.
2. **G. Abromavičius**, S. Kičas, "Post-deposition annealing of ion beam sputtered dielectric mirrors based on hafnia-silica mixtures", Advanced Materials and Technologies, Palanga, Lithuania**,** 2018.
3. **G. Abromavičius**, S. Kičas, "Optical and surface properties of HfO_2-SiO_2 mixture based UV mirrors", Open Readings, Vilnius, 2018.
4. **G. Abromavičius**, T. Juodagalvis, R. Buzelis, S. Kičas and R. Drazdys, "Lydyto kvarco optinių pagrindukų ėsdinimo deguonies plazma taikymas formuojant didelės galios lazeriams skirtus optinius komponentus", Fizinių ir technologijos mokslų tarpdalykiniai tyrimai, Vilnius, Lithuania, 2018.
5. K. Juškevičius, R. Buzelis, R. Samuilovas, S. Abbas, **G. Abromavičius**, A. Puzas, R. Drazdys, "Plasma etching of fused silica substrates for manufacturing high laser damage resistance optical interference coatings", Optical Interference Coatings, Tucson, USA, 2016.

Pranešimai konferencijose, tiesiogiai nesusiję su disertacijos tema

1. **G. Abromavičius**, T. Tolenis, L. Grinevičiūtė, R. Buzelis, S. Kičas, A. Melninkaitis, E. Pupka, "High LIDT mirrors for 355nm wavelength based on combined ion beam sputtering and glancing angle deposition technique", SPIE Laser Damage, Boulder, 2017.
2. **G. Abromavičius**, T. Juodagalvis and R. Drazdys, "Optical and mechanical properties of Al_2O_3 thin films prepared by ion beam sputtering", Open Readings, Vilnius, 2017.
3. **G. Abromavičius**, R. Samuilovas, K. Juškevičius and R. Drazdys, "Al_2O_3 films prepared by reactive magnetron sputtering and their application for making dielectric mirrors", Advanced Materials and Technologies, Palanga, Lithuania**,** 2017.
4. **G. Abromavičius**, R. Drazdys, "Jonapluoščio dulkinimo būdu suformuotų metalo oksidų optinės savybės bei jų taikymas UV

spektrinio ruožo aukšto atspindžio optinių dangų formavimui”, LNFK, Vilnius, Lithuania, 2015.

Autoriaus asmeninis indėlis

Autorius pats atliko daugumos eksperimentų planavimą, arba kitais atvejais aktyviai dalyvavo juos planuojant. Jis taip pat pats suprojektavo ir suformavo visų dielektrinių UV veidrodžių dangas, atliko jų spektrofotometrinius, paviršiaus šiurkštumo matavimus bei visų gautų duomenų analizę. Disertantas aktyviai dalyvavo FS ėsdinimo mažos energijos deguonies plazma bei HfO_2, Sc_2O_3, Al_2O_3 dvikomponenčių mišinių eksperimentų duomenų analizėje. Autorius taip pat paruošė visas, tiesiogiai su disertaciją susijusias publikacijas (išskyrus pirmosios ruošimą, kuriame aktyviai dalyvavo kaip bendraautorius), o taip pat pristatė rezultatus mokslinėse konferencijose.

Bendraautorių indėlis

Tomas Juodagalvis atliko ėsdinimo mažos energijos plazma, HfO_2, Sc_2O_3 ir Al_2O_3 dvikomponenčių mišinių formavimo eksperimentus, taip pat atliko reikalingus matavimus.

Dr. Rytis Buzelis atliko LIDT bei CRD matavimus.

Dr. Vidas Pakštas atliko ir interpretavo XRD matavimus.

Dr. Simonas Kičas suteikė naudingų patarimų planuojant dielektrinių UV veidrodžių eksperimentus bei prisidėjo prie jų rezultatų interpretavimo.

Romanas Samuilovas ir Dr. Kęstutis Juškevičius iniciavo ėsdinimo argono plazma eksperimentų planavimą, analizavo gautus duomenis ir aktyviai dalyvavo ruošiant susijusią publikaciją.

Literatūros apžvalga

1 disertacijos skyriuje yra pateikiama literatūros apžvalga. Aptariamas optinių pagrindukų apdirbimas, poliravimo likučiai ir jų įtaka pagrindukų atsparumui lazerinei spinduliuotei, įvairūs papildomo apdirbimo metodai, įskaitant plazmos bei jonų technologijas. Toliau yra apibūdinama jonapluoščio dulkinimo technologija, jos fizikiniai pagrindai, pagrindiniai komponentai bei pagrindinės jonapluoščio dulkinimo būdu suformuotų dielektrinių dangų savybės. Sekančiuose poskyriuose yra pateikiamos pagrindinių UV spektrinio ruožo dangų formavimui naudojamų oksidų savybės. Toliau seka dielektrinių medžiagų mišinių optinių, mikrostruktūrinių bei mechaninių savybių apžvalga. Taip pat aprašomas dielektrinių dangų optinis atsparumas, įskaitant impulsinės pažaidos modelį, lazerinę pažaidą UV spektriniame diapazone bei pagrindinius metodus, skirtus didinti optinį dangų atsparumą. Paskutiniuose poskyriuose apibendrinami įtempiai, jų mechanizmai plonuose sluoksniuose ir optinėse dangose, bei pagrindinės įtempių modifikavimo metodikos.

Eksperimentinės metodikos

Eksperimentuose naudoti lydyto kvarco pagrindukai buvo plaunami ultragarsinėje plovyklėje UCS40 (Optimal Technologies).

Plazminis ėsdinimas buvo atliekamas naudojantis skirtingais radiodažniniais plazmos šaltiniais – PSC301 (Evatec AG) ir IS300 (CCR GmbH).

Ploni sluoksniai ir dangos buvo formuojamos jonapluoščio dulkinimo įrenginiu IBS-LAB (Cutting Edge Coatings GmbH). Terminis atkaitinimas buvo atliekamas naudojant SNOL 13/1100 krosnelę (Umega Group).

Optinės savybės buvo tirtos spektrofotometru bei panaudojus gęstančio impulso rezonatoriuje metodiką. Lūžio rodiklių, ekstinkcijos koeficientų dispersijos bei fiziniai storiai buvo nustatyti atliekant modeliavimą programiniu paketu OptiChar v.8.85.

Lazerio pažeistos vietos buvo analizuojamos optiniu mikroskopu Olympus BX bei Nikon Eclipse LV100 šviesaus bei tamsaus lauko režimuose.

Lazerio sukeltos pažaidos slenksčiai buvo matuojami naudojant 1-į-1 metodiką, 355 nm bei 266 nm ~2.5-3 ns trukmės impulsus. Testai buvo atlikti pagal kiek pakeistą metodiką, aprašytą ISO 21254-1, naudojant mikrofokuso artinį. Buvo panaudota lazerinės pažaidos matavimo sistema, sukurta Optinių Dangų Laboratorijoje.

Bandinių paviršiaus šiurkštumai bei pažeistų vietų kraterių gyliai buvo analizuoti atominių jėgų mikroskopu „Dimension Edge“ (Bruker).

Dangų rentgeno struktūrinė analizė buvo atlikta bendradarbiaujant su FTMC Medžiagų struktūros charakterizavimo skyriumi.

Įtempių įvertinimui buvo naudoti matavimų duomenys, gauti profilometru Dektak 150 (Veeco).

Detalesnė eksperimentinės metodikos informacija yra pateikta 2 skyriuje.

Rezultatai

Tezių rezultatai pateikiami tokiu būdu: A skyriuje yra pristatomi ir analizuojami FS pagrindukų ėsdinimo argono bei mažų energijų deguonies plazma rezultatai, jų taikymas kuriant padidinto optinio atsparumo skaidrius optinius komponentus UV spektriniam ruožui; B skyriuje yra analizuojama HfO_2-SiO_2 mišinių pagrindu suformuotų dielektrinių veidrodžių 266 nm bangos ilgiui atkaitinimo įtaka jų mikrostruktūrinėms, optinėms, bei LIDT savybėms; C skyriuje yra aptariama atkaitinimo įtaka HfO_2, Sc_2O_3 ir Al_2O_3 dvikomponenčių mišinių optinėms, paviršinėms savybėms, įtempiams, bei diskutuojama apie jų galimą taikymą kuriant daugiasluoksnes dangas UV diapazonui, pasižyminčias kompensuotais įtempiais.

A. Lydyto kvarco pagrindukų apdirbimas argono, deguonies plazmomis

Lydytas kvarcas yra plačiai naudojama medžiaga gaminti optinių komponentų, skirtų UV spektrinio diapazono lazerių pluoštų valdymui, pagrindukams. Pagrindukų gamybą sudaro įvairūs žingsniai – pjovimas, šlifavimas, poliravimas. Galutinis poliravimo procesas sukuria taip vadinamus Bilbio ir popaviršinių defektų sluoksnius, kurie ženkliai sumažina pralaidžių optinių komponentų atsparumą lazerinei UV spinduliuotei. Šio reiškinio priežastis yra minėtuose sluoksniuose esantys poliravimui naudotų medžiagų likučiai, kurie sugeria krintančią spinduliuotę.

Papildomas poliruoto pagrinduko paviršiaus apdorojimas jonais ar plazma yra vienas iš perspektyviausių metodų šalinant minėtus defektų sluoksnius, kadangi tai yra bekontaktis ir paviršiaus neteršiantis procesas (kai yra naudojami optimalūs proceso parametrai). Visgi, toks apdirbimas taip pat gali sukelti ir nepageidaujamus efektus, tokius kaip paviršiaus šiurkštumo padidėjimas, atominės gardelės deformacija, paviršinio sluoksnio sutankinimas, ypatingai jeigu yra naudojamos didelės jonų energijos. Dėl šių priežasčių, efektyvus sugeriančių popaviršinių defektų pašalinimas naudojant plazmą turi tuo pačiu nepabloginti kitų svarbių optinių pagrindukų parametrų.

FS pagrindukų, pagamintų to paties tiekėjo, ėsdinimas Ar plazma buvo atliktas naudojantis “RADIANCE” dulkinimo įrenginyje (Evatec AG), turinčiame radiodažninį (RF-*radio frequency*) plazmos šaltinį. Ėsdinimo procesas buvo atliekamas 0.23 Pa slėgyje, naudojant 1kW šaltinio galią. Iš pradžių buvo atliktos kalibravimo procedūros, kurių dėka buvo nustatyta ėsdinimo sparta. Tuomet buvo atlikti skirtingų gylių (20 nm, 50 nm, 100 nm, 200 nm ir 400 nm) ėsdinimai. Svarbu paminėti, kad kalibracijos metu buvo nustatyta ėsdinamo gylio paklaida neviršijo 7%. Norint išsiaiškinti, ar plazma apdorotas bandinių paviršius nebuvo galimai užterštas dėl plazmos šaltinyje esančio tinklelio erozijos, buvo atlikti keli ėsdinimo procesai, bei matuojamas bandinių pralaidumas 200 – 900 nm spektriniame diapazone Nustatytos pralaidumo vertės po plazminio apdorojimo praktiškai sutapo su neėsdintų pagrindukų charakteristikomis - tai rodo, jog jei ir buvo kažkokia nežymi paviršiaus tarša, jos nebuvo galima aptikti pagal pokyčius UV spektriniame ruože.

Vienas iš galimų nepageidaujamų optinių pagrindukų plazminio apdirbimo efektų yra jų paviršiaus optinės kokybės degradavimas, t.y. paviršiaus šiurkštumo didėjimas bei plokštiškumo mažėjimas. Atlikti matavimai (1 pav.) parodė, jog paklaidų ribose minėti parametrai nepablogėjo, lyginant su pradinėmis vertėmis, atskirais atvejais plokštiškumas net šiek tiek pagerėjo.

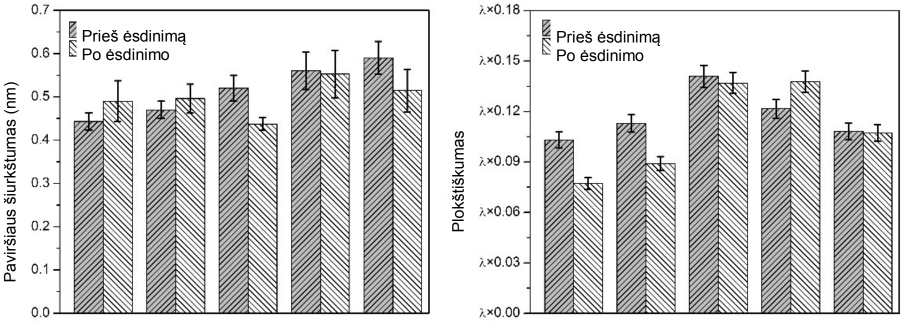

1 pav. FS pagrindukų paviršiaus šiurkštumo (a) bei plokštiškumo (b) verčių palyginimas prieš ir po ėsdinimo argono plazma. Plokštiškumo matavimui naudoto interferometro lazerio bangos ilgis buvo λ = 633 nm.

Atlikus atsparumo 355 nm bangos ilgio lazerinei spinduliuotei matavimus, buvo nustatyta, jog visi ėsdinti bandiniai pasižymėjo ~ 4 – 8 kartais didesnėmis LIDT vertėmis, lyginant su neapdorotais bandiniais (2 pav.). Didžiausias, 8 kartų pokytis buvo užfiksuotas plazma pašalinus 50 nm ir

100 nm storio sluoksnius. Reikia pabrėžti, jog komerciškai poliruotų pagrindukų atsparumai lazerio spinduliuotei yra priklausomi nuo konkretaus gamintojo ir jo naudojamų poliravimo technologijų, bei gali kisti nuo 5 J/cm^2 iki 22 J/cm^2. Dėl šios priežasties, bendru atveju skirtumai tarp neėsdinto ir plazma apdoroto pagrinduko LIDT verčių gali būti didesni, arba mažesni.

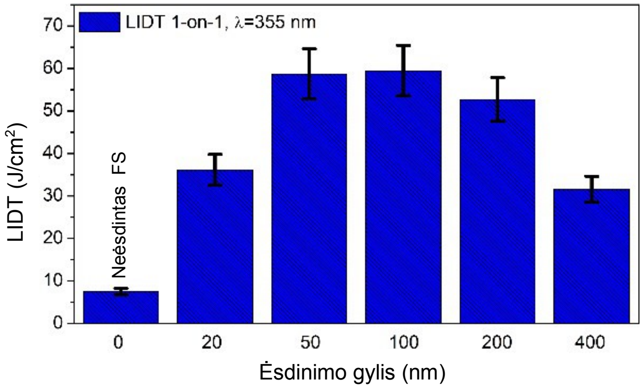

2 pav. Argono plazma ėsdintų bei neapdorotų FS pagrindukų LIDT palyginimas.

Nuėsdinus 400 nm storio sluoksnį, bandinių LIDT padidėjo du kartus mažiau, nei 50 nm bei 100 nm atvejais. Tai gali būti susiję su atsirandančia paviršiaus tarša dėl ilgesnės paviršiaus ėsdinimo trukmės. Keičiant plazmos tankį ir energiją, didinant galią galima padidinti ėsdinimo spartą. Visgi, ėsdinimas su ženkliai didesnių energijų Ar^+ plazma gali sukelti jonų implantavimą paviršiuje ir papildomų defektų sukūrimą. Pagrindukų ėsdinimai, naudojant skirtingus šio plazmos šaltinio režimus, nebuvo įtraukti į šios disertacijos darbų apimtį.

Sekančiame etape buvo nuspręsta pritaikyti gautus rezultatus pralaidžių optinių komponentų gamybai. Argono plazma apdoroti FS pagrindukai (ėsdinimo gylis 100 nm) buvo padengti skaidrinančia (AR) bei poliarizuojančia (Pol) dangomis. Abiejų tipų dangos yra pralaidžios 355 nm bangos ilgio spinduliuotei (Pol dangos atveju – P poliarizacijos šviesai), todėl krintantis lazerio impulsas sklinda kiaurai visą optinį komponentą. Jei ėsdinimo metu yra pašalinamas lazerinę spinduliuotę sugeriantis Bilbio sluoksnis, turėtų išaugti tokio komponento optinis atsparumas. Pasirinktos optinės dangos buvo suformuotos EBE technologija, naudojant HfO_2 bei SiO_2 medžiagas.

3 pav. parodyta šių dangų LID tikimybių kreivės. Abejais atvejais, naudojant argono plazma apdorotus pagrindukus, buvo užregistruotas didesnis nei dviejų kartų LIDT padidėjimas– 2.4 karto AR@ 355 dangai ir 2.1

karto Pol@ 355 dangai, lyginant su analogiškai padengtais plazma neapdorotais pagrindukais.

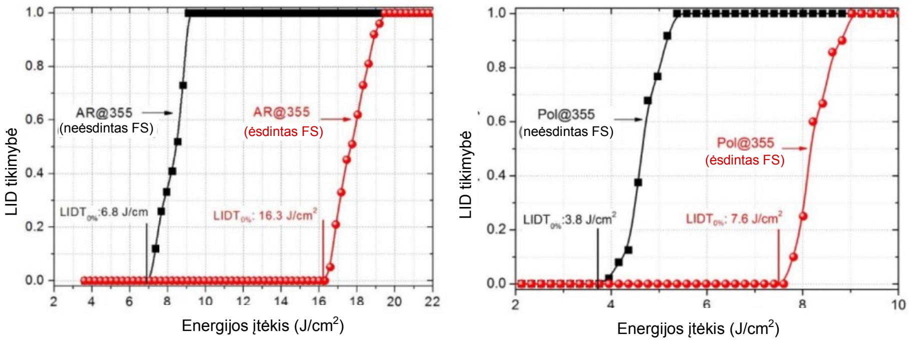

3 pav. AR@355 bei Pol@355 dangų, suformuotų ant neapdorotų, bei Ar$^+$ plazma ėsdintų pagrindukų, lazeriu indukuotos pažaidos tikimybinės kreivės.

FS pagrindukų bombardavimas Ar$^+$ jonais gali sukelti papildomų paviršiaus pažeidimų dėl atomų perstūmimo, spalvinių centrų ar gardelės defektų sukūrimo [198]. Ėsdinimas mažos energijos deguonies plazma tokiu atveju gali būti alternatyvi technologija. Juo labiau, O$^+$ jonai yra reaktyvūs, todėl taip pat efektyviai šalina nuo paviršiaus organinę taršą [199].

Sekantys FS pagrindukų ėsdinimo eksperimentai buvo atlikti naudojant mažų energijų (<300 eV) deguonies plazmą. Šiam tikslui buvo panaudotas RF plazminis šaltinis Copra IS300 (CCR Technology GmbH), įdiegtas elektronpluoščio garinimo kameroje Vera 1100 (VTD Vakuumtechnik Dresden GmbH). Pagrindukai buvo įtvirtinti 40 cm atstumu nuo šaltinio, plazmos kritimo kampas su bandinių paviršiaus normale sudarė apie 40 laipsnių.

Prieš atliekant eksperimentus, buvo išmatuoti plazmos energijų spektrai, keičiant šaltinio darbinius parametrus (4 pav.).

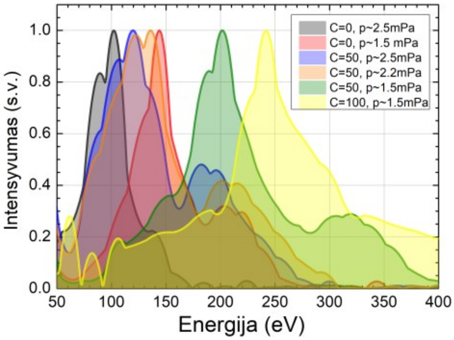

4 pav. Išmatuoti deguonies plazmos jonų energijų spektrai.

Copra IS300 šaltinio generuojama plazma nėra monoenergetinė. Yra matomi aiškūs maksimumai spektruose, kurių padėtys keičiasi nuo 100 eV iki 240 eV. Toliau tekste bus naudojamas terminas “plazmos energija”, kuris reikš tiesiog pagrindinio jonų energijų spektro maksimumo padėtį.

Pradinių eksperimentų tikslas buvo įvertinti skirtingų energijų deguonies plazmos įtaką ėsdintų pagrindukų paviršiaus šiurkštumui bei optiniam atsparumui. Visais atvejais išmatuotas 250 ± 30 nm gylio nuėsdintų FS pagrindukų paviršių šiurkštumo pokytis siekė apie 0.1 nm (5 pav. (a)). Pradinis pagrindukų šiurkštumas iš esmės nekinta, ir tokie pagrindukai yra pilnai tinkami formuoti optinius komponentus, skirtus lazerinėms sistemoms. 5 pav. (b) yra pavaizduoti LIDT matavimai 355 nm bangos ilgiui. Bandiniai, apdoroti 130 eV ir 140 eV energijos plazma pasižymėjo labai aukštomis LIDT vertėmis, atitinkamai 67 ± 3 J/cm^2 ir 75 ± 4 J/cm^2. Šios vertės yra palyginamos su [200] tyrime paskelbtomis lydyto kvarco tūrinio LIDT reikšmėmis, kurios siekė 70-90 J/cm^2, naudojant 1-į-1 testavimo metodiką, esant 9.3 ns trukmės impulsams. Konkurse, skirtame pasiekti kuo didesnį skaidrinančių dangų, optimizuotų $\lambda = 355$ nm bangos ilgiui, atsparumą [201], nustatytos nedengto FS pagrinduko vertės neviršijo 50 J/cm^2. Disertacijoje pademonstruotas ženklus plazma ėsdinto FS pagrinduko LIDT padidinimas greičiausiai yra susijęs su efektyviu popaviršiniame sluoksnyje esančių poliravimo likučių pašalinimu, tačiau reikia papildomai atlikti detalius cheminės analizės tyrimus, norint galutinai atsakyti į šį klausimą. Ėsdinimas naudojant didesnės energijos (200 eV bei 245 eV) deguonies plazmą neleido padidinti bandinių optinio atsparumo. Tai gali būti susiję su efektyvesniu volframo tinklelio dulkinimu ir tuo pačiu, jau pasireiškiančiu papildomu paviršiaus užteršimu, sukeliančiu krintančios lazerio spinduliuotės sugertį. Kita galima priežastis būtų didenių energijų jonų implantavimas, sukuriantis papildomus defektus Vėlgi, norint patikrinti šias hipotezes, reikalingi papildomi tyrimai [198].

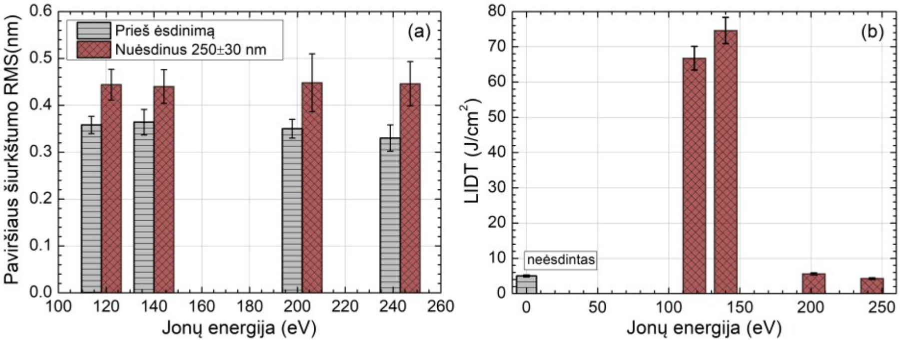

5 pav. Neėsdintų ir ėsdintų FS pagrindukų, naudojant skirtingos energijos deguonies plazmą, paviršiaus šiurkštumo RMS (a) ir LIDT (b).

Sekančiame etape, naudojant geriausiu rezultatu pasižymėjusį ėsdinimą 140 eV jonų energiją turinčia plazma, buvo varijuojamas ėsdinimo gylis. 6 pav. (a) parodyti paviršių šiurkštumai po 39 ± 4 nm ir 540 ± 20 nm gylių ėsdinimų, kurie vėlgi, iš esmės nepakito.

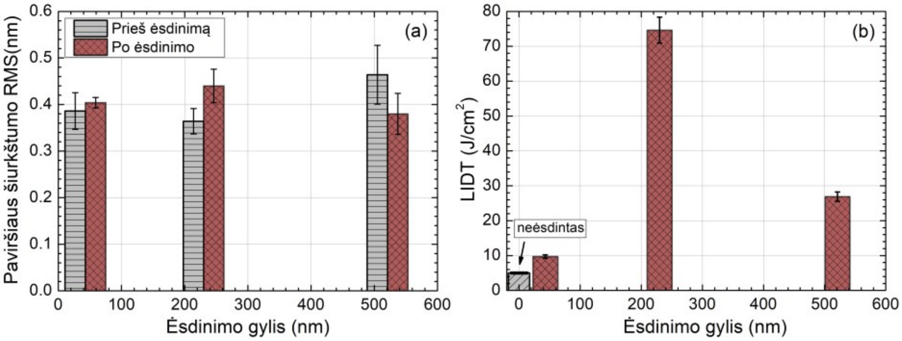

6 pav. Neėsdintų ir ėsdintų FS pagrindukų, naudojant 140 eV energijos plazmą ir keičiant ėsdinimo gylius, paviršiaus šiurkštumo RMS (a) ir LIDT (b).

6 pav. (b) atvaizduotos LIDT vertės, gautos nuėsdinus 39 ± 4 nm storio sluoksnį, yra 2 kartus didesnės nei plazma neapdoroto bandinio ir siekia 10 J/cm^2, o 540 ± 20 nm atveju yra 27 ± 1 J/cm^2. Šiuo atveju mažesnio ėsdinimo gylio gali neužtekti, kad efektyviai pašalinti poliravimo medžiagų likučius. Šią prielaidą patvirtina keleto mokslinių publikacijų rezultatai. Hongjie ir kt. atlikę tradicinio chemiškai-mechaniškai poliruoto Fs pagrinduko 30 nm storio pašalinimą jonais nustatė 10 kartų Fe ir Ce elementų koncentracijos sumažėjimą, tačiau atlikus ~ 60 nm gylio ėsdinimą, minėtų elementų koncentracija sumažėjo 100 kartų, lyginant su pradinėmis vertėmis [25]. Taip pat svarbu paminėti, kad Bilbio sluoksnio, kurį sudaro poliravimo medžiagų likučiai, storis gali stipriai skirtis, priklausomai nuo optinių pagrindukų gamintojo.

Siekiant patikrinti FS pagrindukų ėsdinimo mažos energijos deguonies plazma efektą galutiniam pralaidaus optinio komponento atsparumui lazerio spinduliuotei, neapdoroti, o taip pat plazma ėsdinti agrindukai buvo padengti AR dangomis, optimizuotomis $\lambda = 355$ nm bangos ilgiui. Al_2O_3 (d = 52 nm) and SiO_2 (d = 58 nm) sluoksniai buvo nusodinti naudojant IBS technologijos įrenginį. Suformuoti optiniai komponentai buvo papildomai atkaitinti $T = 300$ °C temperatūroje, siekiant užtikrinti pilną sluoksnių oksidaciją ir išvengti papildomų sugerties nuostolių pačioje dangoje.

7 pav. aiškiai matyti FS pagrinduko apdorojimo O^+ plazma efektas galutiniam komponento optiniam atsparumui. AR danga, suformuota ant

ėsdinto pagrinduko turėjo 3.4 kartus didesnį LIDT (14 ± 0.7 J/cm^2), lyginant su plazma neapdoroto pagrinduko atveju.

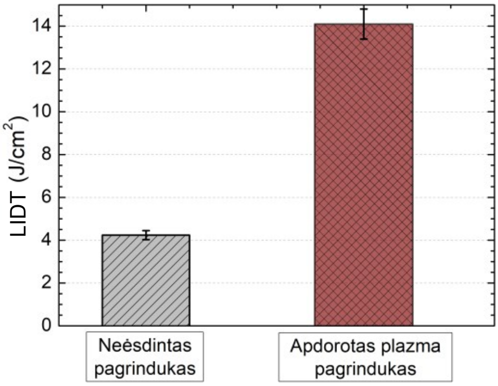

7 pav. AR dangų 355 nm bangos ilgiui, optinių atsparumų palyginimas. Dangos suformuotos ant neėsdinto bei ant deguonies plazma apdoroto (energija 140 eV, ėsdinimo gylis $d = 220 \pm 10$ nm) FS pagrindukų.

Pasiektas rezultatas yra palyginamas su zolių-gelių būdu suformuotų AR dangų atsparumu (19.5 J/cm^2, esant 8 ns trukmės impulsams), kurios buvo padengtos ant ėsdintų FS pagrindukų Li ir kt. tyrime [203]. Reikia paminėti, jog zolių-gelių metodas yra laikomas vienas iš didžiausią lazerinį atsparumą leidžiančių pasiekti skaidrinančių optinių dangų formavimo metodų.

Norint labiau suprasti gautus skirtumus tarp plazmos ėsdinimu paruošto ir neėsdinto skaidrinto optinio komponento atsparumų, optiniu mikroskopu buvo papildomai atlikta pažeistų vietų analizė. 8 pav. (a) pavaizduota AR danga padengto, plazma apdoroto pagrinduko pažeidimų krateriai esant skirtingoms lazerio impulsų energijoms, o (b) dalyje – tokio pat ta pačia danga dengto neėsdinto FS pagrinduko.

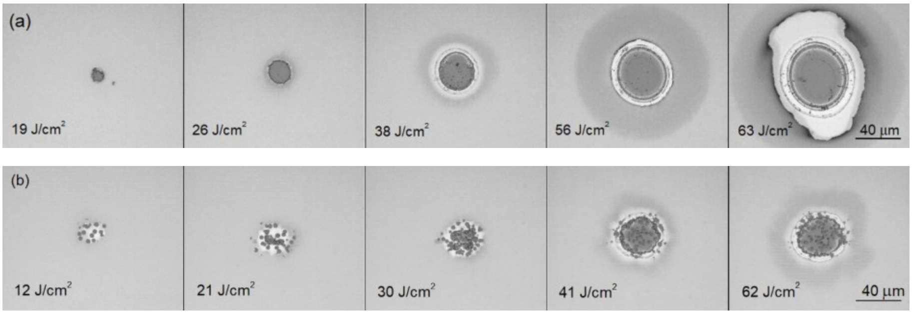

8 pav. Deguonies plazma ėsdinto (a) ir neėsdinto (b) pagrindukų, padengtų ta pačia skaidrinančia danga, optimizuota 355 nm bangos ilgiui, pažeistų vietų vaizdai.

Matyti, jog dangai, suformuotai ant plazma apdoroto pagrinduko, lazerio impulsai sukelia sluoksnių atšokimą, tuo tarpu neėsdinto pagrinduko atveju yra stebimi taškiniai pažeidimai, greičiausiai atsirandantys dėl lazerio energiją sugeriančių poliravimo likučių dalelių.

9 pav. pavaizduoti nustatyti pažeistų vietų gyliai pagrinduko paviršiaus atžvilgiu, esant skirtingoms impulsų energijoms. Gyliai buvo nustatyti naudojant kraterių AFM skenogramų duomenis.

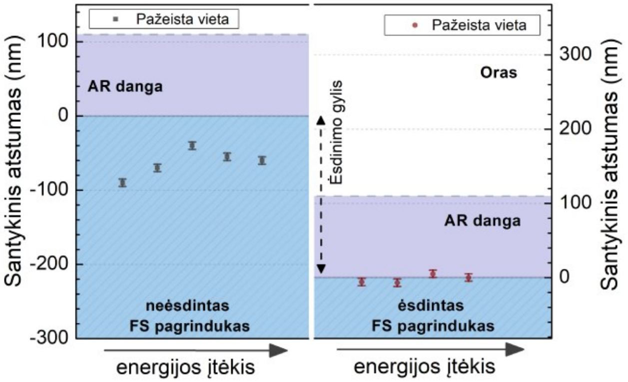

9 pav. Pažeistų vietų gylių palyginimas AR dangomis padengto neapdoroto, bei plazma ėsdinto FS pagrindukų atveju. Pirmu atveju lazerinių impulsų, sukėlusių pažeidimus energijos didėja nuo 12 J/cm^2 iki 62 J/cm^2, antruoju – nuo 19 J/cm^2 iki 62 J/cm^2.

Deguonies plazma prieš dangos suformavimą apdoroto pagrinduko atveju pažeidimas įvyksta dangos – pagrinduko sandūroje, kai tuo tarpu neėsdinto pagrinduko atveju lazerio impulsai yra sugeriami 40-80 nm gylyje po pagrinduko paviršiumi dėl likusių poliravimo medžiagų dalelių.

Atlikti tyrimai rodo, jog parinkus tinkamą ėsdinimo argono plazma gylį, FS pagrinduko optinis atsparumas padidinamas 4-8 kartus, o naudojant plazma apdorotus pagrindukus AR bei Pol dangų, optimizuotų 355 nm bangos ilgiui formavimui, jų atsparumas padidėja 2-3 kartus. Pritaikius ėsdinimo mažų energijų deguonies plazma metodiką, ir tokiu būdų pašalinus poliravimo medžiagų likučiais užterštą popaviršinį Bilbio sluoksnį, pralaidžių optinių komponentų atsparumas UV spektriniame ruože padidėja daugiau nei 3 kartus.

B. HfO_2-SiO_2 mišinių pagrindu suformuotų dielektrinių veidrodžių tyrimai

Hafnio oksidas yra plačiai naudojama aukšto lūžio rodiklio medžiaga, naudojama gaminant didelio optinio atsparumo komponentus aukštos galios UV lazerinėms sistemoms. Didelis draustinės juostos tarpas (5.6-6.2 eV) yra vienas iš esminių HfO_2 privalumų, tačiau šis parametras gali būti dar labiau padidintas maišant hafnio oksidą su didesnį draustinės juostos tarpą turinčiu silicio oksidu. Keletas atliktų studijų jau pademonstravo tokio metodo potencialą didinant daugiasluoksnių dangų, skirtų 355 nm lazerio spinduliuotei, atsparumą 1.7-2 kartus. Taip pat yra naudojamos ir kitos metodikos didinti dangų optinį atsparumą, taikomos po dangos formavimo, tokios kaip terminis atkaitinimas, ekspozicija deguonies plazmoje, kondicionavimas lazeriu. Terminis atkaitinimas yra vienas plačiausiai naudojamų būdų dėl savo paprastumo bei efektyvumo.

Jonapluoščio dulkinimo būdu suformuoti sluoksniai paprastai turi amorfinę mikrostruktūrą. Taikant atkaitinimą atitinkamose temperatūrose, galima sukelti sluoksnių kristalizaciją, kuri taip pat priklauso nuo konkrečios medžiagos bei sluoksnių storių. Keletas tyrimų, atliktų su plonais hafnio sluoksniais parodė, jog šios medžiagos draustinės juostos tarpas priklauso nuo jos mikrostruktūros. Jis yra šiek tiek didesnis kristalinėms fazėms ir mažesnis – amorfinėms. Kadangi nėra publikuotų tyrimų, susijusių su HfO_2 arba jo pagrindu suformuotų bei atkaitintų ir perėjusių į kristalinę fazę daugiasluoksnių dangų atsparumu UV spektrinio ruožo lazeriniams impulsams, buvo iškelta idėja suformuoti dielektrinius veidrodžius 266 nm bangos ilgiui, atlikti skirtingus kaitinimus išlaikant amorfinę, bei sukeliant aukšto lūžio rodiklio sluoksnių fazinį virsmą į kristalinę struktūrą, bei išanalizuoti šių dangų mikrostruktūrines, optines savybes bei LIDT.

Eksperimentinės dangos buvo suformuotos naudojantis IBS įrenginiu (Cutting Edge Coatings GmbH). Aukšto lūžio rodiklio medžiagų sluoksniams formuoti buvo pasirinktas grynas hafnio oksidas, o taip pat skirtingi HfO_2-SiO_2 mišiniai, turintys atitinkamai 82% ir 46% HfO_2 frakcijas. Pagrindiniai dangų duomenys yra apibendrinti 1 lentelėje.

1 lentelė. Pagrindiniai eksperimentinių veidrodžių duomenys.

Bandinio pavadinimas	H medžiaga	L medžiaga	Struktūra	H sluoksnio fizinis storis (nm)	L sluoksnio fizinis storis (nm)
Hf_100%	HfO_2	SiO_2	(HL)^12L	29	44
Hf_82%	82%HfO_2+18%SiO_2	SiO_2	(HL)^16L	32	44
Hf_46%	46%HfO_2+54%SiO_2	SiO_2	(HL)^23L	37	44

Pradiniai kaitinimo eksperimentai buvo skirti nustatyti temperatūrą, kurioje atkaitinus įvyksta dangų H medžiagos sluoksnių kristalizacija. Dėl skirtingų hafnio oksido koncentracijų skirtingų bandinių sluoksniuose, nustatyta kritinės temperatūros vertė buvo mažiausia gryno hafnio pagrindu suformuotai dangai, ir didžiausia - 46%HfO_2+54%SiO_2 mišinio pagrindu suformuotai dangai. Tuomet buvo paruoštas bandinių, atkaitintų trijose skirtingose temperatūrose, rinkinys: T_c–200 °C; T_c ir T_c+100 °C, kur T_c – atkaitinimo temperatūra, kuriai esant įvyko H medžiagos kristalizacija. Konkrečios atkaitinimo temperatūrų vertės kiekvieno bandinio atveju yra nurodytos 2 lentelėje.

2 lentelė. Atkaitinimo temperatūros, taikytos skirtingiems bandiniams.

Bandinio pavadinimas	T_c–200 °C	T_c	T_c+100 °C
Hf_100%	400	600	700
Hf_82%	700	900	1000
Hf_46%	800	1000	1100

Daugiasluoksnių dangų sklaidos nuostoliai gali priklausyti nuo sluoksnių mikrostruktūros, jų paviršiaus šiurkštumo [204]. 10 pav. pavaizduota visų bandinių XRD spektrai. Suformuotos dangos pasižymėjo amorfine struktūra. Gryno hafnio oksido sluoksniai Hf_100% veidrodžio struktūroje po atkaitinimo 600 °C temperatūroje perėjo į kristalinę kubinę fazę. Suformuotų mišinių pagrindu dangų atveju prireikė kur kas aukštesnių temperatūrų, kad jų mišinių sluoksniai kristalizuotųsi (T_c = 900 °C Hf_82% dangai ir T_c = 1000 °C Hf_46% dangai). Taip pat reikia paminėti, jog nustatytas hafnio oksido kristalinės būsenos fazės tipas skiriasi nuo kituose tyrimuose identifikuotos panašių atkaitintų dangų fazės, kuri buvo monoklininė [82, 116, 173].

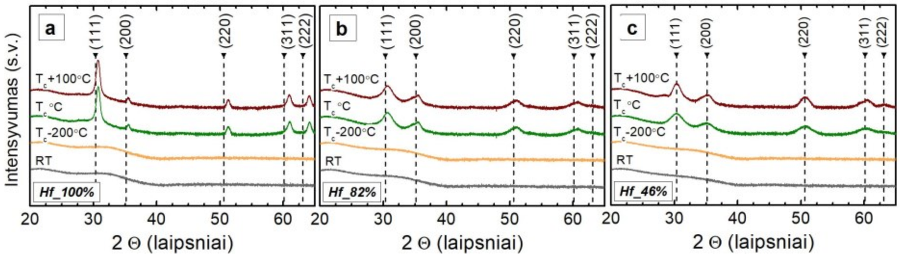

10 pav. Padengtų (RT) bei atkaitintų HR dangų XRD spektrai. Atkaitinimo temperatūrų vertės yra nurodytos 2 lentelėje.

Pagal XRD matavimus nustatyti kristalitų dydžiai yra pavaizduoti 11 pav.

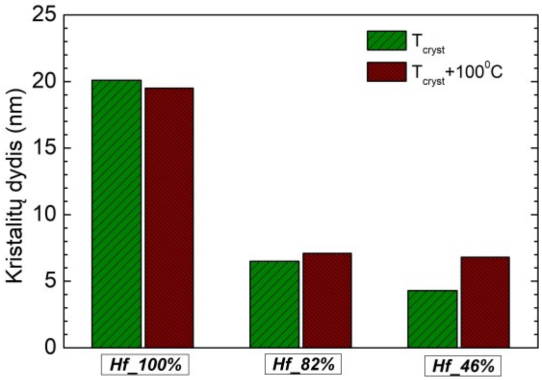

11 pav. Atkaitintų HR dangų, suformuotų naudojant gryną hafnio oksidą bei skirtingus jo mišinius su silicio oksidu, H medžiagos sluoksnių kristalitų dydžiai. Atkaitinimo temperatūrų vertės yra nurodytos 2 lentelėje.

Hf_100% dangų atveju, hafnio oksido sluoksnio kristalitų dydžiai siekė 20 nm. Mišinius savo struktūroje turinčių dangų atveju dėl esančios SiO_2 frakcijos susiformavę kristalitai siekė tik 6.8 nm ir 4.3 nm, atitinkamai Hf_82% ir Hf_46% bandiniams. Pastarosios dangos atveju po kaitinimo iki T_c+100 °C kristalitai padidėjo iki ~7 nm. Svarbu paminėti, jog lazerio spinduliuotę visiškai praleidžiančių daugiasluoksnių didelio storio UV dangų atveju, mažesni kristalitų dydžiai turėtų lemti mažesnius sklaidos nuostolius.

Eksperimentinių dangų paviršiaus šiurkštumo RMS vertės yra parodytos 12 pav., o tipinės amorfinių bei polikristalinių dangų AFM skenogramos – 13 pav.

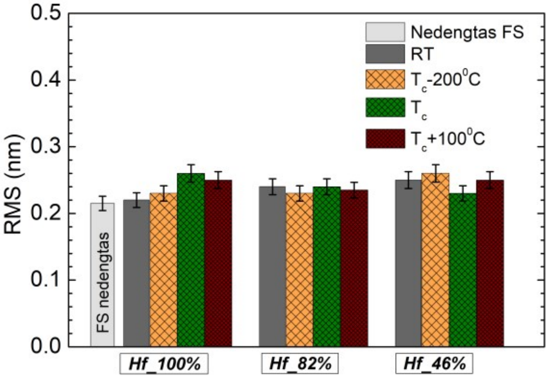

12 pav. Suformuotų bei atkaitintų HR dangų paviršiaus šiurkštumo RMS. Atkaitinimo temperatūrų vertės yra nurodytos 2 lentelėje.

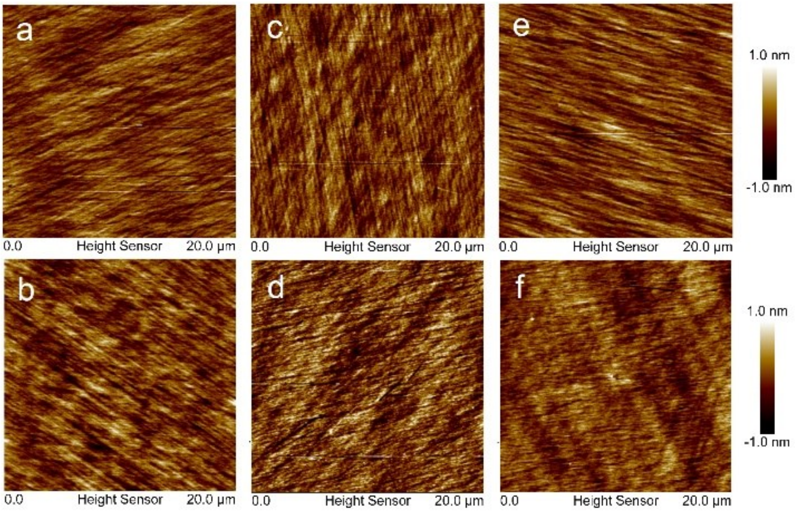

13 pav. Suformuotų Hf_100% (a), Hf_82% (c), Hf_46% (e), ir atkaitintų T_c temperatūrose Hf_100% (b), Hf_82% (d), Hf_46% (f) dangų paviršiaus AFM skenogramos. Atkaitinimo temperatūrų vertės yra nurodytos 2 lentelėje.

Galima pastebėti, jog nei vienos iš atkaitintų dangų paviršių glotnumas nepasikeitė, nepaisant įvykusios didelio lūžio rodiklio sluoksnių kristalizacijos. AFM skenogramose taip pat galima įžvelgti pagrinduko paviršiaus tekstūros atsikartojimą dangos paviršiuje, nepaisant įvykusio fazinio virsmo dangos sluoksniuose. Stebimo reiškinio priežastis gali būti išorinis SiO_2 sluoksnis, kuris išliko amorfinis po visų terminių atkaitinimų.

Bandinių pralaidumo spektrai yra pavaizduoti 14 pav.

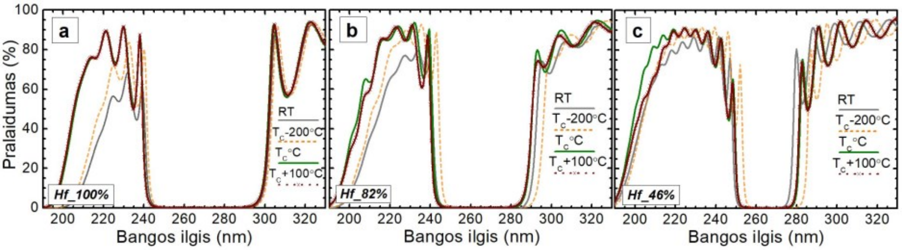

14 pav. Suformuotų (RT) ir atkaitintų HR dangų pralaidumo spektrai. Atkaitinimo temperatūrų vertės yra nurodytos 2 lentelėje.

Po atkaitinimo T_c−200 °C temperatūrose, visų dangų spektruose pralaidumas ~210-230 nm ruože didėja. Tai galima aiškinti sumažėjusia sugertimi dėl pagerėjusios stechiometrijos, kaip buvo nustatyta keliose studijose [82, 172, 177, 211]. Atkaitinus T_c temperatūrose, gaunamas ženklus pralaidumo padidėjimas ~200-240 nm diapazone. Čia didžiausias pokytis įvyko Hf_100% bandinio atveju (nuo $T = 10\%$ iki $T = 70\%$ ties $\lambda = 210$ nm). Atkaitinto $T = 500$ °C temperatūroje SiO_2 ekstinkcijos koeficientas yra keliomis eilėmis mažesnis ($k = 2 \cdot 10^{-4}$), lyginant su HfO_2 ($k = 2 \cdot 10^{-2}$), todėl pagrindinė padidėjusio pralaidumo priežastis yra pokyčiai hafnio bei hafnio-silicio mišinių sluoksniuose, įvykę atkaitinimo metu. Šie sluoksniai po terminio apdorojimo ir fazinio virsmo greičiausiai taip pat įgauna didesnės draustinės juostos plotį. Šiam paaiškinimui galutiniai patvirtinti reikėtų papildomų tyrimų, tačiau jis gerai atitinka publikuotus duomenis, rodančius, jog HfO_2 sluoksnių draustinės juostos plotis padidėja, įvykus kristalizacijai [206, 208, 209].

Eksperimentinių veidrodžių atspindžio vertės $\lambda = 266$ nm bangos ilgiui yra pateiktos 15 pav.

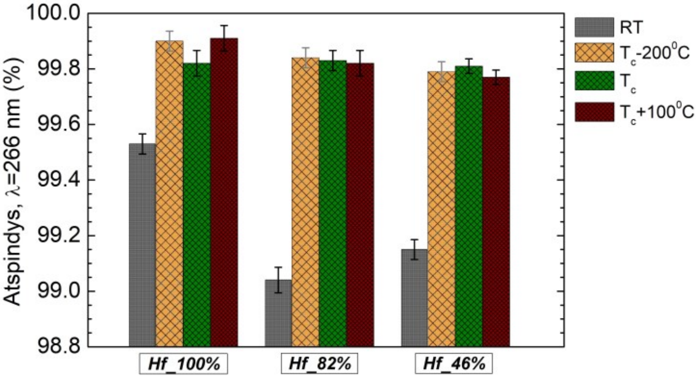

15 pav. Suformuotų (RT) bei atkaitintų HR dangų atspindžio vertės $\lambda = 266$ nm bangos ilgiui. Atkaitinimo temperatūrų vertės yra nurodytos 2 lentelėje.

Atkaitinimas T_c–200 °C temperatūrose visų dangų atveju lėmė atspindžio padidėjimą per 0.4% - 0.8%, kuris buvo didesnis mišinių pagrindu suformuotoms dangoms. Šis pokytis taip pat rodo, jog H medžiagų sluoksniuose kaitinimo metu mažėja sugertis. Likutiniai nuostoliai dangose susideda iš sklaidos ir likusios sugerties. Tai pat reikia pastebėti, jog pritaikius T_c kaitinimą, atsiradęs dangos sluoksnių kristališkumas nesumažino atspindžio verčių, todėl galima daryti prielaidą, jog šių polikristalinių dangų sklaida nėra didesnė nei amorfinių dangų.

Lazerio sukeltos pažaidos testų rezultatai (1-į-1) yra pateikti 16 pav.

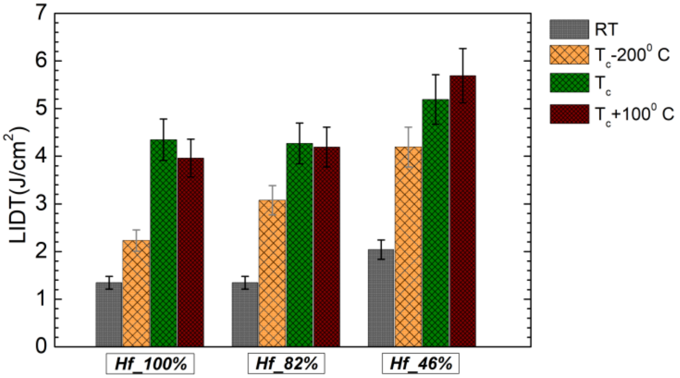

16 pav. Suformuotų (RT) bei atkaitintų HR dangų LIDT (1-į-1 testas) $\lambda = 266$ nm bangos lazerio impulsui. Atkaitinimo temperatūrų vertės yra nurodytos 2 lentelėje.

Hf_46% dielektrinis veidrodis pasižymėjo didžiausiu 2.0 ± 0.2 J/cm^2 optiniu atsparumu tarp suformuotų dangų, tikėtinai dėl didesnio draustinės juostos tarpo 46%HfO_2+54%SiO_2 mišinio sluoksniuose bei mažesnės sugerties. Gautas rezultatas atitinka mokslinėse publikacijose skelbtus hafnio-silicio oksidų mišinių dangų optinio atsparumo tendencijas, kalbant tiek apie vienasluoksnes [141], tiek apie daugiasluoksnes dangas [72, 116]. Santykinai panašūs skirtumai tarp skirtingų H medžiagų pagrindu suformuotų bandinių išliko po T_c–200 °C atkaitinimo, tik visų dangų LIDT vertės ženkliai padidėjo, mišinių atveju – net du kartus. Atkaitinus T_c temperatūrose, kuriose įvyko H medžiagų sluoksnių kristalizacija, Hf_100% dangos lazerinis atsparumas išaugo beveik 2 kartus (iki LIDT = 4.3 ± 0.4 J/cm^2), lyginant su T_c–200 °C bandiniu, ir tuo pačiu pasiekė Hf_82% (T_c) dangos optinį atsparumą. Pagal jau aptartus atspindžio koeficiento rezultatus galima daryti išvadą, jog optinė sugertis Hf_100% dangoje 266 nm bangos ilgiui jau nebesikeičia atkaitinus iki T_c, todėl viena iš galimų ženklaus LIDT išaugimo priežasčių gali būti padidėjęs hafnio oksido sluoksnių efektyvinės draustinės energijos juostos plotis įvykus kristalizacijai. Atkaitintų T_c temperatūroje Hf_82% bei Hf_46%

veidrodžių LIDT taip pat padidėjo per 20–40%, lyginant su T_c–200 °C variantais. Kaitinant dar aukštesnėse, T_c+100 °C temperatūrose, optinis dangų atsparumas paklaidų ribose jau nepasikeitė. Didžiausias 5.5 ± 0.6 J/cm^2 LIDT buvo išmatuotas Hf_46% dangai, atkaitintai iki T_c+100 °C. Nepaisant to, jog šiame tyrime nebuvo atlikti daugybinių impulsų atsparumo testai, pasiekti rezultatai rodo tokio metodo potencialą, kai yra kombinuojamas mišinių panaudojimas dangos struktūroje ir jos atkaitinimas aukštose temperatūrose, sukeliant kristalizaciją jos sluoksniuose.

Pažeistų Hf_100% and Hf_46% dangų vietų morfologijos yra pateiktos 17 pav. Pažeidimai, padaryti naudojant 4% - 7% didesnius lazerio impulso energijos įtėkius, nei LIDT vertės, yra parodyti a, e, c ir g paveiksliukuose. Kraterių, atsiradusių paveikus 21-29% didesnės energijos įtėkio impulsais, nei LIDT vertės, vaizdai yra pateikti b, f, d ir h. Matomas aiškus skirtumas lyginant gryno hafnio oksido bei $46\%HfO_2+54\%SiO_2$ mišinio pagrindu suformuotų dangų pažeidimus - Hf_100% atveju pažeidimai yra sukelti mikrono eilės dydžio defektų, kai tuo tarpu Hf_46% atveju yra stebimas dangos nusilupimas, kai tik impulsų energija vos viršija jos optinio atsparumo ribą. Morfologijos skirtumai taip pat yra matomi lyginant amorfinių, bei polikristalinių struktūrų pažeidimus, gautus veikiant ~30% didesnės energijos, nei LIDT, impulsams. Amorfinius hafnio oksido sluoksnius turinčios Hf_100% dangos pažeidimo kraterio dugnas yra glotnus (17 pav. (b)), kai tuo tarpu patyrusios kristalizaciją dangos kraterio dugno paviršius pasižymi granuline struktūra (17 pav. (d)). Hf_46% amorfinių bei kristalinių bandinių atveju skiriasi pažeidimo kraterių kraštai.

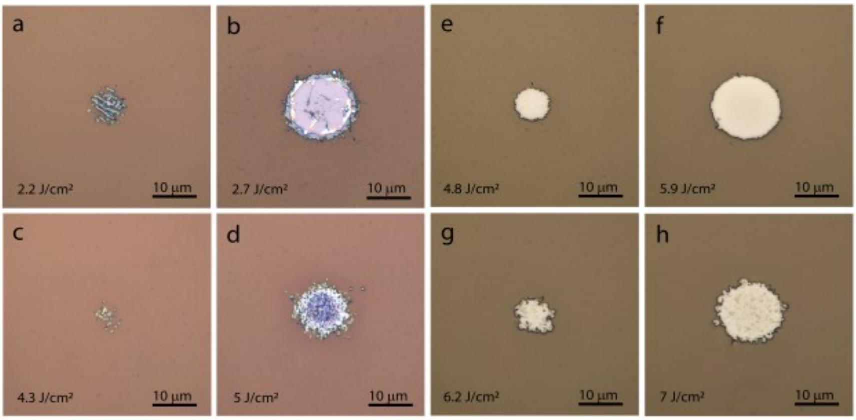

17 pav. Pažeidimų, veikiant skirtingos energijos įtėkių lazerio impulsais, morfologijos. Hf_100% danga, atkaitintos T_c-200 °C temperatūroje (a), (b); T_c (c), (d). Hf_46% danga, atkaitintos T_c-200 °C temperatūroje (e), (f); T_c (g), (h). Atkaitinimo temperatūrų vertės yra nurodytos 2 lentelėje.

Pažeistos šiek tiek didesnių (8–10%, lyginant su LIDT vertėmis) energijos įtėkių vietos buvo papildomai skenuotos atominių jėgų mikroskopu, siekiant nustatyti pažeidimų dangose gylį. 18 pav. e pavaizduota atkaitintoje amorfinėje (trumpo punktyro linija) bei kristalinėje (ilgo punktyro linija) Hf_100% dangoje išmatuoti pažeidimų gyliai, kartu su normuotu elektrinio lauko intensyvumo pasiskirstymu septyniuose išoriniuose dangos sluoksniuose.

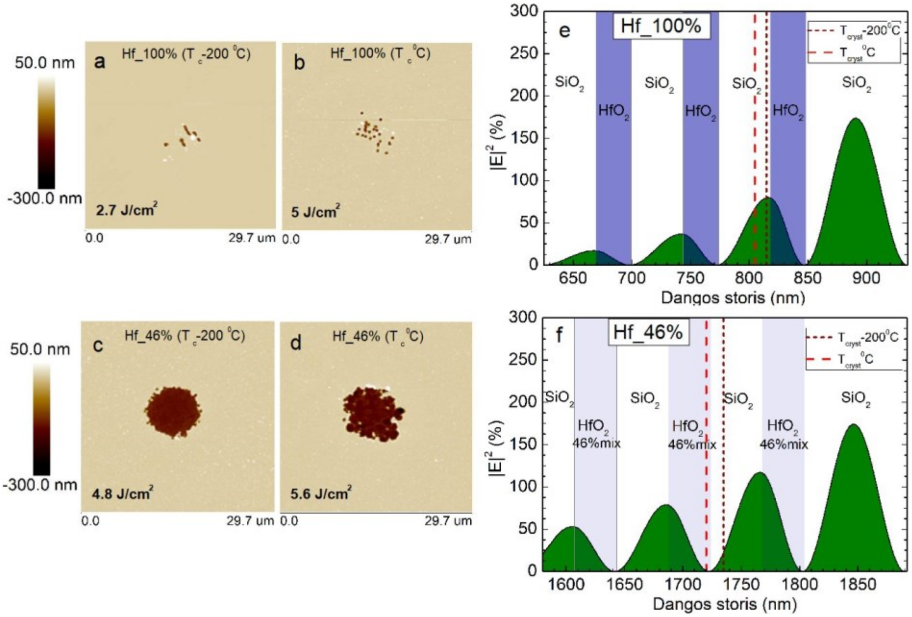

18 pav. Atkaitintų Hf_100% ir Hf_46% veidrodžių pažeidimų, sukeltų 7–17% didesnių energijų impulsais, lyginant su jų LIDT, pažeidimų morfologijų AFM skenogramos. Atkaitintas T_c–200 °C amorfinis Hf_100% bandinys (a), atkaitintas T_c ir polikristalinis Hf_100% (b). Atkaitintas T_c–200 °C amorfinis Hf_46% (c), atkaitintas T_c ir polikristalinis (d). Išmatuoti pažeistų vietų gyliai atkaitintos amorfinės Hf_100% dangos (trumpo punktyro linija) bei atkaitintos polikristalinės (ilgo punktyro linija) dangos atvejais pavaizduoti kartu su normuotu elektrinio lauko pasiskirstymu išoriniuose dangos sluoksniuose (e). Analogiškai, atkaitintų Hf_46% dangų atvejis pavaizduotas (f). Atkaitinimo temperatūrų vertės yra nurodytos 2 lentelėje.

Pažeidimų vietos abiejais atvejais praktiškai sutampa su antrąja HfO_2 ir SiO_2 sluoksnių sandūra, kurioje kaip tik yra elektrinio lauko intensyvumo maksimumas. Submikroninio dydžio atskirtų mikrokraterių morfologija rodo, jog šiuo atveju pažaidą greičiausiai inicijuoja nanometrinio dydžio absorbuojantys Hf metalo klasteriai, apie kuriuos buvo diskutuojama keliose publikacijose [156, 212, 213]. Hf_46% veidrodžio dangos kraterių gylių analizė analogišku principu yra pateikta 18 pav. f. Tiek atkaitintos amorfinės, tiek kristalinės dangos pažeidimų morfologija rodo, jog šiuo atveju minėtų metalo klasterių hafnio-silicio oksido mišinio sluoksniuose nėra, ir, eksponavus dangą 266 nm lazerio impulsu, įvyksta sluoksnių atsilupimas trečiojoje, SiO_2/HfO_2-SiO_2 sandūroje. Stebimą efektą sudėtinga paaiškinti, kadangi šiuo atveju pažeidimas įvyksta sluoksnių sandūroje, kurioje kaip tik yra elektrinio lauko intensyvumo minimumas. Norint nustatyti stebimo reiškinio priežastis, reikėtų atlikti papildomus eksperimentus ir tyrimus.

Atliktas tyrimas rodo puikias galimybes kurti ženkliai didesnio atsparumo daugiasluoksnes dielektrines dangas UV spektriniam diapazonui, jų konstrukcijai panaudojus hafnio-silicio oksidų mišinius bei suformuotų dangų atkaitinimą aukštose temperatūrose, tokiu būdu sukeliant kristalizaciją aukšto lūžio rodiklio medžiagos sluoksniuose.

C. HfO_2, Sc_2O_3 ir Al_2O_3 dvikomponenčių mišinių sluoksnių įtempių, optinių bei paviršinių savybių tyrimai

Jonapluoščio dulkinimo technologija įgalina suformuoti tankias, precizinių spektrinių savybių daugiasluoksnes dangas, pasižyminčias mažais optiniais nuostoliais, atsparumu aplinkos poveikiui. Visgi, dideli gniuždantieji įtempiai gali būti vienu iš šių dangų esminių trūkumų, nulemiančių pagaminto optinio komponento plokštiškumo degradaciją, ir tuo pačiu – optines aberacijas, lazerio impulso bangos fronto iškraipymą. Yra keletas metodų, naudojamų siekiant sumažinti ar kompensuoti esamus įtempius – priešingos pagrinduko pusės padengimas atitinkamo storio SiO_2 sluoksniu, terminis suformuoto komponento atkaitinimas, dengimo proceso parametrų optimizavimas. Terminis atkaitinimas yra vienas iš efektyviausių ir plačiausiai naudojamų metodų, tačiau kai kurių medžiagų atveju, atsirandanti sluoksnių kristalizacija bei jos nulemti sklaidos nuostoliai dangoje apriboja šio metodo taikymą.

Dielektrinių medžiagų, kurias galima sėkmingai naudoti UV spektrinio ruožo dangų formavimui IBS technologijos pagalba, pasirinkimas yra gana ribotas. Paprastai HfO_2, Sc_2O_3 ir Al_2O_3 yra naudojami kaip aukšto lūžio rodiklio medžiagos, o SiO_2 – kaip žemo lūžio rodiklio medžiaga. Šiame skyriuje bus pristatyti skirtingų sudėčių dvikomponenčių HfO_2, Sc_2O_3 ir Al_2O_3 mišinių optinių, paviršinių savybių, bei jų įtempių pokyčiai, taikant atkaitinimą skirtingose temperatūrose iki 900 °C. Taip pat yra analizuojamos tokių mišinių panaudojimo galimybės projektuoti amorfines daugiasluoksnes dangas UV spektriniam diapazonui su kompensuotais įtempiais.

Eksperimentams atlikti buvo naudojama ta pati vakuuminė IBS kamera (žr. B skyrių). 25.4 mm diametro bei 1 mm storio FS pagrindukai buvo padengti eksperimentiniais mišinių sluoksniais, kurių optinis storis siekė 7 ketvirčius 355 nm bangos ilgiui, o fizinis – nuo ~290 nm iki ~380 nm, priklausomai nuo medžiagų mišinio ir jo sudėties. Skirtingų sudėčių HfO_2-Al_2O_3, Sc_2O_3-Al_2O_3 ir HfO_2-Sc_2O_3 mišiniai buvo gauti keičiant zoninio taikinio padėtį dulkinančio jonų pluošto atžvilgiu (19 pav.).

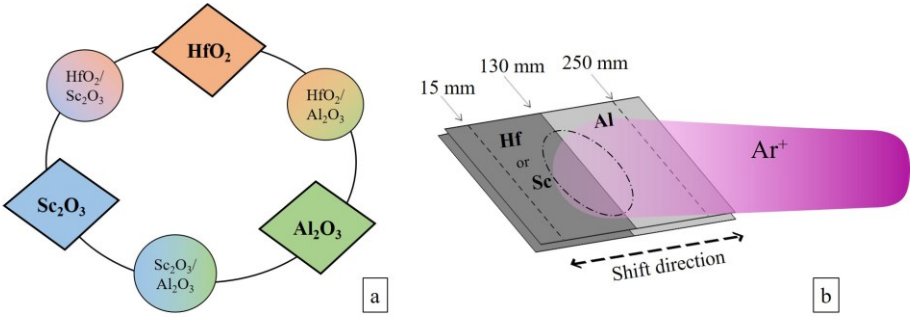

19 pav. Pasirinktos medžiagos, bei jų mišiniai (a). Eksperimentinių sluoksnių dengimas, naudojant zoninio taikinio padėties keitimą jonų pluošto atžvilgiu (b). Schematiškai pavaizduotos skirtingos (15 mm, 130 mm ir 250 mm) taikinio pozicijos.

Išmatuoti bandinių pralaidumo spektrai, nustatytos lūžio rodiklių bei ekstinkcijos koeficientų dispersijos yra pavaizduotos 20 pav. Paprastumo dėlei, toliau tekste bus įvardinta tik aukštesnio lūžio rodiklio medžiagos dalis mišinyje. Kadangi hafnio bei skandžio oksidų lūžio rodikliai yra labai panašūs ir pralaidumo spektrai, esant skirtingoms taikinio padėtims, praktiškai nesiskiria, modeliuojant išmatuotus spektrus nėra įmanoma nustatyti dedamųjų medžiagų kiekių. Tačiau, minėtų medžiagų sluoksnių augimo spartos yra labai panašios, todėl pagal taikinio poziciją galima apytikriai nusakyti gauto mišinio sudėtį (3 lentelė).

3 lentelė. Apytikslės HfO_2 bei Sc_2O_3 dedamosios mišiniuose priklausomai nuo taikinio pozicijos

Taikinio pozicija (mm)	HfO_2 dalis (%)	Sc_2O_3 dalis (%)
15	100	0
100	~70	~30
130	~50	~50
160	~30	~70
250	0	100

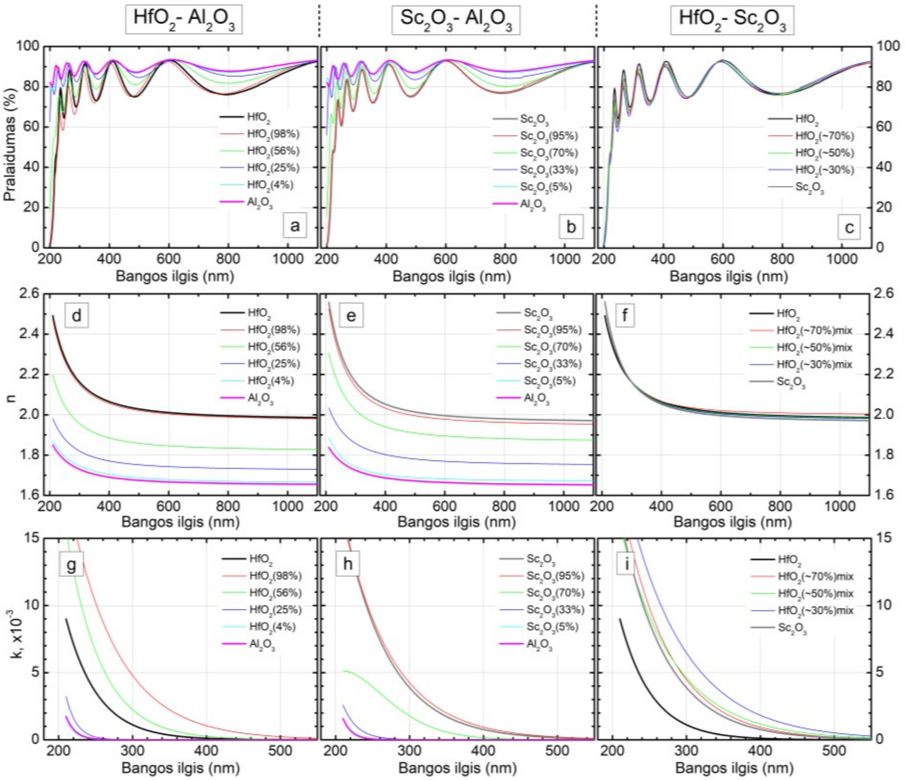

20 pav. Suformuotų HfO_2-Al_2O_3, Sc_2O_3-Al_2O_3, HfO_2-Sc_2O_3 mišinių ir atitinkamų grynų medžiagų pralaidumo spektrai (a, b, c), lūžio rodiklių (d, e, f) ir ekstinkcijos koeficientų (g, h, i) dispersijos.

Hafnio-skandžio oksidų mišinių lūžio rodiklių vertės yra praktiškai vienodos. Kitų porų atveju, mišinio lūžio rodiklis priklausė nuo dedamųjų dalių santykio, ir jo vertė buvo tarp atitinkamos aukštesnio bei žemesnio lūžio rodiklio medžiagos. Analogiškos tendencijos taip pat buvo gautos kituose mišinius analizuojančiuose darbuose [129, 142, 217]. Kai kurių suformuotų mišinių ekstinkcijos vertės buvo didesnės nei atitinkamų grynų medžiagų. Sluoksnių formavimo metu oksidacijai reikalingas deguonies kiekis buvo apskaičiuotas interpoliuojant tarp atitinkamiems gryniems oksidams formuoti reikalingų optimalių deguonies verčių. Kadangi, jos buvo gana skirtingos, tikėtina, jog mišinių formavimo metu naudoti O_2 kiekiai visgi nebuvo optimalūs. Tačiau, reaktyvių dujų kiekio optimizavimas proceso metu nebuvo pagrindinis šio tyrimo tikslas.

Kadangi IBS būdu suformuoti amorfiniai sluoksniai po terminio atkaitinimo gali kristalizuotis [82], analizuojant paviršiaus šiurkštumo pokyčius, buvo ieškoma atkaitinimo temperatūrų rėžių, kuriuose vyksta faziniai virsmai. Keliose publikacijose nustatyta, jog plonų kristalinių sluoksnių paviršiaus šiurkštumas yra didesnis, nei amorfinių sluoksnių [86, 218-220]. 21 pav. a) matyti, jog HfO_2 ir HfO_2 (98%) mišinio atveju tokia kritinė fazinio virsmo temperatūra T_c buvo tarp 500 °C ir 600 °C, o Al_2O_3 atveju 800 °C < T_c ≤ 900 °C.

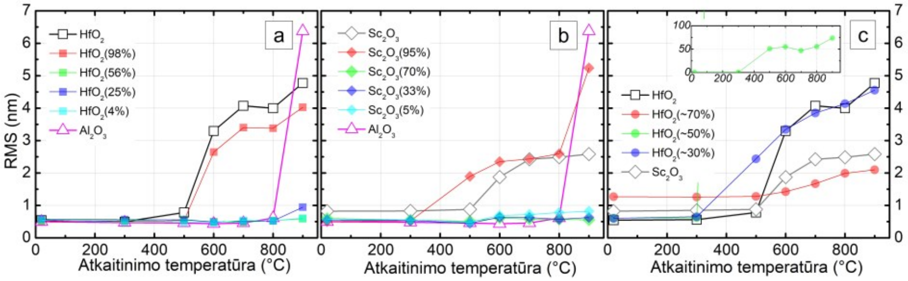

21 pav. HfO_2-Al_2O_3 (a), Sc_2O_3-Al_2O_3 (b), HfO_2-Sc_2O_3 (c) mišinių paviršiaus šiurkštumo RMS pokyčiai atkaitinus pasirinktose temperatūrose.

Kiti hafnio-aliuminio oksidų mišiniai - HfO_2 (25%), HfO_2 (56%) ir HfO_2 (4%) nepatyrė tokių pokyčių ir išliko amorfiniai. Gauti rezultatai atitinka impulsinio lazerinio nusodinimo būdu suformuotų hafnio aliuminato sluoksnių atkaitinimo metu nustatytas kristalizacijos temperatūras, kurios viršija 900 °C [221].

Gryno skandžio oksido sluoksniai patyrė fazinį virsmą 500 °C < T_c ≤ 600 °C diapazone (21 pav. b). Esant 5% Al_2O_3 frakcijai mišinyje, kritinės temperatūros rėžis sumažėjo iki 300 °C < T_c ≤ 500 °C, o kitų Sc_2O_3-Al_2O_3 mišinių sluoksnių paviršiaus šiurkštumas nesikeitė, kol nebuvo atliktas kaitinimas 900 °C temperatūroje.

Visai kitokia situacija buvo hafnio-skandžio mišinių atveju. HfO_2 (70)% mišinys dar prieš atkaitinimą pasižymėjo didesniu paviršiaus šiurkštumu. Tai gali būti susiję su galima polikristaline struktūra, susidariusia jau sluoksnio formavimo metu. Kitų HfO_2-Sc_2O_3 mišinių faziniai virsmai vyko 300 °C < T_c ≤ 500 °C ir 500 °C < T_c ≤ 600 °C ruožuose. Apskritai, šių mišinių fazinė būsena nėra tokie stabili esant vidutinėms atkaitinimo temperatūroms, lyginant su prieš tai aptartų mišinių poromis.

22 pav. a, b, c pavaizduota lūžio rodiklio verčių 355 nm bangoje pokyčiai, o 22 pav. d, e, f parodytas $\lambda_{0.001}$ bangos ilgio kitimas, didėjant atkaitinimo temperatūroms.

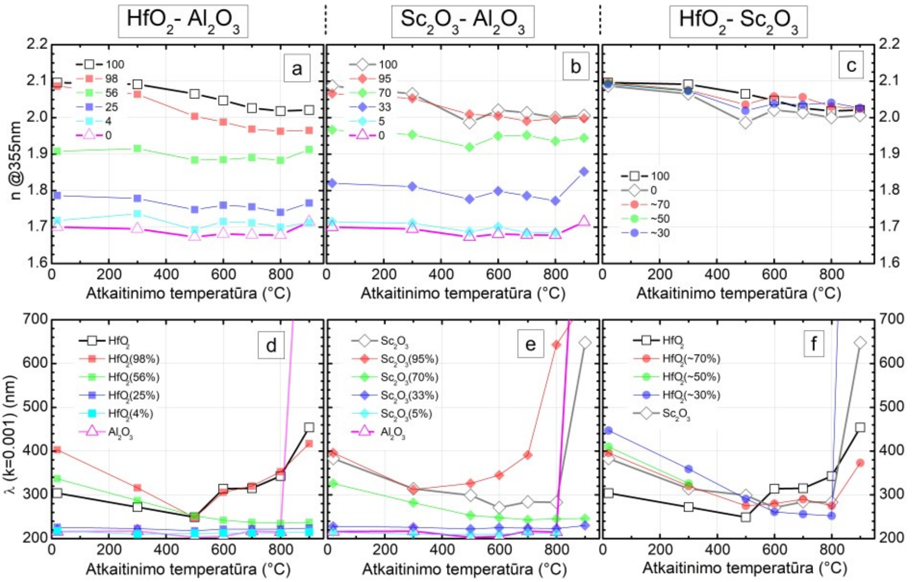

22 pav. HfO_2-Al_2O_3 (a, d), Sc_2O_3-Al_2O_3 (b, e), HfO_2-Sc_2O_3 (c, f) mišinių sluoksnių lūžio rodikliai bei λ ($k = 0.001$) priklausomai nuo atkaitinimo skritingose temperatūrose.

$\lambda_{0.001}$ bangos ilgis čia yra apibrėžiamas $k = 0.001$ kriterijumi, t.y. tai yra bangos ilgis, kuriame sluoksnio ekstinkcijos koeficientas pasiekia 0.001 vertę. Kadangi ekstinkcijos koeficientas nuosekliai didėja trumpesnių bangų ruože, $\lambda_{0.001}$ mažėjimas rodo, kad sluoksnis darosi labiau optiškai pralaidus, ir jo sugertis mažėja. Kaip jau buvo minėta, vertinama, jog lūžio rodiklio nustatymo paklaida nėra didesnė, nei 0.5%, tai atitinka $\Delta n = 0.01$, kai $n = 2$.

HfO_2 ir HfO_2 (98%) mišinių lūžio rodiklis (22 pav. a) nuosekliai mažėja didėjant T. Kitų mišinių atveju, šis parametras keitėsi mažiau, o aliuminio oksido sluoksnio lūžio rodiklis padidėjo įvykus kristalizacijai po 900 °C atkaitinimo. 22 pav. d matyti, jog gryno hafnio oksido ir jo mišinių su aliuminio oksidu ekstinkcija nuolatos mažėjo, didinant T iki 500 °C. Tai galima susieti su padidėjusia oksidacija bei pagerėjusia stechiometrija, kaip parodyta tiriant papildomo atkaitinimo įtaką vienasluoksnėms ir daugiasluoksnėms dangoms [172, 173, 222]. Po kaitinimo 600 °C temperatūroje buvo užfiksuota padidėjusi HfO_2 ir HfO_2 (98%) mišinių ekstinkcija, kuri yra susijusi su išaugusia sklaida dėl įvykusios kristalizacijos. Visų kitų likusių hafnio aliuminio oksidų mišinių ekstinkcija palaipsniui mažėjo, arba liko tokia pati, didinant atkaitinimo temperatūrą iki pat 900 °C. Al_2O_3 sluoksnio ekstinkcija ženkliai padidėjo atkaitinus ties 900 °C, dėl perėjimo iš amorfinio į kristalinį būvį [223, 224].

Sc_2O_3 lūžio rodiklis mažėjo vykdant terminius apdorojimus pradiniuose žingsniuose, tačiau, įvykus kristalizacijai po 600 °C atkaitinimo, padidėjo, vėliau vėl šiek tiek mažėjo. Sc_2O_3 mišinio, turinčio 5% Al_2O_3, lūžio rodiklis šiek tiek mažėjo didinant *T*, kai tuo tarpu kitų Sc_2O_3-Al_2O_3 mišinių lūžio rodiklio pokyčių tendencijos atitiko gryno Sc_2O_3 atvejį. Sc_2O_3 ekstinkcija mažėjo didinant *T*, netgi įvykus kristalizacijai. Tai gali reikšti, jog polikristalinę struktūrą sudarė maži kristalitai, neįnešantys sklaidos nuostolių, kurie savo ruožtu ženkliai padidėjo po kaitinimo 900 °C temperatūroje. Sc_2O_3 (95%) mišinio fazinis virsmas įvyko atkaitinus ties 500 °C ir ekstinkcija didėjo, didinant temperatūrą. Kitų tarpinių Sc_2O_3-Al_2O_3 mišinių ekstinkcija nuosekliai mažėjo arba nesikeitė atliekant kaitinimus vis aukštesnėse temperatūrose.

HfO_2-Sc_2O_3 mišinių, kaitintų iki 500 °C, lūžio rodiklių vertės išsidėstė tarp atitinkamų grynų oksidų. Tačiau, atkaitinus 700 °C temperatūroje, HfO_2 (70%) mišinio lūžio rodiklis viršijo atitinkamas grynų medžiagų vertes. Kompozitinių dangų ekstinkcija buvo didesnė nei hafnio bei skandžio oksidų. Po atkaitinimo 600 °C temperatūroje, HfO_2 (30%) mišinio ekstinkcija tapo mažiausia tarp visų bandinių. HfO_2 (50%) mišinyje po atkaitinimo 500 °C temperatūroje įvyko fazinis virsmas, po kurio drastiškai padidėjo paviršiaus šiurkštumas, sukėlęs didelius optinius nuostolius. Dėl šios priežasties optinių savybių modeliavimas tapo netikslus, tad atkaitintiems didesnėse nei 300 °C temperatūrose šiems bandiniams nėra pateikta ekstinkcijos duomenų. Po kaitinimo iki 900 °C, visų bandinių ekstinkcija padidėjo.

23 pav. pavaizduoti suformuotų ir atkaitintų bandinių įtempiai.

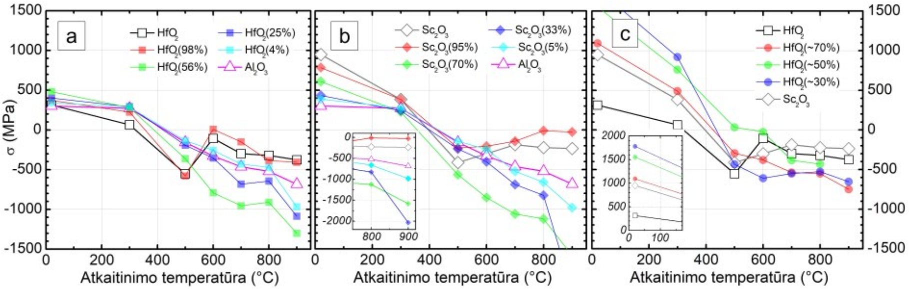

23 pav. HfO_2-Al_2O_3 (a), Sc_2O_3-Al_2O_3 (b), HfO_2-Sc_2O_3 (c) mišinių sluoksnių įtempiai priklausomai nuo atkaitinimo temperatūros.

Gryno HfO_2 bei HfO_2 (98%) mišinio su aliuminio oksido bandinių įtempiai ženkliai sumažėjo ($\Delta\sigma$ = 600 MPa) po kristalizacijos atkaitinus 600 °C temperatūroje (23 pav. a). Įdomiausios tendencijos buvo stebimos HfO_2 (56%) ir HfO_2 (25%) mišinių atveju. Jų pradiniai gniuždantieji įtempiai buvo per $\Delta\sigma \sim$ 150-200 MPa didesni, nei atitinkamų grynųjų medžiagų sluoksnių įtempių vertės. Sekančiame 500 °C atkaitinimo žingsnyje visų HfO_2-Al_2O_3 mišinių įtempiai tapo tempiamieji. Sekančiuose žingsniuose (600 °C ir 700 °C) tempiamieji įtempiai toliau didėjo, ypatingai HfO_2 (56%) atveju. Šuoliškas įtempių padidėjimas matomas atkaitinus 900 °C temperatūroje.

Suformuotų Sc_2O_3-Al_2O_3 mišinių įtempių vertės (23 pav. b) pasiskirstė tarp atitinkamų grynųjų medžiagų verčių. Atkaitinus 500 °C temperatūroje, gryno skandžio oksido bei Sc_2O_3 (95%) mišinio įtempiai tapo tempiamaisiais, tačiau po kaitinimo 600 °C, jie vėl sumažėjo ir priartėjo prie nulinių verčių. Likusių Sc_2O_3-Al_2O_3 mišinių sluoksnių įtempiai taip pat pasikeitė iš gniuždančiųjų į tempiamuosius, kurių vertės toliau didėjo, didinant atkaitinimo temperatūras.

Visų HfO_2-Sc_2O_3 mišinių sluoksnių gniuždantieji įtempiai buvo didesni, nei grynųjų medžiagų. Jie stipriai sumažėjo po pradinių kaitinimų ir tapo tempiamaisiais, ir po kaitinimų aukštesnėse, nei 600°C temperatūrose, ženklesnių pokyčių nebuvo stebima.

SiO_2 sluoksnių įtempių kitimas atliekant kaitinimą yra pristatytas Kičo ir kt. tyrime [144]. Atkaitintas SiO_2 turi tokius įtempius: ~380 MPa (400 °C) ir ~225 MPa (500 °C). Standartinio Brego veidrodžio atveju, SiO_2 sluoksniai yra didesnio fizinio storio, nei aukšto lūžio rodiklio sluoksniai, ir šis skirtumas priklauso lūžio rodiklių skirtumų tarp medžiagų.

Pagal prieš tai aptartus mišinių optinių savybių bei įtempių pokyčius priklausomai nuo atkaitinimo, žemiau išvardinti mišiniai, naudojant atitinkamas atkaitinimo temperatūras, gali būti kombinuojami kartu su SiO_2 daugiasluoksnių dangų UV diapazonui su kompensuotais įtempiais projektavimui:

a) HfO_2(56%)-Al_2O_3(44%) (σ = -360 MPa esant 500 °C), HR dangos atkaitinimas turėtų būti atliekamas 450 °C < T < 500 °C);

b) Sc_2O_3(70%)-Al_2O_3(30%) (σ = -560 MPa esant 500 °C), HR dangos atkaitinimas turėtų būti atliekamas 400 °C < T < 500 °C);

c) HfO_2(~70%)-Sc_2O_3(~30%) (σ = -295 MPa, esant 500 °C), HR dangos atkaitinimas turėtų būti atliekamas 450 °C < T < 500 °C).

Tolimesnių eksperimentų, kurių metu būtų formuojamos daugiasluoksnės dangos su kompensuotais įtempiais, nebuvo galima atlikti, kadangi turimoje jonapluoščio dulkinimo įrangoje galėjo būti naudojamas tik dviejų medžiagų taikinys. Šiuo atveju iš atitinkamo parinkto tirtų aukšto lūžio medžiagų mišinio ir SiO_2 sluoksnių sudarytos daugiasluoksnės dangos dengimas nebuvo galimas.

Pagrindiniai rezultatai ir išvados

1) Lydyto kvarco pagrindukų paviršiaus ėsdinimas argono plazma, pašalinant 50-100 nm storio paviršinį sluoksnį, ženkliai padidino jo LIDT, nepabloginus jo pradinių optinių, paviršiaus šiurkštumo bei plokštiškumo savybių. Skaidrinanti ir poliarizuojanti dielektrinės dangos, optimizuotos 355 nm bangos ilgiui, padengtos ant plazma apdoroto pagrinduko, turėjo daugiau nei 2 kartus didesnį optinį atsparumą, lyginant su tomis pačiomis dangomis, suformuotomis ant plazma neapdorotų pagrindukų.
2) Naudojant 140 eV energijos deguonies plazmą ir pašalinus 220 ± 10 nm storio FS pagrinduko paviršinį sluoksnį, jo optinis atsparumas ženkliai padidėjo ir pasiekė 75 ± 4 J/cm^2, 3ns trukmės $\lambda = 355$ nm lazerio impulsams. Skaidrinanti danga $\lambda = 355$ nm bangos ilgiui, padengta ant mažos energijos deguonies plazma apdoroto FS pagrinduko pasižymėjo 14 ± 0.7 J/cm^2 optiniu atsparumu, 3.4 kartus didesniu, lyginant su plazma neapdorotu pagrinduku. Pademonstruotas optinio atsparumo esminis padidinimas rodo puikias galimybes efektyviai panaudoti mažos energijos deguonies plazmos ėsdinimo metodiką kuriant didelio optinio atsparumo komponentus UV spektriniam ruožui.
3) Taikant atkaitinimą aukštose temperatūrose ir sukeliant hafnio-silicio oksidų mišinių sluoksnių struktūros kristalizaciją dielektrinių veidrodžių struktūroje, yra padidinamas optinių elementų atspindys, bei pralaidumas UV srityje ir išlaikomos pradinės paviršiaus šiurkštumo vertės.
4) Atkaitintas 1100 °C temperatūroje dielektrinis veidrodis, suformuotas naudojant 46%HfO_2+54%SiO_2 mišinį bei SiO_2, turėjo didžiausią 5.5 ± 0.6 J/cm^2 optinį atsparumą 266 nm lazerio impulsams. Gauti rezultatai rodo naujos metodikos, kombinuojant hafnio-silicio mišinius bei atkaitinimą aukštose temperatūrose, keičiant jų mikrostruktūrą, potencialą, kuriant padidinto optinio atsparumo daugiasluoksnes dangas UV spektriniam ruožui.
5) Atkaitinimo įtakos skirtingų sudėčių dvikomponenčių HfO_2, Sc_2O_3 ir Al_2O_3 mišinių optinėms, paviršiaus savybėms bei įtempiams analizė leido nustatyti potencialius variantus bei atkaitinimo temperatūrų rėžius, tinkančius daugiasluoksnių dangų su kompensuotais įtempiais UV spektriniam ruožui, projektavimui ir gamybai.

CURRICULUM VITAE

Name: Giedrius
Surname: Abromavičius
Date of birth: 1979 03 23
Place of birth: Panevėžys
E-mail: giedrius.abromavicius@ftmc.lt
Education:

1986 – 1997	Panevėžys secondary school No 5
1997 – 2001	Bachelor’s degree in Physics at Vilnius University
2001 - 2003	Masters’s degree in Physics at Vilnius University
2013 – 2017	PhD studies at the Center for Physical Sciences and Technology and Vilnius University

ACKNOWLEDGEMENTS

I would like to give my all gratitude to my family - my beloved wife, my mother, my late dad, my sister for never ending patience, support, love and faith. Also, big thanks to my supervisor Dr. Ramutis Drazdys for his help, support and belief.

Special thanks to Tomas Juodagalvis for his sincere efforts and devotion in related experimental work. Only with his assistance, presented amount of the results was possible. I am also grateful to other colleagues for their valuable suggestions and timely inspirations – Dr. Tomas Tolenis, Dr. Simonas Kičas and Dr. Kęstutis Juškevičius.

Huge thanks to my closest team mates for wonderful atmosphere in Optical Coating Laboratory – Audrius Valavičius, Simas Melnikas, Alexandr Belosludtsev and the others. Also, grateful thanks for my all friend and fellows for the encouraging discussions during the hardest times before the dawn.

LIST OF PUBLICATIONS AND THEIR COPIES

Scientific papers directly related to the thesis:

1. K. Juškevičius, R. Buzelis, **G. Abromavičius**, S. Abbas, A. Belosludtsev, R. Drazdys, S. Kičas, “Argon plasma etching of fused silica substrates for manufacturing high laser damage resistance optical interference coatings,“ Optical Materials Express, **7** (10), **2017.**
2. **G. Abromavičius**, T. Juodagalvis, R. Buzelis, K. Juškevičius, R. Drazdys, S. Kičas, “Oxygen plasma etching of fused silica substrates for high power laser optics”, Applied Surface Science, **453**, **2018.**
3. **G. Abromavičius**, S. Kičas, R. Buzelis, “High temperature annealing effects on spectral, microstructural and laser damage resistance properties of sputtered HfO_2 and HfO_2-SiO_2 mixture-based UV mirrors”, Optical Materials **95**, **2019.**

NOTES

Vilniaus universiteto leidykla
Saulėtekio al. 9, III rūmai, LT-10222 Vilnius
El. p. info@leidykla.vu.lt,
www.leidykla.vu.lt
Tiražas 20 egz.